INTRODUCTION

The Nuclear Physics Laboratory at the University of Washington pursues a broad program of research in nuclear physics and related fields. Research activities are conducted locally and at remote sites. The current program includes "in-house" research on nuclear collisions and fundamental interactions using the local tandem Van de Graaff and superconducting linac accelerators, as well as local and remote non-accelerator research on fundamental interactions and user-mode research on relativistic heavy ions at large accelerator facilities in the U.S. and Europe.

The filling of the SNO detector with heavy water was completed in April, 1999, and the complete detector was put into operation. During the past year the SNO data acquisition system developed by UW has been performing extremely well and reliably. The detector has been acquiring good quality production neutrino data since November 1999. These results suggest that the extreme care taken to maintain cleanliness during construction has paid off. The radioactive backgrounds are equal to, or better than, design goals. We are now organizing our resources to focus on keeping pace with the incoming data, running and maintaining the detector. In addition we are preparing for upgrading the SNO detector with the ^{3}He neutral current detector array.

The neutral current detectors for SNO are nearing completion, with about 95% of the detectors built and 75% underground in Sudbury. SNO is presently taking data with pure heavy water; during this time the NCD electronics will be commissioned and the alpha backgrounds of the detectors will be measured in preparation for their installation.

The electronics for the NCD array are built around a pair of multiplexed 4-channel high-speed digitizing oscilloscopes and 96 channels of spectroscopy ADCs. The Shaper-ADC boards have been successfully completed, and the multiplexers and controller boards are under construction.

The emiT experiment has set a limit on the "D" time reversal sensitive component in beta decay that is slightly better than the current world average. A paper describing this result will soon be submitted. An upgrade to the apparatus is underway, and a new measurement is planned in the coming year.

Our initial studies of lead perchlorate solution as a Cerenkov medium for neutrino detection have aroused an enthusiastic response among the neutrino community. This detector has promise for long baseline oscillation studies, supernova and other astrophysical neutrino studies and possibly proton decay. We are focusing our effort on understanding the optical properties of the liquid and the Cerenkov response of such a detector.

Preliminary ^{7}Be(p,g)^{8}B data has been taken, and most systematic errors have been reduced to a level compatible with our goal of a 5% determination of the astrophysical S-factor. In addition, we are initiating the first-ever direct measurement of the correction for loss of ^{8}B from the target due to backscattering.

In our cluster studies a triple coincidence experiment has provided direct evidence for multifragmentation of C_{60} into three complex fragments. From a separate experiment we have tentative evidence for production of a stable dianion of Si_2O_5 by fragmentation of the $NaSi_2O_5$ monoanion.

UW URHI activities in NA49 at CERN and STAR at RHIC continue at a rapid pace. Recent developments in NA49 event-by-event analysis are providing quantitative information on dynamical and flavor fluctuations, resonance effects in multiplicity correlations and possible evidence for correlated particle emission coupled to radial flow to produce recently-observed large-scale two-particle momentum correlations. The STAR event-by-event program has passed a milestone with the recent completion of Mock Data Challenge 3, a collaboration-wide effort in which several EbyE analysis techniques were applied to up to 25,000 simulated Au-Au events in a pilot study which tested many elements of STAR EbyE analysis infrastructure.

Preparations for using the STAR detector at RHIC for Hanbury-Brown Twiss interferometry are progressing well. The HBT simulation and analysis software is being tested extensively in preparation for the initial physics run at RHIC this Summer. The STAR HBT Physics Working Group has developed a detailed plan for the analysis of Year-One STAR data that addresses many physics issues in the new and unexplored regime of energy density that will open with the operation of RHIC.

The E\"ot-Wash group's recent work addressing the question "what is the weight of gravity itself?" (i.e. testing the equivalence principle for gravitational self-energy) was featured in Physics Today, Scientific American, Science, and Sky and Telescope. We removed an ambiguity in the classic lunar laser-ranging test by comparing, in effect, the accelerations of miniature earths and moons toward the sun. Our results were sufficiently precise that we could unambiguously determine that gravity has the weight predicted by Einstein to about 1 part in 1000.

We have recently begun a new round of experiments that test the gravitational inverse-square law at sub-millimeter separations. This work is motiviated by recent theoretical speculations of "large" extra dimensions, which predict fundamentally new behavior in this regime.

We have completed our "Big G" apparatus and conducted our first precision measurement of the gravitation constant. The measurement has much smaller systematic and statistical uncertainties than previous determinations.

As always, we encourage outside applications for the use of our facilities. As a convenient reference for potential users, the table on the following page lists the vital statistics of our accelerators. For further information, please write or telephone Professor Derek, W. Storm, Executive Director, Nuclear Physics Laboratory, University of Washington, Seattle, Washington 98195; (206) 543-4080, (e-mail: storm@npl.washington.edu) or can also refer to our web page: http://www.npl.washington.edu.

We close this introduction with a reminder that the articles in this report describe work in progress and are not to be regarded as publications or to be quoted without permission of the authors. In each article the names of the investigators have been listed alphabetically, with the primary author to whom inquiries should be addressed underlined.

Derek Storm, Editor

storm@npl.washington.edu, (206) 543-9522

Barbara Fulton, Assistant Editor

2000 TANDEM VAN DE GRAAFF ACCELERATOR SPECIFICATIONS

TANDEM VAN DE GRAAFF ACCELERATOR

A High Voltage Engineering Corporation Model FN purchased in 1966 with NSF funds; operation funded primarily by the U.S. Department of Energy. See W.G. Weitkamp and F.H. Schmidt, "The University of Washington Three Stage Van de Graaff Accelerator," Nucl. Instrum. Meth. **122**, 65 (1974).

Some Available Energy Analyzed Beams

Ion	*Max. Current (particle m A)*	*Max. Energy (MeV)*	*Ion Source*
^{1}H or ^{2}H	50	18	DEIS or 860
^{3}He or ^{4}He	2	27	Double Charge-Exchange Source
^{3}He or ^{4}He	30	7.5	Tandem Terminal Source
^{6}Li or ^{7}Li	1	36	860
^{11}B	5	54	860
^{12}C or ^{13}C	10	63	860
* ^{14}N	1	63	DEIS or 860
^{16}O or ^{18}O	10	72	DEIS or 860
F	10	72	DEIS or 860
* Ca	0.5	99	860
Ni	0.2	99	860
I	0.01	108	860

* Negative ion is the hydride, dihydride, or trihydride.

Additional ion species available include the following: Mg, Al, Si, P, S, Cl, Fe, Cu, Ge, Se, Br and Ag. Less common isotopes are generated from enriched material.

BOOSTER ACCELERATOR

We give in the following table maximum beam energies and expected intensities for several representative ions. "Status of and Operating Experience with the University of Washington Superconducting Booster Linac," D.W. Storm *et al.*, Nucl. Instrum. Meth. A **287**, 247 (1990).

Available Energy Analyzed Beams

Ion	*Max. Current (pm A)*	*Max. Practical Energy MeV*
p	>1	35
d	>1	37
He	0.5	65
Li	0.3	94
C	0.6	170
N	0.03	198
O	0.1	220
Si	0.1	300
^{35}Cl	0.02	358
^{40}Ca	0.001	310
Ni	0.001	395

Contents

1 Fundamental Interactions

1.1 A precise measurement of the ^{32}Ar superallowed branch

E. G. Adelberger, M. Bhattacharya, A. Garcia,* T. Glasmacher,† V. Guimares,*
A. K. Komives,* P. F. Mantica,† H. E. Swanson and S. L. Tabor‡

A recent measurement[1] of the $e - \nu$ angular correlation coefficient in the superallowed (SA) decay of ^{32}Ar at ISOLDE (deduced from the Doppler broadening of the SA proton peak) placed a stringent limit on the contribution of scalar currents to the standard model. The main source of systematic uncertainty in this measurement was the uncertainty in the mass of ^{32}Ar (-2180 ± 50 keV). In order to reduce this systematic uncertainty below the statistical uncertainty, the mass of ^{32}Ar had to be known with an accuracy of <4 keV. The authors in Ref [1] circumvented this problem by invoking the Isobaric Multiplet Mass Equation for A=32, T=2 quintet, and used the precisely known masses of the other 4 members of the multiplet to predict the mass of ^{32}Ar with an uncertainty of 3 keV. A more direct determination of the mass of ^{32}Ar would be desirable.

We recently performed an experiment at the National Superconducting Cyclotron Laboratory with a goal of measuring the SA decay branch of ^{32}Ar with an accuracy of better than 1%. Using this branching ratio and the precisely known half life[2] of ^{32}Ar one can compute the partial half-life for the ^{32}Ar SA decay. The partial half-life in conjunction with the expected ft value (twice the precisely measured value for T=1→T=1 pure Fermi decays) can then be used to infer the mass of ^{32}Ar with an accuracy of ∼10 keV. In addition the results from this experiment can also be used to check isospin-mixing calculations for $0^+ \rightarrow 0^+$ SA decays needed for the determination of V_{ud} and in turn for unitarity tests of the CKM matrix.

In our experiment ^{32}Ar was produced by the fragmentation of a ∼53 MeV/u ^{40}Ar beam. The fragments were mass-separated using the A1200 fragment mass analyzer and implanted at the center of a 500 μm thick PIPS detector which also served as our delayed proton counter. This detector was sandwiched between two detectors of same dimensions used for detecting the betas as well as for rejecting fast particles from the beam. Another 500 μm PIPS detector located upstream of the telescope provided energy loss and time of flight information needed to identify the incoming fragments. The telescope was surrounded by 5 large HPGe detectors (3 of them segmented clover detectors) to look for β-delayed γ decays of ^{32}Ar.

Analysis of the data is in progress. Careful attention is being paid to determine the number of ^{32}Ar ions implanted in the implantation detector and to the absolute proton detection efficiency of this detector.

*University of Notre Dame, Notre Dame, IN 46556.
†NSCL, Michigan State University, East Lansing, MI 48824.
‡Florida State University, Tallahassee, FL 32306.
[1] E.G. Adelberger *et al.*, Phys. Rev. Lett. **83**, 1299 (1999).
[2] Unpublished data from the ISOLDE experiment of Ref [1].

1.2 ^{4}He$(\alpha,\gamma)^{8}$Be

R. Hazama, K. A. Snover, D. W. Storm and J. P. S. Van Schagen*

We are in the process of completing the analysis of the high-precision measurement[1] of the ^{4}He$(\alpha,\gamma)^{8}$Be reaction. The goal of this experiment is the determination of the isovector M1 and E2 decay widths for a precision test of CVC and second-class currents in the mass-8 system. Last year we reported[2] how we had used the ^{10}B(^{3}He,pγ)^{12}C, ^{13}C(^{3}He,pγ)^{15}N, and ^{15}N(p,γ)^{16}O reactions to produce photons of 15.1, 8.3, and 13.3 MeV, respectively. These measurements give us detector response line shapes at those various energies, and the coincidence measurements enable us to determine the photon detector efficiency. Additional measurements of the ^{12}C(p,γ)^{13}N reactions at the E_p = 14.23 MeV resonance also provide an efficiency measurement, using the results of Marrs, *et al.*[3]

We have expanded the Sandorfi and Collins[4] lineshape parameterization by adding a second low-energy exponential tail, and, for two of the three detectors, an additional high energy tail. Using the three energies, 15.1, 13.3, and 8.3 MeV, along with spectral shapes calculated in 1 MeV increments with GEANT, we have determined the energy dependence of the parameters, in order to apply them to the broad γ-ray energy spectrum which is due to the width of the final state (first excited state) in ^{8}Be. Then the yield in any ^{4}He$(\alpha,\gamma)^{8}$Be spectrum can be determined by fitting the data to a predicted shape resulting from the convolution of the parameterized detector response with the spectral shape predicted by the R-matrix calculations that we described in last year's Annual Report.[5] This scheme uses estimated R-matrix parameters to obtain the yields, and then by fitting the excitation functions, precise values of these parameters will be obtained. Thus iteration may be necessary.

Once the data have been fit and all the relative R-matrix parameters have been determined, the absolute isovector M1 width must be determined from absolute cross sections. For this determination, we need absolute efficiencies, which are obtained from the photon yields (in coincidence with protons) and the singles proton yields, in the (^{3}He,pγ) measurements. We have found that the efficiencies for the spectra obtained without using the plastic-annulus veto are reproducible over time. However, for some detectors the threshold setting on the plastic veto seems to shift, so the efficiencies obtained using the plastic veto vary by a few percent from one measurement to the next. Furthermore, the absolute efficiencies obtained with the ^{10}B(^{3}He,pγ)^{12}C reaction differ by about 5% from those obtained from the ^{12}C(p,γ)^{13}N measurement. We are presently investigating possible sources of these discrepancies.

---

*Presently at WRQ, Seattle, 98109.
[1] Nuclear Physics Laboratory Annual Report, University of Washington (1999) p. 5.
[2] Nuclear Physics Laboratory Annual Report, University of Washington (1999) p. 4.
[3] R.E. Marrs, E.G. Adelberger, and K.A. Snover, Phys. Rev. C **16**, 61 (1977).
[4] A.M. Sandorfi and M.T. Collins, Nucl. Instrum. Methods **222**, 479 (1984).
[5] Nuclear Physics Laboratory Annual Report, University of Washington (1999) p. 6.

1.3 Time reversal in β decay - the emiT experiment

M. C. Browne,* H. P. Mumm, A. W. Myers, R. G. H. Robertson, T. D. Steiger, T. D. Van Wechel, D. I. Will, J. F. Wilkerson and emiT Collaboration†

The emiT experiment is a search for time-reversal (T) invariance violation in the beta decay of free neutrons. Both CP (charge conjugation - parity) and explicit T violation have been observed in the neutral K meson system. (Theoretically one expects that a combined CPT symmetry exist in all Lorentz-invariant field theories, thus CP and T symmetries must be intimately related.) However, some 35 years since the discovery of CP violation, neither CP nor T violation has been seen in any other system and possible origins are still not well understood. Although CP(T) violation can be accommodated within the standard model of nuclear and particle physics, it may also be an indication of physics beyond the standard model.

The standard model predicts T-violating observable in beta decay to be extremely small (Second order in the weak coupling constant) and hence beyond the reach of modern experiments.[1] However, potentially measurable T-violating effects are predicted to occur in some non-standard models such as those with left-right symmetry, exotic fermions, or lepto-quarks.[2,3] Thus a precision search for T-violation in neutron beta decay provides an excellent test of exotic physics.

The emiT experiment probes the T-odd P-even triple correlation between the neutron spin and the momenta of the neutrino and electron, $D\sigma_n \cdot P_e \times P_\nu$, in neutron beta decay. The coefficient of this correlation, D, is measured by detecting decay electrons in coincidence with recoil protons from a polarized neutron beam. This test is complementary to the more sensitive electric dipole moment (EDM) searches. EDMs violate both T and P and thus result from different physical processes.

emiT uses a beam of cold (2.7 meV), polarized neutrons from the Cold Neutron Research Facility at NIST in Gaithersburg, MD. The detector was installed on the NG-6 beamline at NIST from November of 1996 until September of 1997. A total of roughly 14 million coincidence events were recorded with a maximum sustained coincidence rate of ~ 7 Hz. Analysis of these data has been completed.[4] The result, $D = -0.1 \pm 1.3 \times 10^{-3}$, represents a small improvement over the current world average. It is limited by statistical uncertainty; however, systematic effects are not insignificant. The largest, $D_{ATP} = 4 \times 10^{-4}$, results from an asymmetric neutron beam combined with a slightly misaligned (Transverse) neutron polarization. The primary reason for the unexpectedly large magnitude of this effect was the lack of detector symmetry due to disabled channels in the proton detection segments (Normally the highly symmetric detector is fairly insensitive to such effects). The root cause of this problem was excessive energy loss in the proton detectors and the associated dead time, noise, and electronic failures due to high voltage sparks. Work on an upgrade to the apparatus (see Sec. 1.4) which will solve the problems experienced during the first run is currently in progress at the NPL. A new measurement is planned at NIST in 2001.

---

*Los Alamos National Laboratory, Los Alamos, NM 87545.

†Los Alamos National Laboratory, the National Institute of Standards and Technology (NIST), the University of California at Berkeley/Lawrence Berkeley National Laboratory, the University of Michigan, the University of Notre Dame, and NPL.

[1] M. Kobayashi and T. Maskawa, Prog. Theor. Phys. **49**, 652 (1973).

[2] P. Herczeg, *Progress in Nuclear Physics*, W.-Y.P Hwang, ed., Elsevier Sciences (1991) p. 171.

[3] E.G. Wasserman, *Time Reversal Invariance in Polarized Neutron Decay*, Ph.D. thesis, Harvard University, (1994).

[4] L.J. Lising *et al.*, Phys. Rev. C, to be submitted.

1.4 Upgrades to the emiT detector

M. C. Browne,* H. P. Mumm, A. W. Myers, R. G. H. Robertson, T. D. Steiger, T. D. Van Wechel, D. I. Will and J. F. Wilkerson

Past experiments searching for T violation in the β decay of polarized neutrons have reached a sensitivity to D of 1.4×10^{-3}. Technological advances in neutron polarization and an optimized detector geometry should allow emiT to attain a sensitivity to D of 3×10^{-4}, given the current capture flux available at the NG-6 beamline at NIST (1.4×10^{9} n/cm^{2}s). This level of sensitivity represents a factor of five improvement over previous neutron T tests, and may permit restrictions to be placed on several extensions to the Standard Model that allow values of D near 10^{-3}.

The emiT detector consists of four electron detectors (plastic scintillators) and four proton detectors (large-area PIN diode arrays) arranged in an alternating octagonal array concentric with the neutron beam. The average angle between any given proton detector and it's opposing electron detector is 135°. This configuration was chosen to take advantage of the electron–proton angular distribution which is strongly peaked around 160° due to the disparate masses of the decay products. When compared to the 90° geometry used in previous experiments, this choice results in an increased signal rate equivalent to roughly a factor of three increase in neutron bean flux.[1]

The protons produced in the decay of free neutrons have a relatively low energy. (The Q-value for the decay is 782 keV, producing protons with energies $\leq$ 751 keV.) While this allows for a delayed coincidence trigger between the proton and electron (eliminating much of the background due to cosmic rays) it makes detection difficult. The PIN diode array and associated electronics are therefore held at a nominal voltage of -30 kV which accelerates the protons to detectable energies and focuses them onto the PIN diode detectors.

During the first run, high voltage related problems stemming from higher than expected energy loss in the PIN diodes led to damaged electronic components and a non-symmetric detector. Systematic effects were less effectively canceled due to the lack of full detector symmetry and a more complex data analysis scheme was required.[2]

To assure that the second run is not affected by these problems, a number of detector upgrades are currently in progress at NPL. Sensitive electronics have been isolated through the use of analog fiber-optic links. The DAQ electronics have been extensively reworked. Lower power consumption will decrease the cooling requirements, and sharper ADC thresholds will allow better background rejection. This should allow operation at lower voltages thus increasing the stability of the detector. The fiber-optic links and new ADC cards have been constructed and are performing extremely well.

In addition, upgrades to the DAQ software will allow closer monitoring of the detector status and will improve the capability for real time data analysis. A tentative decision to replace the PIN diodes with Surface Barrier detectors has been made based on comparative studies of PIPS, PIN and Surface Barrier detectors. Investigations into the source of the observed high voltage instability are continuing. Finally, an upgrade to the NIST reactor will result in a factor of approximately two higher cold neutron flux. It is expected that emiT will resume collecting data in the fall of 2000, likely reaching the design goal of $D < 3 \times 10^{-4}$ early in 2001.

*Los Alamos National Laboratory, Los Alamos, NM 87545.

[1] E.G. Wasserman, *Time Reversal Invariance in Polarized Neutron Decay*, Ph.D. thesis, Harvard University (1994).

[2] L.J. Lising *et al.*, Phys. Rev. C, to be submitted.

1.5 PNC spin rotation of cold neutrons in a liquid helium target

E. G. Adelberger, J. H. Gundlach, D. Haase,* G. Hansen,† P. Huffman,‡ B. R. Heckel, D. Markoff,* U. Schmidt, H. E. Swanson, M. Snow† and F. Wietfeldt‡

When a neutron beam traverses a material target, the weak interaction between the target and beam causes the neutron spin vector to rotate about the beam momentum, giving rise to the PNC neutron spin rotation observable. When the target is liquid helium, the PNC spin rotation angle is a measure of the neutron-alpha weak coupling constant, which in turn is sensitive to the weak pion-nucleon coupling constant, f_π. We are building an experiment to measure the PNC neutron spin rotation in a liquid helium target using a cold neutron beam at the NIST reactor. This experiment receives support from the NSF as well as the Nuclear Physics Laboratory.

The first data runs, completed in 1997, revealed a need for a higher neutron counting rate and a more reliable cryostat. The experimental apparatus is being rebuilt to allow a measurement of the PNC spin rotation angle at the level of 10^{-7}, six times smaller than the first data runs.

There are three components of the apparatus that must be completed before new data can be taken.

1) The cryostat has been rebuilt with reliable vacuum and cryogenic seals. It has been shipped to NIST and has been successfully cooled to 4K at NIST.

2) A long wavelength neutron filter is required to improve the neutron beam polarization. Such a filter, based upon super-mirror reflections, has been demonstrated by Dubbers' group at the Institut Laue-Langevin. U. Schmidt has designed a similar filter for use by the spin rotation experiment. This filter is being made in Heidelberg and will be tested at NIST as soon as possible.

3) The target insert inside the cryostat must be modified to create and hold superfluid helium. P. Huffman. at NIST, is designing the new insert system. The final design will be completed in the spring of 2000.

While the above three major components are being completed, additional improvements are being made to the apparatus. G. Hansen is working on ways to improve the magnetic shielding. His conclusion is that an additional shield of 'cryoperm' be added inside the cryostat. Such a shield will be built and tested. Hansen is also working on a system of fluxgate magnetometers inside of the target region to monitor the magnetic field. H.E. Swanson is creating a more flexible data acquisition system for the experiment.

The goal of the collaboration is to take new PNC spin rotation data in 2001.

---

*TUNL, North Carolina State University, Durham, NC 27708.

†IUCF, Indiana University, Bloomington, IN 47408.

‡NIST, Gaithersburg, MD 20899.

1.6 Charge exchange reactions and hadronic probes of weak strength

E. G. Adelberger, M. Bhattacharya, C. D. Goodman* and Colleagues in IUCF experiments E356 and E406

Matrix elements for the Gamow-Teller (GT) operator between various nuclear states provide particularly interesting nuclear structure information because these matrix elements simply and directly show the relationships between the quantum states of neutrons and of protons in nuclei. Beyond the inherent nuclear structure interest in measuring GT matrix elements there are applications of GT measurements in neutrino physics and in astrophysics. Neutrino detection by absorption of neutrinos on nuclei occurs through Fermi and GT transitions, and some detection schemes rely exclusively on GT transitions. Some steps in astrophysical nucleosynthesis occur through electron absorption and emission in GT transitions. The density of hot electrons in supernova explosions is controlled by electron capture into GT states.

Beta decay is without question the most reliable way to measure GT matrix elements. However, because of the very limited energy window that it can explore, it is incapable of measuring GT giant resonances or GT transitions involved in some neutrino detectors.

Charge-exchange reactions offer an alternative for measuring GT matrix elements without the energy limitations of beta decay. However, the specific Fermi and GT cross sections, needed to convert reaction cross sections to Fermi and GT strengths, do not have a smooth mass number dependence that can be accurately predicted by reaction dynamics theory. It was discovered at IUCF that the ratio of specific Fermi to GT cross sections on the other hand, has a strong incident proton energy dependence that is universal (*i.e.* no mass dependence). One can exploit this energy dependence of the ratio of specific cross sections to extract the number of Fermi counts in a spectrum (the Fermi peak is usually not resolved from nearby and underlying GT transitions) and normalize the spectra to GT strength by normalizing to the Fermi transition, bypassing reaction dynamics uncertainties.

The best way to test the accuracy of charge exchange reactions in predicting GT strengths is to compare GT strengths obtained from charge exchange reactions to their β-decay values in nuclei where multiple GT transitions, spanning a wide range of excitation energies, are allowed. Two such nuclei are the ^{37}Cl and ^{40}Ar. For both of these nuclei a large number of GT transitions have been observed in the β decay of the isospin mirror and the GT strengths obtained from the β decay studies should be identical to those deduced from $0°(p,n)$ reactions to the extent that isospin symmetry is exact.

^{37}Cl(p,n)^{37}Ar studies were carried out at IUCF several years ago but the data were not fully analyzed. We are reanalyzing this data with refined data handling techniques. Also, we recently performed ^{40}Ar(p,n)^{40}K measurements at IUCF and are in the process of analyzing the data and preliminary results indicate a fair agreement between β-decay and charge-exchange reactions in this case.

*IUCF, 2401 Milo B. Samson Lane, Bloomington, IN 47408.

1.7 A precision measurement of the Newtonian constant

J. H. Gundlach and S. Merkowitz

The gravitational constant is one of the fundamental constants in nature and can only be determined by direct measurement. In the last ten years several measurements were carried out but the uncertainty of each was larger than the value of Luther and Towler[1] published in 1982. In addition some of the measurements scattered far outside of the ±128ppm uncertainty of the 1986 CODATA[2] value, putting the accuracy of our knowledge of G into question.

We developed a new torsion balance technique that offers several significant advantages over previous torsion balance methods.[3] A torsion balance apparatus was placed on a turntable located between a set of attractor masses. First, the turntable was rotated at a constant rate so that the pendulum experiences a sinusoidal torque due to the gravitational interaction with the attractor masses. A feedback was then turned on to accelerate the torsion balance apparatus precisely so that the torsion pendulum did not twist with respect to the turntable. The angular acceleration of the turntable, which contains the gravitational angular acceleration, was determined from the second time derivative of the turntable angle. Since the torsion fiber did not experience any appreciable deflection our measurement is independent of many torsion fiber properties and in particular avoids in- and anelasticity problems that may have led to a bias in previous measurements.

The largest quoted systematic uncertainty in the best torsion balance measurement to date is due to the pendulum mass distribution. We used a thin vertical plate as the pendulum in conjuction with selecting the purely quadrupole angular acceleration. This trick frees us from having to know the pendulum mass distribution exactly.

The attractor masses were located on a separate but coaxial turntable. This turntable rotated with a constant angular velocity difference to the pendulum turntable so that the signal occured at a constant and higher frequency that was selected by the operator. The rotation of the attractor masses allowed us to effectively remove gravitational interactions due to mass changes in the environment and reduce 1/f-noise.

We recorded four ≈100 hour long data sets. After each data set the spheres were moved to positions 90° away on the attractor turntable shelves. The orientation of the spheres was also changed to average out density fluctuations and non-spherocity. The coordinates of the spheres were measured before and after each data set. We used specially fabricated measuring tools mostly made of invar. Before and after each distance measurement the tools were compared to invar ball bar standards that were calibrated at NIST to within 0.3μm.

We ran tests in which the turntable and signal velocities were varied, the ambient magnetic field was exaggerated, and large rotating temperature gradients in phase with the attractor spheres were induced and found the gravitational acceleration was independent of these effects. A second data set with four of the eight attractor spheres removed was taken to verify the linearity of our system and agreement within errors was found. Numerical simulations were conducted to check the accuracy of our data analysis.

[1] G.G. Luther and W.R. Towler, Phys. Rev. Lett. **48**, 121 (1982).
[2] E.R. Cohen and B.N. Taylor, Rev. Mod. Phys. **59**, 1121 (1987).
[3] J.H. Gundlach *et al.*, Phys. Rev. D **54**, R1256 (1996).

Our *preliminary* value for the gravitational constant is

$$G = 6.6742 \pm 0.0001 \times 10^{-11} m^3 kg^{-1} s^{-2}.$$

At about ±15ppm this value represents a substantial increase in precision and is not subject to the most significant sources of systematic error or potential bias associated with other torsion balance measurements. Our value is higher than the 1986 CODATA value and is therefore only in marginal agreement. It may however be noted that the weighted average of all other measurements published after 1995 is also higher, by 248±63ppm, than the accepted value.

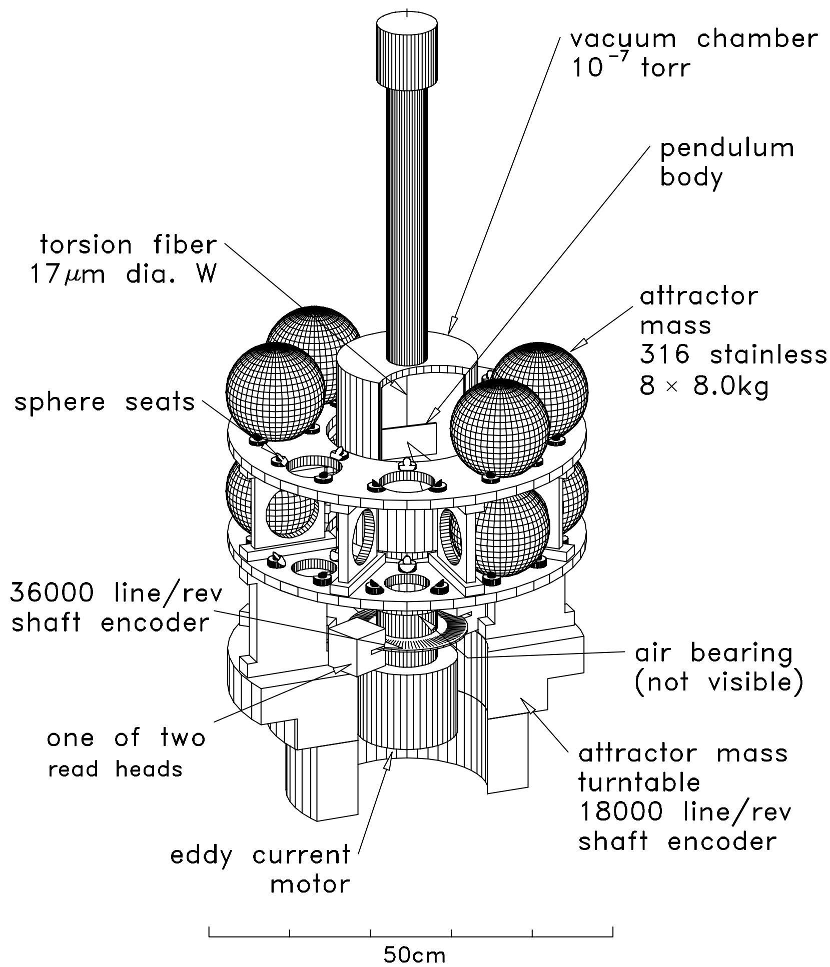

Figure 1.7-1. Cut-away view of the apparatus. The torsion balance consisting of a flat vertical plate hung from a thin tungsten fiber is mounted on an air bearing turntable. The apparatus rotates continuously and smoothly changes its angular velocity so that the torsion fiber is not twisted. The gravitational angular acceleration is transfered to the turntable and a high resolution shaft encoder is used to read out the angular acceleration. Eight stainless steel spheres produced an almost pure gravitational quadrupole field. To discriminate gravitational accelerations from other nearby masses, the attractor spheres are rotated on a second turntable.

1.8 Calculation of the source strength for the Eöt-wash III torsion balance

E. G. Adelberger, K. Choi and B. R. Heckel

We calculated the source strength ($\vec{I}$)for the Eöt-Wash III torsion balance which is designed to search for violations of the equivalence principle (EP) from new fundamental forces with Yukawa range > 1m. Since our experiment is sensitive only to the horizontal differential acceleration, we only need to calculate the horizontal component of the source strength,

$$\vec{I}_{\perp} = G \int d^3 r \rho_s(\vec{r}) (\frac{q_5}{\mu})_s (1 + \frac{r}{\lambda}) \frac{e^{-r/\lambda}}{r^2} (\hat{\imath} \sin\theta\cos\phi + \hat{\jmath} \sin\theta\cos\phi), \quad (1)$$

where $\vec{r}$ denotes the position of the source elements, G is Newton's constant, q_5 and λ are the "charge" and range of the EP-violating interaction, μ is the mass in AMU and ρ is the density.

The calculation of $\vec{I}_{\perp}$ involves two steps: first modeling, second integration of the effective source masses. We used the MULTI and M2CAD14 program, written by Eric Adelberger and Nathan Collins, and AutoCad to model the source near the pendulum, such as a sand box, magnet and coil, pits under the magnet, cranes, concrete blocks and beams in the cyclotron room, the pond above the cyclotron room, and the Nuclear Physics Laboratory (NPL) building (Fig. 1.8-1). We also used a commercial program called "Surface Display System" (SDS) to model the sources such as the hillside excavations for the NPL, the topographic terrain out to a radius 40km, including Lake Washington, part of Puget Sound, and the bedrock underground down to 20km.

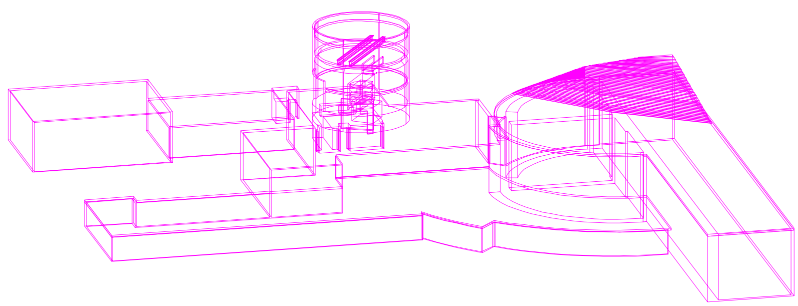

Figure 1.8-1. Entire NPL Building.

We used rectangular coordinates with $\hat{x}$ = East, $\hat{y}$ = North, $\hat{z}$ = up to integrate over the effective sources. Except for sources in the NPL Building which were calculated by the MULTI program, we integrated each part of the source separately on a 3-dimensional rectangular grid using the Richardson method.

The results of calculation,[1] expressed in the magnitude $|\vec{I}_{\perp}|$ and the direction θ in the EW-NS frame for $q_5 = B$, L, $\frac{(B-L)}{\sqrt{2}}$, and $\frac{(B-2L)}{\sqrt{5}}$, are shown in Fig. 1.8-2, where B and L are the baryon and lepton numbers.

[1]E.G. Adelberger *et al.*, Phys Rev. D **42**, 3283 (1990).
[2]Nuclear Physics Laboratory Annual Report, University of Washington (1999) p. 10.
[3]Germund Dahlquist, *Numerical Methods,* Prentice-Hall, Inc. (1974).

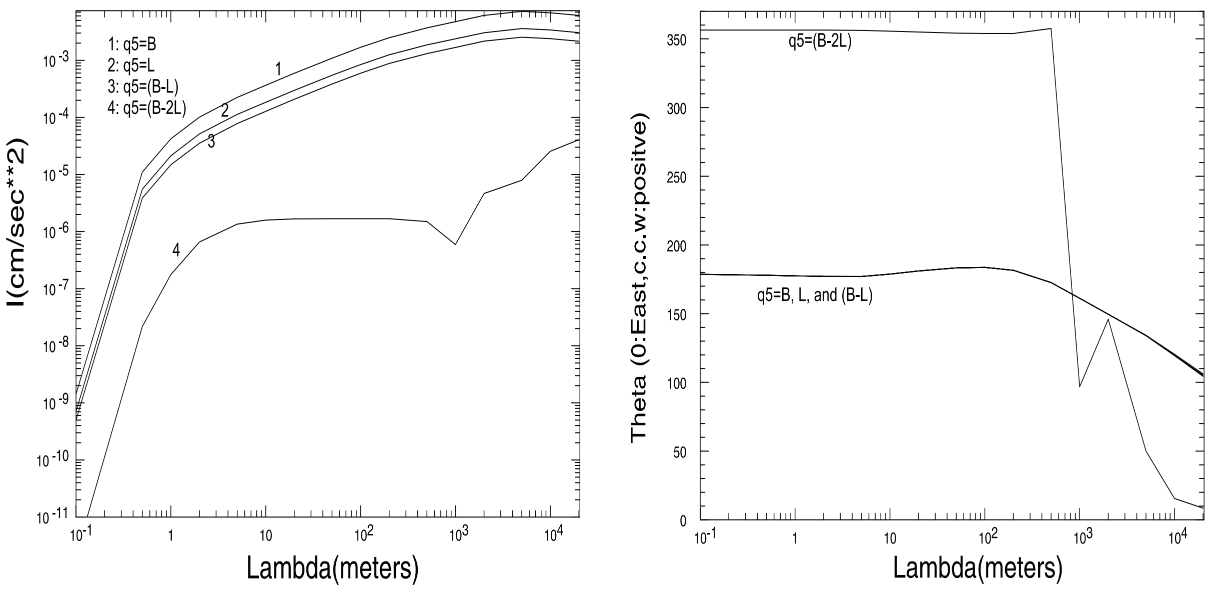

Figure 1.8-2. The source strength ($\vec{I}_{\perp}$) and the direction θ.

1.9 Millimeter-scale test of the gravitational inverse square law

E. G. Adelberger, N. A. Collins, C. Deufel,* J. H. Gundlach, B. R. Heckel, C. D. Hoyle, D. J. Kapner, U. Schmidt and H. E. Swanson

Motivated by higher-dimensional theories which predict deviations from the gravitational inverse-square law at the millimeter scale,[1] we have constructed a torsion balance experiment sensitive to such anomalous effects.

We adapted many components from the Rot-Wash apparatus[2] for this short-range test. The apparatus consists of a specially designed torsion pendulum which hangs as close as possible above a rotating attractor of similar geometry (see Fig. 1.9-1). A thin electrostatic screen separates the pieces. We chose the geometry in order to minimize gravitational torques while accentuating any torque due to a short-ranged Yukawa or power law interaction.

In the last year, much design and construction effort went into this project. Using a Fourier-Bessel expansion of the gravitational potential, we created a program to calculate gravitational and Yukawa torques on the pendulum. This allowed us to choose the best possible geometry. We constructed a 3-axis rotation and translation platform for precise pendulum positioning. Also, mechanisms for attractor alignment as well as an improved optical system were made. We presently await the completion of the tantalum and copper pendulum and attractor pieces.

In the meantime, we constructed a simpler attractor and pendulum from copper and aluminum respectively, each of which has 10 identical holes spaced evenly about the azimuth. Preliminary measurements have been performed with this design. We leveled the pendulum to within 200 μrad of local vertical by rotating it above a differential capacitor. We then made the electrostatic screen and attractor parallel to the pendulum using optical and mechanical methods so that the total angle between them is less than 1 mrad. The pendulum and attractor were made coaxial to within 60 μm with gravitational techniques described in G.L. Smith, *et al.*[2]

We are presently finishing our initial data set which includes pendulum/attractor separations between 0.15 mm and 8 mm. We expect to be able to reach separations of 0.10 mm. We should have significant results from this experiment in the coming months.

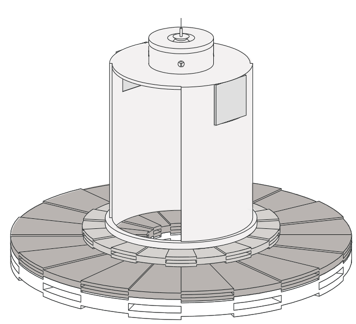

Figure 1.9-1. The pendulum and rotating attractor. The shaded sectors are tantalum, the unshaded ones copper. The mirrors used for the optical readout system and cutouts for gravitational alignment are also shown. The electrostatic screen has been omitted for clarity.

*REU summer student from Wabash College, Crawfordsville, IN 47933.

[1] See, for example, N. Arkani-Hamed, *et al.*, Phys. Lett. **429B**, 263 (1998).

[2] G.L.Smith, *et al.*, Phys. Rev. D **61**, 022001 (1999).

1.10 Final results from the Rot-Wash test of the equivalence principle

E. G. Adelberger, J. H. Gundlach, B. R. Heckel, C. D. Hoyle, G. L. Smith* and H. E. Swanson

We have completed our short-range test of the equivalence principle using the Rot-Wash apparatus. The experiment involved rotating a 3 ton ^{238}U attractor around a torsion pendulum containing a copper/lead composition dipole.

We analyzed new data taken in 1997–98 and re-analyzed previously reported 1996 data.[1] Combining the data sets, we found a differential acceleration of $\Delta a_{Cu-Be} = (1.0 \pm 2.8) \times 10^{-13}$ cm/s^2. Our results set new constraints on equivalence-principle violating interactions with Yukawa ranges down to 1 cm, and improve significantly existing limits between 10 km and 1000 km (see Fig. 1.10-1). For a full account of experimental design, protocol, and results, see G.L. Smith *et al.*[2]

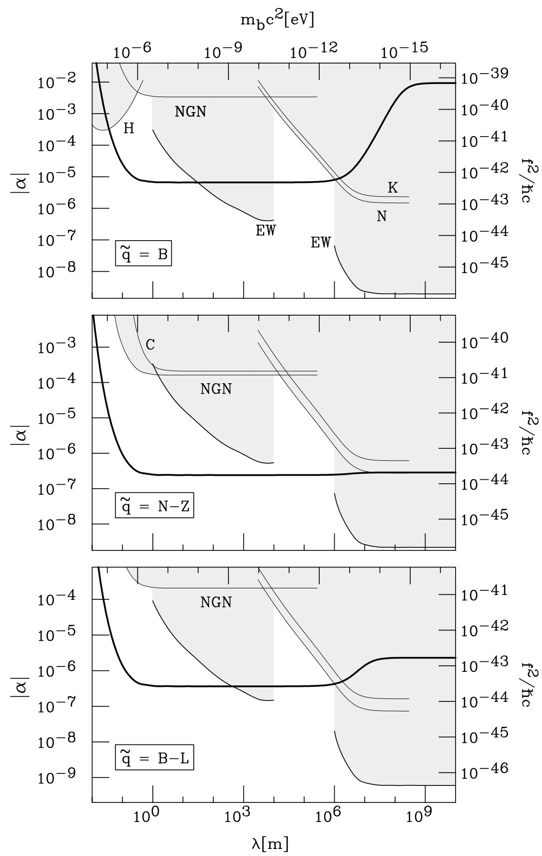

Figure 1.10-1. 95% Confidence limits on coupling strengths of hypothetical Yukawa interactions with range λ and vector charges of baryon number, neutron number minus proton number, and baryon number minus lepton number (top to bottom). The top axis shows exchange boson mass and on the right we see dimensionless “fine structure constants” for such interactions. The heavy curve is from this work; the shaded areas represent previously excluded regions. (For references, see G.L. Smith *et al.*)[2]

*Presently at Skagit Community College, Mt. Vernon, WA 98273.
[1] J.H. Gundlach, *et al.*, Phys. Rev. Lett. **78**, 2523 (1997).
[2] G.L. Smith, *et al.*, Phys. Rev. D **61**, 022001 (1999).

1.11 Progress on the Eöt-Wash III rotating torsion balance

E. G. Adelberger, K. Choi, J. H. Gundlach, B. R. Heckel, C. D. Hoyle, D. J. Kapner, S. M. Merkowitz, U. Schmidt and H. E. Swanson

We are building a new rotating torsion balance to search for violations of the equivalence principle due to new fundamental forces with Yukawa ranges >1 m. As described in previous reports, the balance will consist of a composition-dipole pendulum containing titanium, beryllium, or aluminum test bodies. The pendulum is suspended inside a vacuum chamber and hangs from a constantly rotating turntable.

We completed a new data acquisition and control system written in C++ that runs under Windows 98. The data collection includes averaging filters that can reduce the amount of 60Hz and other high-frequency noise in the data. The operator can now control most of the apparatus from a single program, such as set the turntable speed, rotate the pendulum relative to the turntable, change the settings on the lock-in amplifiers, and lock the turntable. The user can create multiple windows with real-time plots of the data with a variety of settings. The program can perform several special tasks unattended, such as: change the turntable speed without exciting the pendulum, rotate the pendulum with respect to the autocollimator, and execute a calibration run. Future enhancements will include catching and cooling the pendulum. We will also implement a feedback loop that accelerates the turntable to minimize the torsion fiber twist that was successfully used on the apparatus to measure the gravitational constant (see Sec. 1.7).

We built an insulated shed around the experiment and use a water chiller to maintain a constant temperature in the enclosure. Another chiller is used to keep the room temperature constant to within 0.2K (at a single location). The vacuum chamber is enclosed in a insulated jacket that is also kept at constant temperature by circulating chilled water. We re-wired the temperature sensors (AD-590s) and built a new controller box with high and low gain options (set through the data acquisition program). With these changes, the noise on the sensors was reduced to about 1mK. We are currently investigating ways to further improve their sensitivity.

We installed new legs and linear displacement LVDTs (linear variable differential transformers) on the turntable that will allow us to remotely level the turntable. The leg height can be coarsely adjusted with a stepper motor that drives a leveling screw. Fine adjustments are made with a peltier element inside lead feet that change the temperature of the feet allowing us to use their thermal expansion to change their height (see Sec. 1.12).

We installed Q21, Q22, Q31 gravity gradient compensators and have completed first-round measurements of their strength. A second measurement of the gradients is in progress, after which the compensators will be further "tuned" to fully cancel these components of the local mass distribution. A second measurement is necessary because several changes in the room mass distribution were made since the initial measurements.

We designed and built several new components of the apparatus: vacuum chamber, autocollimator, corner-mirror and holder, phi-top stage that includes a stepper motor for changing the height of the pendulum, pendulum parking stand, and two shielded tilt sensor holders. The design for the final pendulum[1] is finished and is being manufactured commercially.

[1] Nuclear Physics Laboratory Annual Report, University of Washington (1999) p. 10.

1.12 Gravity's gravity

E. G. Adelberger, J. H. Gundlach, B. R. Heckel, S. M. Merkowitz, U. Schmidt and H. E. Swanson

We measure the composition dependent acceleration of the four test bodies of our rotating torsion balance towards the sun. Two test bodies have the composition of the earth and the other two the composition of the moon. Our result removes the ambiguity of the lunar-ranging tests of the equivalence principle for gravitational self-energy. Since our last reports[1,2,3,4] we upgraded the Eöt-Wash II torsion balance in various ways:

- Active tilt compensation: The laboratory and therefore our torsion balance change its tilt typically by 1 μrad per day. This tilt causes an additional twist of the fiber of the torsion balance. With a feed through coefficient of typically 10^{-2}, measured by purposely tilting the apparatus, the additional twist of the fiber leads to an false effect of 10 nrad, which is 20 times bigger than our instrumental sensitivity. The uncertainty of the correction for this tilt effect was the major contribution to our systematic error budget. We now reduce this effect by a factor of 50. Our active elements (feet that support the apparatus) consist of a lead tube coupled through a peltier element to a temperature stabilized water reservoir. The peltier element acts as a heat pump and allows us to change the temperature of the lead tube and therefore by thermal expansion its length. With a sophisticated computer controlled feed back loop we managed to control the length of our feet within 10 nm. By replacing two of the three feet with our active ones, we are able to keep our apparatus leveled within 20 nrad over weeks.

- Vibration isolation of the fiber: We insert a small bellows between the prehanger of the fiber and it upper mount. This bellows decouples the vibration of the rest of apparatus from the fiber above 10 Hz and therefore reduces the noise in our signal.

- Improvements of the data acquisition: We changed our data acquisition program from a solely DOS-based to a real-time task switching one. This allow us to introduce a 288 times over sampling together with digital filtering. The maximum error of the computer controlled timing of the ADC conversion is 2μs. Therefore the feed through of the 60 Hz power line and the 120 Hz lock-in synchronization frequencies is reduced by a factor of 2×10^{-4} due to digital filtering. Further the digitizing noise of our data is reduced by a factor of 20. In addition we reduced the electronic channel crosstalk from 2.3×10^{-5} to 7.5×10^{-6}. In combination with some smaller changes in the temperature-measurement electronics the systematic error of our signal due to temperature effects is now smaller by a factor of 10.

We finished a second run of data taking and are working on the data evaluation. For the data taken between June 1999 and February 2000 our preliminary result for a composite-dependent component of the earth-moon differential acceleration toward the sun is $\Delta a_{CD}/a_s = 1.0 \times 10^{-13}$ with a statistical error of 1.4×10^{-13}. We estimate the systematic error to be 0.2×10^{-13} from the current state of the data analysis.

---

[1]S. Baeßler *et al.*, Phys. Rev. Let. **83**, 3585 (1999).
[2]Nuclear Physics Laboratory Annual Report, University of Washington (1999) p. 13.
[3]Physics Today, Nov. 1999, pp 19-21.
[4]Scientific American, Feb. 2000, p. 20.

1.13 A sensitive test for CPT-violation in the electron sector

E. G. Adelberger and B. R. Heckel

Because any quantum field theory is necessarily invariant under the combined symmetries of C, P and T, it is difficult to assess the relative sensitivities of different experimental tests for CPT-violation. Kostelecky and co-workers[1] have developed a general theoretical framework which admits CPT invariance at the cost of breaking Lorentz invariance in a controlled way. Their model posits spontaneously generated vector and axial vector fields, fixed in the universe, with which the usual standard model particles interact in Lorentz covariant form. "Observer Lorentz invariance" is maintained (invariance under arbitrary boosts, translations and rotations of the observer) while "particle Lorentz invariance" (invariance under arbitrary boosts, etc. of a test particle) is broken. Recently Bluhm and Kostelecky[2] showed that the results from a 1998 Eöt-Wash experiment[3] using a torsion pendulum containing nearly a mole [$(7.8 \pm 0.6) \times 10^{22}$] fully polarized electrons spins could be used to set powerful constraints for CPT and Lorentz non-invariance in the electron sector.

The Kostelecky CPT-and-Lorentz-violating Lagrangian for electrons is

$$\mathcal{L} = -a_\mu \psi \gamma^\mu \psi - b_\mu \psi \gamma_5 \gamma^\mu \psi \tag{2}$$

where a_μ and b_μ are vector and axial vector fields fixed in the cosmos. The second term in Eq. 2 (plus CPT-conserving but Lorentz-violating terms in Kostelecky's Lagrangian) lead to an interaction of a polarized electron with the cosmic field

$$\mathcal{H} = -\tilde{b} \cdot \sigma \tag{3}$$

where $\tilde{b} = b+$ (CPT-conserving but Lorentz-noninvariant terms). This would have cause our spin pendulum to experience a torque around $\tilde{\boldsymbol{b}}$.

Torsion balances are sensitive only to the *vertical* component of the torque, but as the earth rotates the vertical axis sweeps out a cone in fixed space. By monitoring the torque on the pendulum as a function of the orientation of the spin relative to axes fixed in space we can detect interactions of the form given in Eq. 2 and by exploiting the phase of the torque signal in our rotating balance we can probe all three components of $\tilde{\boldsymbol{b}}$. The North-South component of $\tilde{\boldsymbol{b}}$ produces a torque that is constant as the earth rotates, while the remaining two components produce torques that vary with a period of a sidereal day.

We have reanalyzed M.G. Harris's thesis data (which he had analyzed for signals fixed in the lab frame) and obtained the following results for the $\hat{x}$, $\hat{y}$, and $\hat{z}$ components of $\tilde{\boldsymbol{b}}$ ($\hat{z}$ points from the center of the earth to its North rotational pole, and $\hat{x}$ points from the earth to the sun at the vernal equinox)

$$\tilde{b}_x = (0.1 \pm 2.1 \pm 0.8) \times 10^{-20}\text{eV} \tag{4}$$
$$\tilde{b}_y = (1.7 \pm 2.3 \pm 0.8) \times 10^{-20}\text{eV} \tag{5}$$
$$\tilde{b}_z = (-10.3 \pm 3.9 \pm 7.6) \times 10^{-20}\text{eV} \tag{6}$$

[1]See for example, D. Colladay and V.A. Kostelecky, Phys. Rev. D **55**, 6760 (1997).
[2]R. Bluhm and V.A. Kostelecky, Phys. Rev. Lett. **84**, 1381 (2000).
[3]M.G. Harris, Ph.D. thesis, University of Washington (1998).

where the first error is statistical and the second systematic. The systematic errors for $\tilde{b}_x$ and $\tilde{b}_y$ are smaller than for $\tilde{b}_z$ because only the components of temperature, magnetic field, gravity gradients and turntable wobble that vary over the course of a sidereal day contribute to $\tilde{b}_x$ and $\tilde{b}_y$, while their average values contribute to $\tilde{b}_z$. The above results provide the most sensitive test, to date, for Lorentz and CPT violation in the electron sector.

2 Neutrino Physics

2.1 The Sudbury Neutrino Observatory

Q. R. Ahmad, J. F. Amsbaugh, M. C. Browne,* T. V. Bullard, T. H. Burritt, P. J. Doe, C. A. Duba, S. R. Elliott, R. Fardon, J. E. Franklin, A. A. Hamian, R. Hazama, G. C. Harper, K. M. Heeger, M. A. Howe, A. W. Myers, J. Orrell, A. W. P. Poon,† R. G. H. Robertson, K. Schaffer, M. W. E. Smith, T. D. Steiger, T. D. Van Wechel and J. F. Wilkerson

The Sudbury Neutrino Observatory (SNO), is a joint Canadian/US/UK effort to measure the spectral distribution and flavor composition of the flux of the higher-energy, ^{8}B neutrinos from the Sun by using a 1000 tonne detector of heavy water. The SNO detector relies on three different neutrino interaction processes.

$$\begin{array}{lcll} ^2H + \nu_e & \rightarrow & p + p + e^- & \text{Charged Current (CC)} \\ ^2H + \nu_x & \rightarrow & p + n + \nu_x & \text{Neutral Current (NC)} \\ e^- + \nu_x & \rightarrow & e^- + \nu_x & \text{Elastic Scattering (ES)} \end{array}$$

Because of this unique sensitivity to the known flavors of neutrinos, SNO should be able to yield a definitive answer to the question of whether neutrino flavor oscillations are occurring in the Sun in a way that is independent of the standard solar models (SSM) of how the Sun works. As a second generation solar neutrino detector, SNO will also have a significant increase in statistical sensitivity compared to present detectors. Assuming an energy threshold of 5 MeV, the SNO detector is expected to observe 12.7 CC events/day (SSM/2), 5.5 NC events/day (SSM), and 1.2 ES events/day (SSM/2).

This past year has been very productive and exciting. In November 1999 the detector made the transition from commissioning to taking production neutrino data. The SNO data acquisition system and tools developed by UW have proven very reliable and user friendly.

Fabrication of the neutral current detection (NCD) proportional counter array is nearing completion. Approximately 92% of the detectors in the array have been constructed and 75% are underground at SNO where their performance is being monitored. The final data acquisition system nears completion. It is anticipated that the complete system will be underground and functioning in Summer 2000. The hardware required to deploy the array has been designed at UW and fabrication by the NPL shop is almost complete.

With the successful operation of the detector and the near completion of the NCD array we are focusing our attention on analyzing the PMT data from the detector. To this end we have formed a collaboration, the "West Coast Alliance" (WCA), which consists of University of Washington, Lawrence Berkeley National Laboratory, Los Alamos National Laboratory and the University of British Columbia.

*Los Alamos National Laboratory, Los Alamos, NM 87545.
†Lawrence Berkeley National Laboratory, 1 Cyclotron Road, Berkeley, CA 94720.

2.2 Initial operation and performance of SNO

K. M. Heeger and the SNO collaboration

Using heavy water as a target, the Sudbury Neutrino Observatory (SNO) has the unique capability to measure both the flux of electron neutrinos as well as the flux of other neutrino flavors. In the first phase of the experiment SNO will run with pure D_2O and make a measurement of the charged-current interaction of neutrinos with deuterium.

SNO is on-line and taking data. Since November of last year SNO has been taking production data while calibrating the detector and measuring background rates at the same time. The electronics and data acquisition are operating smoothly, with typical trigger rates of about 15-20 Hz. The hardware trigger threshold is set to roughly 2 MeV which corresponds to 18 PMTs above pedestal threshold. Currently the average channel threshold is about 0.25 photoelectrons. More than 98.5% of all 9598 PMT channels are fully working. The PMT death rate from all causes is currently 0.5% per year.

In late 1998 serious problems were observed associated with breakdown in the HV connectors leading into the PMT tube bases. This problem was significantly reduced by regassing the light water that surrounds the PMTs with nitrogen. Since then the detector has operated with minimal problems from high voltage breakdown or tube loss. Flashers, which are light-emitting breakdowns inside the PMT, are a potential background to neutrino data. They occur at a rate of about 1/minute and are mostly correlated with seismic events. The signature of these events has been well characterized so that these events can be removed during data cleaning.

A number of calibrations have been performed in SNO to measure the optical response of the detector, its energy resolution, and background rates. The optical calibration, performed using a laser source and a diffuser ball suspended in the D_2O, shows that the timing resolution of the phototubes is near the expected design goal of 1.7 ns. The attenuation length of the heavy water is measured to be greater than 100 m at 550 nm. A triggered ^{16}N source which produces a 6.1 MeV γ-ray is used for the energy calibration near the analysis threshold. The ^{16}N calibration data is in good agreement with the Monte Carlo prediction of roughly 8-9 hits/MeV, electron equivalent.

The analysis threshold for neutrino data is determined by the backgrounds in SNO. Water assays indicate that background levels in the H_2O and D_2O are near the design goals. With full D_2O recirculation ongoing the water cleanliness continues to improve.

	Current in H_2O	*Target in H_2O*	*Current in D_2O*	*Target in D_2O*
Uranium	5.0x10^{-15} g/g	4.5x10^{-13} g/g	1.0x10^{-14} g/g	4.5x10^{-14} g/g
Thorium	1.0x10^{-13} g/g	3.7x10^{-14} g/g	$\leq$ 4.0x10^{-15} g/g	$\leq$ 3.7x10^{-15} g/g
Radon	1.0x10^{-13} g/g	4.5x10^{-13} g/g	1.0x10^{-14} g/g	4.5x10^{-14} g/g

During the initial phase of data taking the SNO detector has performed very well. New calibrations sources, such as U and Th sources, and a ^{8}Li source will come on-line in the next few months to measure the characteristics of principal backgrounds and understand better the detector's energy response. SNO is expected to report its first results later this year.

2.3 Data acquisition in SNO

C. A. Duba, A. A. Hamian, P. Harvey,* M. A. Howe, J. Roberts,† P. M. Thornewell‡ and J. F. Wilkerson

The Sudbury Neutrino Observatory data acquisition (SNO DAQ) system is designed to provide continuous readout of the detector's 9547 photomultiplier tubes (PMTs) with a minimum of dead time. It is made up of four main parts: system initialization and control, hardware readout, event building/recording, and monitoring. Since the SNO DAQ system has been described extensively in past Annual Reports,[1] only a brief overview with the most recent updates is provided here.

The main system interface is the SNO Hardware Acquisition Real-time Control program (SHaRC). A major enhancement to SHaRC was the introduction of a number of pre-defined standard run types, which allow the operator to set up the detector with a single click. New monitoring capabilities were added, including the ability to monitor the battery backup system and safely shut down the detector in the event of a sustained power outage. In addition, SHaRC now maintains and updates a private web page every 15 minutes so that the DAQ group can remotely monitor critical system parameters and system behavior. Two serious bugs, which were causing SHaRC to crash, were discovered and fixed. One was an ftp transfer problem that was causing random crashes during the transfer of log files and the other was a problem writing the log files to disk. With these fixes, SHaRC crashes have been practically eliminated.

Hardware readout is provided through a MVME167 68040 embedded processor running tightly optimized code that places the data into dual port memory for event building. There have been no significant changes to the event readout software in the last year. It has proven to be remarkably robust and trouble-free for the last two years.

The event building and recording software, which runs on a SUN Ultra Sparc 1 workstation, was recently combined into a single program. The new version is simpler for operators as it eliminates the need to run a separate recording program. It is easier to maintain, uses 30 MB less memory, and has more potential for speed optimization. The data throughput rates of the new builder are the same or slightly better than the old builder, with sustained rates of up to 400 kB/s demonstrated. The new builder fixes a number of record/data header ordering problems and ensures that all dispatched records are in the proper sequence in the final ZDAB files. In addition, audible warnings have been added to alert the operators to critical error situations.

Most data monitoring is provided by XSNOED, which can display either the near real time dispatched data stream or offline ZDAB files, and also by SNOSTREAM, which displays running summary plots of detector performance.

The DAQ group maintained an almost continuous onsite presence in 1999, and will continue to provide full offsite support in the upcoming year. With the exception of the new builder/recorder program, there have been only minimal changes to the SNO DAQ software since the start of production running in November 1999. The system has been performing reliably, and there are no major upgrades foreseen in the coming year.

*Queens's University, Kingston, Ontario, Canada.

†Sudbury Neutrino Observatory, Sudbury, Ontario, Canada.

‡F5 Networks Inc., Seattle, WA.

[1] Nuclear Physics Laboratory Annual Report, University of Washington 1997 p.20-23, 1998 p.18-20, 1999 p.16-18.

2.4 Data analysis in the first phase of SNO operation

Q. R. Ahmad, C. A. Duba, A. A. Hamian, R. Hazama, K. M. Heeger, J. Orrell, R. G. H. Robertson, T. D. Steiger and J. F. Wilkerson

SNO production running began on November 2, 1999. Since the data acquisition system is complete and the NCD array is nearly complete, many members of the University of Washington SNO group have turned their focus towards analysis of the phototube data. This analysis is underway on a number of fronts, including work on support analyses which will be used by the entire collaboration, work on a complete solar neutrino analysis in close collaboration with a subset of SNO scientists, and special-interest projects undertaken by individual graduate students.

A crucial first step in the SNO analysis is the data cleaning process, which is designed to remove as much of the non-physics events from the data as possible, leaving a data sample with a vastly improved physics to non-physics event ratio. Identifying physics events like neutrino and muon interactions from this reduced data set will be a significantly easier task than starting with all of the original data. Each of the more than twenty data cleaning cuts has been, or is currently being, studied and characterized in terms of how many physics and non-physics events it flags. Two of these cuts are being studied at UW. One is a cut which flags events with a high charge sum, but with few PMTs hit. The second cut flags "orphans", PMT data bundles which have not been successfully built into a complete event. Once all of the cuts have been fully characterized, the next step will be to identify an optimal set of these cuts which maximizes the non-physics event removal while minimizing the number of "good" events which are rejected.

There are two other main areas of support analysis in which UW has been involved; both are considered "detector support" analyses whose results feed directly back into improving the detector performance on an ongoing basis. One is the study of time-variation of the electronics pedestals. These pedestals are measured on a weekly basis, and keeping track of their stability over time is a good way of identifying problem electronics channels. The second area of detector support analysis is summarizing the detector livetime, both the total time (including calibration and maintenance runs), and the neutrino mode livetime. These results are provided to the collaboration on a weekly basis, and are being used as an aid to help maximize the neutrino mode livetime. Fig. 2.4-1 shows the total SNO livetime from the start of production running until March 14, 2000.

The UW solar neutrino analysis is being performed in conjunction with collaborators from several other SNO institutions, and is progressing rapidly on all fronts. A recent area of focus for UW has been in producing a candidate sample of solar neutrinos. This has included formulating and implementing a run selection scheme, as well as hand-scanning events which survived a series of non-physics removal cuts. The UW group has also taken on responsibilities in fitter studies for vertex reconstruction, and detector acceptance studies.

Muons interacting in the SNO detector are a special interest of a senior UW graduate student (Q.R. Ahmad), and will form the basis of his Ph.D. thesis. In particular, the use of detected neutrons from spallation interactions of muons in the detector as an additional energy calibration is being pursued. In addition, the possibility of using muon events themselves as a way of performing or checking the optical calibration is being investigated.

With the SNO detector running smoothly in production mode, the coming year promises to be a time of significant progress in terms of analysis. The UW group has already made important contributions both to support analyses and towards obtaining solar neutrino results, and expects to be fully integrated in these efforts in the future.

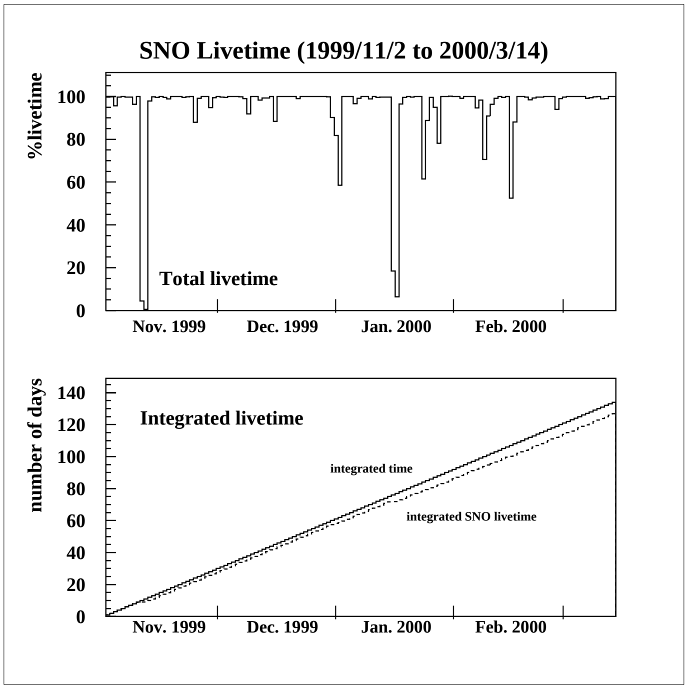

Figure 2.4-1. Top figure: fraction of SNO livetime versus days since start of production running. Bottom figure: integrated SNO livetime since start of production running.

2.5 The neutral current detector project at SNO

J. F. Amsbaugh, M. C. Browne,* T. V. Bullard, T. H. Burritt, P. J. Doe, C. A. Duba, S. R. Elliott, R. M. Fardon, J. E. Franklin, R. Hazama, G. C Harper, K. M. Heeger, A. W. Myers, R. G. H. Robertson, K. K. Schaffer, M. W. E. Smith, T. D. Steiger, T. D. Van Wechel, S. L. Veatch and J. F. Wilkerson

SNO is unique for its neutral current detection capability, with all neutrino flavors interacting with deuterium to produce free neutrons. These neutrons are readily detected, thus measuring the total active neutrino flux from the sun, independent of neutrino oscillations. One technique for neutron detection is to insert an array of ^{3}He proportional counters into SNO. These Neutral Current Detector (NCDs) observe neutrons via the following capture reaction:

$$\mathrm{n} + {}^3\mathrm{He} \rightarrow \mathrm{p} + {}^3\mathrm{H} + 764 \text{ keV}$$

The charged proton and triton ionize the gas, depositing their combined 764 keV of kinetic energy to produce a detectable signal.

The NCDs are made from chemical vapor deposition (CVD) of Ni onto a mandrel to form tubing and endcap components. The CVD process results in ultra low U and Th contamination (1-2 ppt Th). Quartz tubing forms the high voltage and signal feedthrough to a Cu anode wire. The ultra low radioactivity of all components is required to minimize backgrounds from d(γ,n)p reactions in the heavy water and also from alpha tracks in the NCDs which can mimic neutrons.

The array is designed to contain 300 detectors, construction of which is nearing completion. Following is the status as of 3/17/00.

NCDs being stored underground at SNO:	226	=	75%
Built or partially built (at UW):	51	=	17%
Still needing construction:	23	=	8%

The endcaps were previously being built in conjunction with IJ Research in Santa Ana, California. By mutual agreement, the contract with this company was terminated and remaining work was moved to UW. Endcap production has now been successfully implemented at UW for the past 6 months using the RF sputtering machine in the department of physics. The remaining 46 endcaps needed to build the array should be completed in the next few weeks. We are awaiting shipment of the final Ni tubes from CVD Manufacturing, Ontario.

NCDs are stored underground prior to their deployment in SNO. The purpose is to allow the cosmogenic ^{56}Co to decay away with its 79 day half life. This period is also providing an opportunity to measure the intrinsic U and Th levels in the walls of the NCDs. The NCDs are expected to be installed into SNO within the next one to two years.

*Los Alamos National Laboratory, Los Alamos, NM 87545.

2.6 The data path for the SNO neutral current detectors

M. C. Browne* C. A. Duba, A. W. Myers, R. G. H. Robertson, T. D. Van Wechel and J. F. Wilkerson

The data path of the SNO NCD system is in its final stages of refinement. The computer data acquisition system will continuously acquire data from two paths, VME and GPIB. The fast signal path is activated by all signals above a low trigger threshold (ADC threshold). The NCD shaper board then integrates the pulse through a shaper and converts it to a digital value. All of the fast signal path information flows through VME and PCI bus. The slower path digitizes signals with a higher threshold, but below that of the lowest expected neutron pulse. The slower path also incorporates GPIB protocol in addition to VME and PCI to carry its digitized pulse information.

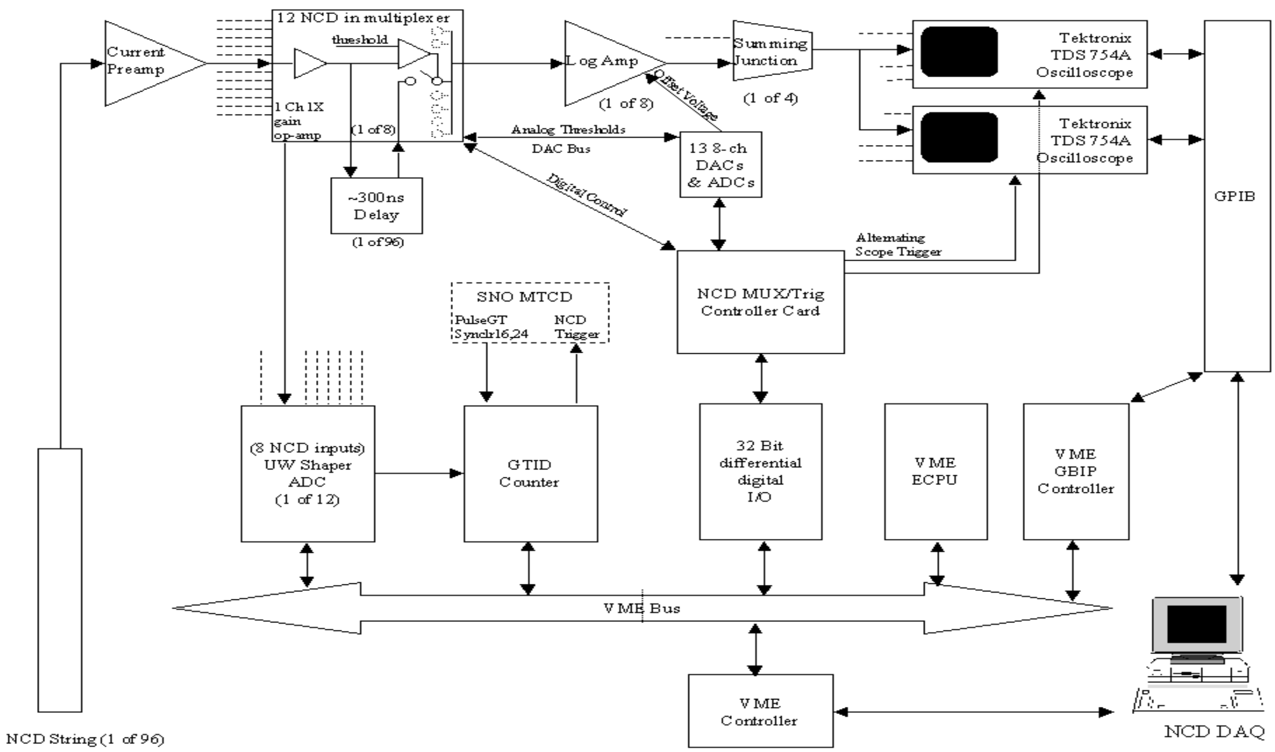

Figure 2.6-1. The path of data through the NCD electronics.

The fast signal path converts each integrated pulse above the low level ADC threshold into an eleven bit digital signal in the shaper boards. The NCD shaper boards are run from a linear VME crate, which itself is controlled by an SBS 618 controller. The 618 communicates to the data acquisition computer through a pair of optical fibers, which significantly reduces the signal-induced noise over electrical controllers.

When the system is complete, the triggering of the shaper board will send a signal to increment the SNO Master Trigger Card, which will assign a 'GTID' to the event, and return a signal to the NCD GTID counter. The NCD GTID counter will also relay the GTID information to the NCD data acquisition through the VME bus. If no additional digitization data arrives, the computer

*Los Alamos National Laboratory, Los Alamos, NM 87545.

places its data into the main SNO data stream through the builder, and sends a copy into the NCD independent data stream.

The slow signal path carries more exacting information about the pulse seen by one of the proportional counter strings. The digitization is triggered by the higher-level digitization threshold within each multiplexer. The multiplexer then sends a signal to the NCD Trigger Controller Card (NCD TCC), which determines the appropriate scope for digitization (see Sec. 7.5).

The data acquisition computer communicates with the controller card through a 32 bit VME I/O module riding on the VME bus. The controller card is able to set the digitization thresholds, offset voltages, and read back the analog thresholds through 13 custom DAC boards. The controller card also relays to the NCD DAQ computer information about possible multiple hits during signal digitization.

The digitized pulse gets to the NCD DAQ computer through GPIB, and the computer immediately sends off copies of the pulse. First, the pulse splits off to the main SNO data stream, with the appropriate GTID number assigned to it. Second, another copy of the pulse runs through LANL's Analyst program, which will compile pertinent characterization numbers. Finally, the raw NCD data stream sends a record of the data down the NCD independent data stream, where it will be saved for cases in which the main SNO data stream might be inactive or unavailable.

2.7 In situ determination of backgrounds from neutral current detectors in the Sudbury Neutrino Observatory: CHIME

J. F. Amsbaugh, P. J. Doe, S. R. Elliott, G. C. Harper, K. M. Heeger, G. Miller,*
A. W. P. Poon† and R. G. H. Robertson

The use of ultra-low background ^{3}He proportional counters as neutron detectors in the SNO detector will provide a means of measuring the neutral-current interaction rate of solar neutrinos. Since the binding energy of the deuteron is only 2.2 MeV, gamma rays from natural decay chains in the proportional counters photodisintegrate the deuteron and thus simulate the neutral current signal. This poses stringent limits on the radiopurity requirements for the counters. An *in-situ* measurement of the background from seven neutral current detectors will determine the activity of ^{232}Th in the neutral current detectors and thus determine an upper limit on the photodisintegration background generated by the radioactivity in the NCD array.

The Neutral Current Detector (NCD) array (see Sec. 2.5) consists of 775 m of ^{3}He proportional counters arranged in 96 strings with 300 counters. The counter bodies are made of about 450 kg of ultra-pure chemical-vapor deposited nickel which contains natural Uranium and Thorium in equilibrium. The photodisintegration gammas are produced in the decays of the ^{232}Th (^{208}Tl $\rightarrow$ ^{208}Pb, E_γ=2.615 MeV) and ^{238}U (^{214}Bi $\rightarrow$ ^{214}Po, E_γ=2.445 MeV) chains and in the decay of the relatively long-lived ^{56}Co (^{56}Co $\rightarrow$ ^{56}Fe, E_γ >2.224 MeV).

A Construction Hardware In Situ Monitoring Experiment (CHIME) has been designed to measure the NCD originated background in the presence of the D_2O contribution prior to the deployment of the entire NCD array. It is an *in-situ* measurement of the construction materials used in the NCD array. Seven individual counters arranged in a close-packed configuration with a total mass of about 5000 g and an overall length of 112 cm will be deployed as a background test source in the SNO detector. The construction materials and procedures for the CHIME counters are essentially identical to those in the real NCD array.

To assure its cleanliness before deployment the CHIME unit was checked for leachable radon. The table below lists the experimental results expressed as microgram equivalents of ^{232}Th and ^{238}U. The poor tracer recovery associated with the CHIME sample is due to physical loss of the sample in processing.

Sample	^{232}Th (^{212}Po)	^{238}U (^{214}Po)	^{238}U (^{226}Ra)	*tracer recovery*
Background	$\leq$ 0.057	$\leq$ 0.0044	$\leq$ 0.0032	82.5%
CHIME	$\leq$ 0.26	$\leq$ 0.035	$\leq$ 0.037	8.1%

The CHIME has been stored underground since December 20, 1998 in order to allow the cosmogenically produced ^{56}Co to decay. The deployment of CHIME is expected to be similar to that of a standard calibration source and will have minimum impact on the SNO operating schedule. The CHIME is negative buoyant and can be deployed along the central axis of SNO using a specially designed deployment mechanism. We plan to perform the CHIME background test experiment later this year.

*Los Alamos National Laboratory, Los Alamos, NM 87545.
†Lawrence Berkeley National Laboratory, Berkeley, CA 94720.

2.8 Deployment of neutral current detectors in the SNO

J. F. Amsbaugh, M. Anaya,* P. J. Doe, G. C. Harper, M. W. E. Smith, W. A. Teasdale* and J. Wouters*

The deployment of the neutral current detectors (NCDs) into the heavy water acrylic vessel of the Sudbury Neutrino Detector (SNO) requires specialized equipment and carefully designed procedures. Care must be exercised to prevent damage to and contamination of the acrylic vessel and heavy water. Each NCD counter is 2–3 meters in length and is stored underground at SNO after manufacture. To minimize SNO down time, the predeployment welding will join counters into segments just small enough for deployment in the deck clean room over the vessel. At deployment, the segments are inserted into the vessel and welded together over the neck. The completed NCD string is lowered to the bottom where a remotely operated vehicle (ROV) can take it to the correct attachment point. Finally, the cable is manipulated and connected to the electronics feedthroughs.

We have been testing the deployment equipment,[1] which replaces the calibration glove box, and developing the procedures at both the UW and a 20 ft deep pool at Los Alamos National Laboratory (LANL) (see Fig. 2.8-1). The global view camera pole and boathook, which manipulate the NCD cables at the bottom of the vessel neck, were assembled over a 39 ft deep tank at UW. The boathook's float provides neutral buoyancy in heavy water and its position counteracts torque when the pole is not vertical. The two worked very well together.

Two sessions of development and testing were done at the LANL pool with what final equipment was finished and prototypes for the rest, except the laser welding fixture. This culminated with a NCD deployment design and plan review on 18-Jun-1999 at LANL. A review panel, two members from the SNO collaboration and two members from outside SNO, were to find things overlooked, comment on the design and procedures developed, paying particular attention to cleanliness and failure mode recovery. Several observers also attended the review which included presentations, a tour of the equipment installed at the pool, and a demonstration deployment of one NCD string with the ROV. Participants got hands-on experience the next day if they so desired. The review in general was positive and several suggestions were made.

A summary of the remaining work includes implementing suggestions and improvements learned from the tests with prototypes. The laser welding fixture and a revised NCD lowering mechanism are designed and are being made. The following have had their design thought out but need to be detailed and finalized, after which they will be made as shop time is available: a lifting device to help remove the glove box, lower the ROV into the acrylic vessel, and place the deployment plate; a neck view camera system; revised glove mountings; a predeployment welding station, using the new welding fixture; and various devices to aid in handling, tilting, and inserting the long NCD segments.

The expected welding equipment completion should enable weld team training to occur in time for predeployment welding to begin in late summer, assuming NCD counter production has finished. Before and during this welding, final NCD deployment procedures can be developed and reviewed, followed by training the deployment teams. Thus the earliest the NCD deployment could begin is 3–6 months after the underground predeployment welding has started.

---

*Los Alamos National Laboratory, Los Alamos, NM 87545.

[1]Nuclear Physics Laboratory Annual Report, University of Washington (1999) p. 22.

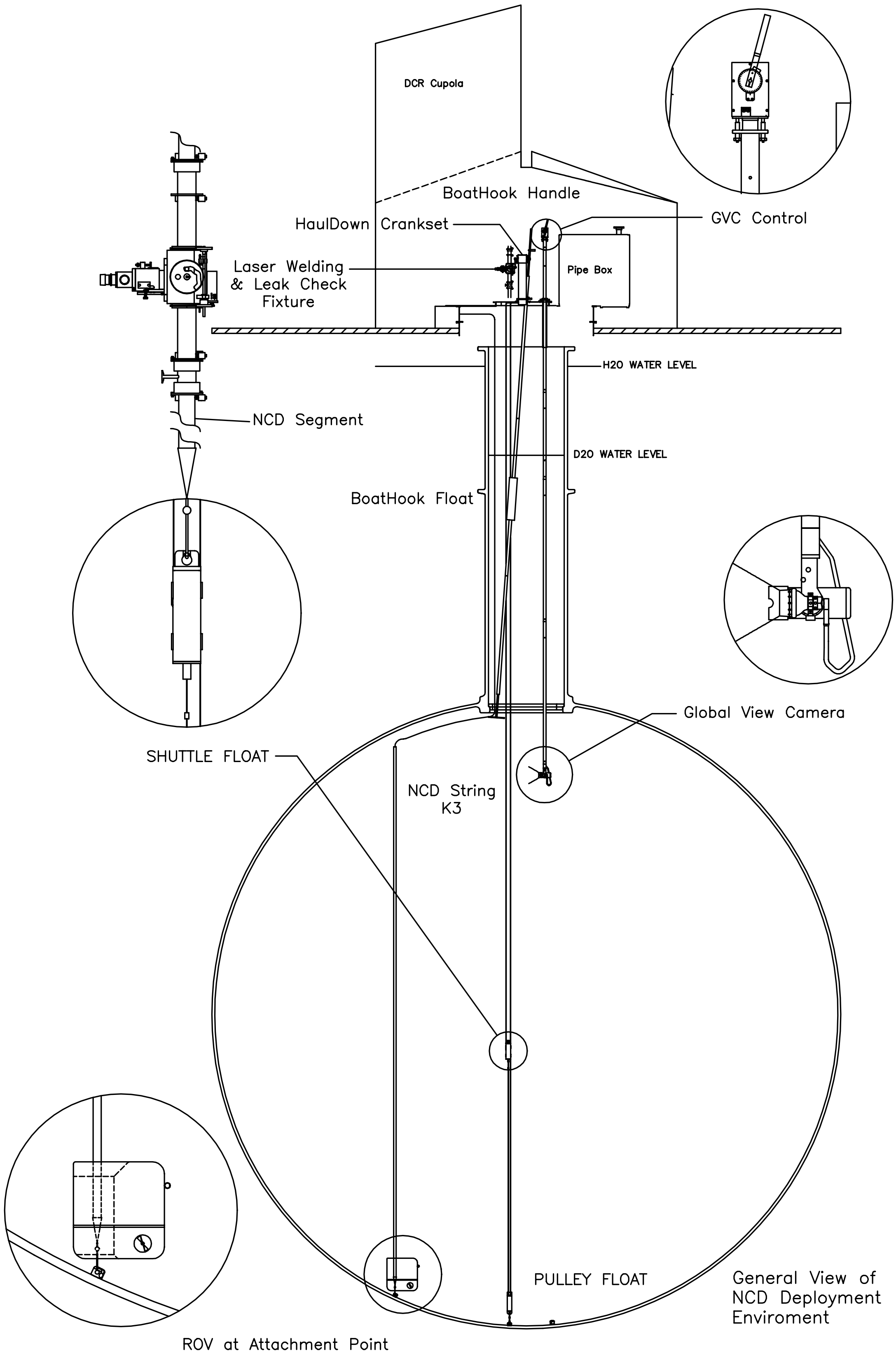

Figure 2.8-1. The NCD deployment equipment.

2.9 SAGE: The Russian American Gallium Experiment

S. R. Elliott and J. F. Wilkerson

The Russian-American Gallium Experiment (SAGE) is a radiochemical solar neutrino flux measurement based on the inverse beta decay reaction, ^{71}Ga(ν,e$^-$)^{71}Ge. The threshold for this reaction is 233 keV which permits sensitivity to the p-p neutrinos which comprise the dominant contribution of the solar neutrino flux. The target for the reaction is in the form of 55 tonnes of liquid gallium metal stored deep underground at the Baksan Neutrino Observatory in the Caucuses Mountains in Russia. About once a month, the neutrino induced Ge is extracted from the Ga. ^{71}Ge is unstable with respect to electron capture ($t_{1/2} = 11.43$ days) and, therefore, the amount of extracted Ge can be determined from its activity as measured in small proportional counters. The experiment has measured the solar neutrino flux extractions between January 1990 and December 1997 with the result; $67.2^{+7.2,+3.5}_{-7.0,-3.0}$ SNU which has been published.[1] (The former set of uncertainties are statistical and the later set are systematic.) This is well below the standard solar model expectation of 138 SNU. Fig 2.9-1 shows a plot of the extraction data. Data now exists through the end of 1999 and it is being prepared for publication.

The collaboration has used a 517-kCi ^{51}Cr neutrino source to test the experimental operation. The energy of these neutrinos is similar to the solar ^{7}Be neutrinos and thus makes an ideal check on the experimental procedure. We have published this result in 1996. The result,[2] expressed in terms of a ratio of the measured production rate to the expected production rate, is 0.95 ± 0.11. This indicates that the discrepancy between the solar model predictions and the SAGE flux measurement cannot be an experimental artifact.

We expect to receive DOE funding for FY00 that will directly support SAGE. A CRDF proposal has been submitted and is in the review process.

SAGE is a mature experiment whose operation has become routine. The University of Washington plays a role in the analysis of the data. This past year we assisted in the design and construction of new proportional counters for the experiment. With the publication of the archive papers, the focus is now on the long term measurement of the solar neutrino flux to reduce the statistical uncertainty to a level comparable to the systematic uncertainty.

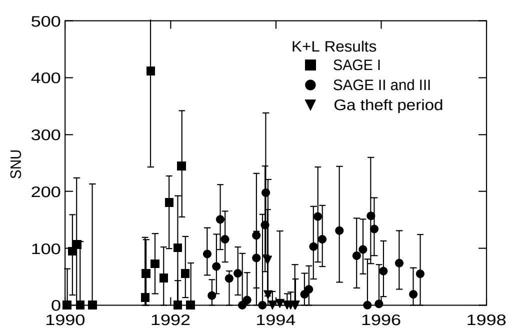

Figure 2.9-1. The individual measurements of the solar neutrino production rate. The uncertainties are statistical only.

[1]J.N. Abdurashitov *et al.*, Phys. Rev. C **56**, 055801 (1999).
[2]J.N. Abdurashitov *et al.*, Phys. Rev. Lett. **77**, 4708 (1996).

2.10 Neutrino detection using lead perchlorate

P. J. Doe, S. R. Elliott, C. Paul,* R. G. H. Robertson and J. F. Wilkerson

Due to its large cross section and relative cheapness, lead is an attractive neutrino detection medium. Both charged and neutral current reactions are available to distinguish electron neutrinos from other neutrino flavors.

$$\begin{aligned} \nu_e +^{208} Pb \;&\Rightarrow\; ^{208}Bi^* + e^- \\ &\quad\;\Downarrow \\ &\quad\; ^{207}Bi + x\gamma + n \\[1em] \nu_x +^{208} Pb \;&\Rightarrow\; ^{208}Pb^* + \nu_x^{'} \\ &\quad\;\Downarrow \\ &\quad\; ^{208-y}Pb + x\gamma + yn. \end{aligned}$$

Unfortunately, detector schemes utilizing lead tend to be complicated and do not lend themselves to the massive scales required for neutrino studies.

One of us (S.R.E.) noted that Lead Perchlorate ($Pb(ClO_4)_2$) is highly soluble in water; 500g of $Pb(ClO_4)_2$ can be dissolved in 100g H_2O with a resultant density of 2.7 g/cc. This solution appears quite transparent to the eye and raises the question as to whether one could realize massive Pb detectors using the water Čerenkov technique. The presence of ^{35}Cl enables the free neutron to be detected with high efficiency by means of the 8.4 MeV capture gamma rays. This is the same technique employed by the SNO detector. Finally, at a cost of $10k/tonne in 100 tonne quantities, detectors on the order of kilo-tonnes are conceivable.

There are a number of physics possibilities with such a detector. Using Pb as a target would make a powerful supernova detector. The average energies of neutrinos emitted by a supernova are expected to follow a hierarchy: $E_{\nu_e} < E_{\bar{\nu}_e} < E_{\nu_{\mu,\tau}}$ The observation of high energy ν_e would be an indication of oscillations to μ, τ flavors.

The large cross section and delayed coincidence ν_e signature of Pb could provide a high statistics oscillation experiment at a beam stop where a short duration beam spill allows the temporal separation of any monoenergetic ν_e which result from ν_μ oscillation. The hydrogen content of $Pb(ClO_4)_2$ solution also makes the detector sensitive to $\bar{\nu}_\mu \rightarrow \bar{\nu}_e$ oscillations. Measuring the cross section for neutrino interactions in Pb is also of importance to supernova modelers investigating the explosion mechanism and transmutation of nuclei.

To determine if a $Pb(ClO_4)_2$ Čerenkov detector can be built we have investigated the optical properties of the solution. The spectral transmission is given in Fig 2.10-1. This is very encouraging since there are no obvious absorption lines. We constructed a special apparatus in order to measure

*Presently at Ratheon, Redondo Beach, CA.

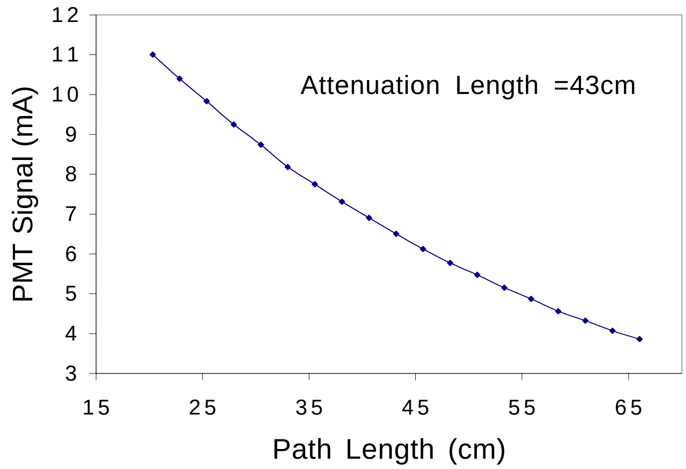

Figure 2.10-1. Spectral transmission of light though a 1 cm long cell containing an 80% solution of $Pb(ClO_4)_2$. The transmission is referenced to deionized water.

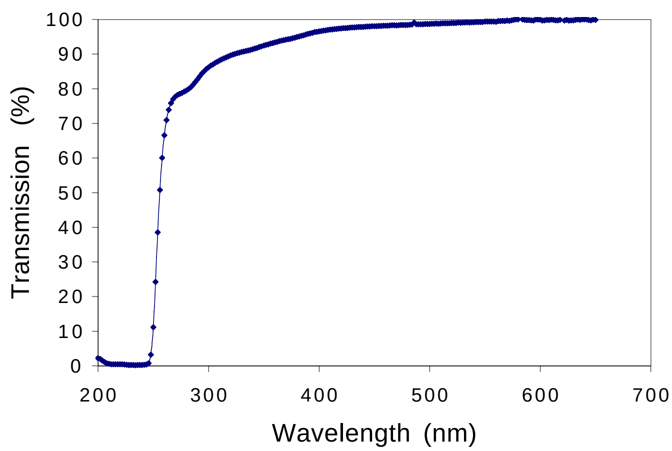

Figure 2.10-2. Attenuation of 430 nm light passing through an 80% solution of $Pb(ClO_4)_2$.

the attenuation of light. The results are given in Fig 2.10-2. An attenuation length of $\approx$0.5m is not sufficient to build a large Čerenkov detector. Diluting the solution only further reduced the attenuation length. This suggests that the loss of light is due to scattering, perhaps due to the formation of Pb salts or polymeric molecules such as $Pb_4(OH)_4$, possibly as a result of reactions with dissolved O_2 and CO_2. We are not aware of any physical reason why large attenuation lengths are not achievable in $Pb(ClO_4)_2$, (as they are in salt water), therefore we plan to determine what steps are necessary to achieve this.

2.11 Spectroscopy of double-beta and inverse-beta decays from ^{100}Mo for neutrinos

H. Ejiri, J. Engel,* R. Hazama, P. Krastev,† N. Kudomi‡ and R. G. H. Robertson

Spectroscopic studies of two β-rays from ^{100}Mo are shown to be of potential interest for investigating both the Majorana ν mass by neutrinoless double β-decay($0\nu\beta\beta$) and low energy solar ν's by inverse β-decay with a multi-ton ^{100}Mo detector. The unique features of the present approach with ^{100}Mo are as follows.

1) The β_1 and β_2 with the large energy sum of $E_1 + E_2$ are measured in coincidence for the $0\nu\beta\beta$ studies, while the inverse β-decay induced by the solar ν and the successive β-decay are measured sequentially in an adequate time window (about 30 s) for the low energy solar-ν studies. The isotope ^{100}Mo is just the one that satisfies the conditions for the $\beta\beta$-ν and solar-ν studies, as shown in Fig. 2.11-1.

2) The large Q value of $Q_{\beta\beta}$=3.034 MeV gives a large phase-space factor $G^{0\nu}$ to enhance the $0\nu\beta\beta$ rate and a large energy sum of $E_1 + E_2 = Q_{\beta\beta}$ to place the $0\nu\beta\beta$ energy signal well above most background (BG) except ^{208}Tl and ^{214}Bi. The energy and angular correlations for the two β-rays can be used to identify the ν-mass term.

3) The low threshold energy of 0.168 MeV for the solar-ν absorption allows observation of low energy sources such as pp and ^{7}Be. The GT strength to the 1^+ ground state of ^{100}Tc is measured to be large: $(g_A/g_V)^2B(GT)$=0.52±0.06 by both the (^{3}He,t) reaction and electron capture. Then ^{100}Mo is found to have large capture rates even for low energy solar ν's. The solar-ν capture rates are 639 SNU for pp ν, 206 SNU for ^{7}Be ν and 27 SNU for ^{8}B ν. The solar-ν sources are identified by measuring the inverse-β energies. Since only the ^{100}Tc ground state can absorb ^{7}Be ν and pp ν, the ratio of ^{7}Be to pp is independent of the uncertainty($\sim$ 15%) of the $B(GT)$ value.

4) The measurement of two β-rays (charged particles) enables one to localize in space and in time the decay-vertex points for both the $0\nu\beta\beta$ and solar-ν studies. β, γ associated with BG are also measured. The tightly localized event in space and time, together with relevant $\beta\gamma$ measurements, are key points for selecting $0\nu\beta\beta$ and solar-ν signals and for reducing correlated and accidental BG by factors $\sim 10^{-5}$.

5) Possible detectors for the present objective are under study. One realistic possibility is an ensemble of plastic scintillator modules read out by wavelength- shifter fibers to get adequate energy and spatial resolutions.

*Dept. Physics and Astronomy, University of North Carolina, Chapel Hill, NC 27599.
†Dept. Physics, University of Wisconsin, Madison, WI 53706.
‡Research Center for Nuclear Physics, Osaka University, Ibaraki, Osaka 567-0047, Japan.

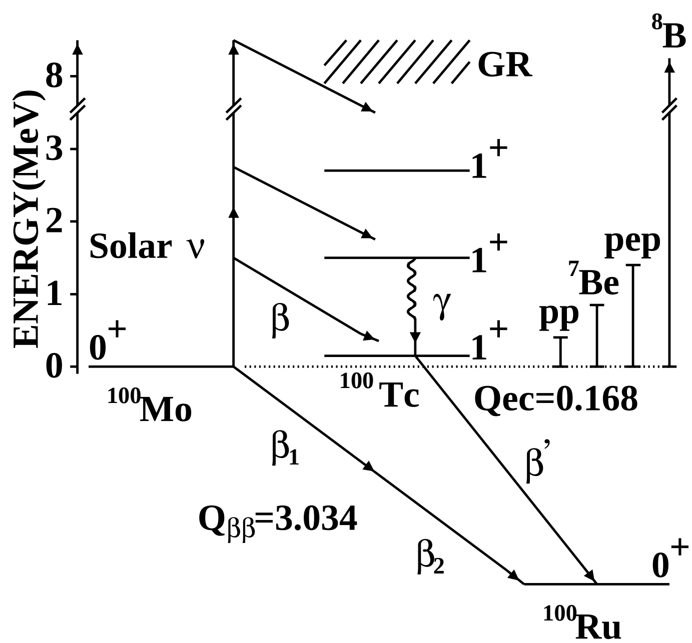

Figure 2.11-1. Level and transition schemes of ^{100}Mo for double beta decays ($\beta_1\beta_2$) and two beta decays ($\beta\beta^{'}$) induced by solar ν.

2.12 Nuclear spin isospin responses for low energy neutrinos

H. Ejiri

Nuclear spin isospin responses for low energy neutrinos of current astroparticle physics interests have been studied. Neutrinos are key particles for new particle physics beyond the standard minimal electro-weak theory, and sensitive probes for studying stellar evolution and astronuclear processes in the sun and stars.

Low energy neutrinos with energies of $E_\nu \simeq 0.1 \sim 50$ MeV have been studied extensively by using nuclei as micro-laboratories for investigating elementary particles and fundamental interactions. Nuclear weak processes involved are vector and axial-vector weak interactions. Accordingly, nuclear isospin and spin-isospin responses for neutrinos are crucial in studying the low energy neutrinos through nuclear weak processes.

Nuclei show spin isospin responses characteristic of nuclear spin isospin structures such as nuclear spin isospin core-polarizations and nuclear spin isospin giant resonances. Nuclear spin isospin responses have recently been investigated by means of hadronic charge-exchange reactions. Nuclear spin isospin responses are investigated also by relevant electromagnetic processes.

Discussions on nuclear spin isospin responses relevant to low energy neutrino studies in nuclei have been made with emphasis on current subjects as follows:

1. Neutrino studies in nuclear micro-laboratories and nuclear responses for neutrinos.
2. Nuclear spin isospin responses, nuclear spin isospin giant resonances, and nuclear medium effects on nuclear spin isospin responses.
3. Nuclear spin isospin responses studied by hadronic charge-exchange spin-flip and non spin-flip reactions.
4. Nuclear spin isospin responses for neutrinos associated with double beta decays.
5. Nuclear spin isospin responses for solar neutrinos studied by nuclear inverse beta decays and nuclear detectors for solar neutrinos.
6. Nuclear spin isospin responses for supernova and accelerator-based neutrinos.

3 Nucleus-Nucleus Reactions

3.1 ^{40}Ca + ^{208}Pb fusion barrier distributions: status report

A. L. Caraley, A. R. Junghans, T. L. McGonagle and R. Vandenbosch

During this past year we began an experiment to measure fission fragment cross sections for ^{40}Ca + ^{208}Pb, at laboratory energies from 195 to 232 MeV, with the goal of determining the distribution of fusion barriers for this system.

The experimental configuration was similar to that used by Bierman *et al.*[1] A silicon surface barrier E-ΔE telescope of $\sim$7 msr was used to detect primary fission fragments. Coincident fragments were detected in a 7-strip silicon detector[2] which was positioned on the opposite side of the beam such that the entire angular distribution of the complementary fragments was subtended. Two additional silicon surface barrier detectors were placed at $\pm$ 30° to monitor the beam energy and quality and to provide for normalization to Rutherford scattering. At the beginning of each period of beamtime the monitor detectors were calibrated in energy using elastically scattered ^{40}Ca, provided by the laboratory's tandem Van de Graaff accelerator. To obtain the beam energies needed for measurement of the experimental excitation function the booster linear accelerator was used in conjunction with the tandem.

Data of sufficient statistics were first collected during a two-week beamtime in December 1999. (Earlier attempts failed due to beam quality/quantity difficulties caused by the damaged low-energy tube in the tandem. See Sec. 8.1 for details.) During the December run, fission data sets were collected at 9 beam energies, of the nearly 25 needed to complete the excitation function. Additional beamtime was scheduled for January 2000 in order to complete the measurement. However, a preliminary determination of the fusion barrier distribution revealed inconsistencies within the December data. A more detailed off-line analysis was conducted. It was determined that an undetected and unexplained failure in the strip detector had resulted in the loss of fragment-fragment coincidence counts. Unfortunately, it was not possible to perform any systematic corrections to the measured data in order to determine a true coincidence yield.

As a result of these difficulties, it was decided that the beamtime scheduled for January 2000 be used to investigate the failure of the strip detector. Tests of the overall strip detector collection efficiency, as well as that of each individual strip, were made under a variety of operating conditions. An evaluation of those tests is still in progress and will comprise much of the Undergraduate Independent Study material of T.L. McGonagle. (Preliminary results are presented in Sec. 7.7.)

[1] J. D. Bierman, P. Chan, J. F. Liang, M. P. Kelly, A. A. Sonzogni, and R. Vandenbosch, Phys. Rev. Lett. **76**, 1587 (1996).

[2] Micron Semiconductor Limited, Lancing, Sussex, England.

3.2 ^{19}F + ^{181}Ta evaporation residue cross sections as a probe of fission dynamics

A. L. Caraley

As reported earlier,[1] fission fragment and evaporation residue cross sections from the ^{19}F + ^{181}Ta system were measured at several beam energies from E_{lab}= 121 to 195 MeV. This experiment was part of a series of experiments conducted to study both the fusion-fission and fusion-evaporation channels of this system. The primary goal of these experiments was to investigate the energy dependence of the statistical model level density parameter using experimental α-particle multiplicities and spectral shapes. This investigation has been completed[2] and the final results prepared for publication.[3]

Our efforts have now turned to a closer examination of the fission and evaporation residue cross section results themselves. In part (a) of Fig. 3.2-1 statistical model calculations using a Monte Carlo version of CASCADE[4,5] (solid line) and JOANNE[6] (dotted line) are compared to our experimental results, as well as to those of Hinde *et al.*[7] (Parameters used: a_n=A/11 MeV^{-1}, a_f/a_n=1.04 and k_f=1.00.) The measured cross sections remain at ∼300 mb from 121 to 195 MeV, while the calculated values decrease by approximately a factor 2 over the same energy range. Of particular interest is the observation that at beam energies above ∼120 MeV the measured residue cross sections are in excess of standard statistical model predictions. This corresponds to a compound nucleus excitation energy threshold for non-statistical fission of approximately 75 MeV. Similar thresholds have been reported for this system, based on measurements of pre-scission neutrons[8,9] and giant-dipole-resonance γ-rays.[10,11] Excess residue cross sections have been observed previously in a few other systems;[12,13,14] analyses of these results have focused on the role of nuclear viscosity in slowing down the fission decay of the compound nuclei formed in these reactions.[13,15,16] A similar analysis of our ^{19}F+^{181}Ta results is described here, although alternative explanations are not ruled out.[17]

As a preliminary examination of the role of fission hindrance in producing the observed excess residue cross sections, a MC CASCADE calculation was performed with the maximum excitation energy allowed for fission set to 80 MeV. The results of this calculation are depicted by the dashed line in Fig. 3.2-1(a) and indicate that some degree of fission hindrance is consistent with our data. The influence of several different aspects of fission hindrance are compared in Fig. 3.2-1(b).

[1] Nuclear Physics Laboratory Annual Report, University of Washington (1998) p.31.
[2] Nuclear Physics Laboratory Annual Report, University of Washington (1999) p.31.
[3] A.L. Caraley, B.P. Henry, J.P. Lestone, R. Vandenbosch, Phys. Rev. C, to be submitted.
[4] F. Pühlhofer, Nucl. Phys **A280**, 267 (1977).
[5] M.G. Herman, U. of Rochester Nuclear Structure Laboratory Report UR-NSRL-318 (1987), unpublished.
[6] J.P. Lestone *et al.*, Nucl. Phys. **A559**, 277 (1993).
[7] D.J. Hinde *et al.*, Nucl. Phys. **A385**, 109 (1982).
[8] J.O. Newton *et al.*, Nucl. Phys. **A483**, 126 (1988).
[9] D.J. Hinde *et al.*, Nucl. Phys. **A452**, 550 (1986).
[10] D. Fabris *et al.*, Phys. Rev. Lett. **73**, 2676 (1994).
[11] R. Butsch *et al.*, Phys. Rev. C **41**, 1530 (1990).
[12] K.-T. Brinkmann *et al.*, Phys. Rev. C **50**, 309 (1994).
[13] B. B. Back *et al.*, Phys. Rev. C **60**, 044602 (1999).
[14] A. L. Caraley, SUNY Stony Brook Ph. D. thesis (1997).
[15] I. Diószegi *et al.*, Phys. Rev. C **61**, 024613 (2000).
[16] D. J. Hofman *et al.*, Phys. Rev. C **51**, 2597 (1995).
[17] J.P. Lestone, Phys. Rev. C **59**, 1540 (1999).

MC CASCADE and JOANNE calculations with fission delay times of 30×10^{-21} s are given by the short-dashed line and dotted line, respectively. (A total fission delay time, τ_{delay}, of $(20–40)\times10^{-21}$ s has been derived[18] from the work of Thoennessen and Bertsch.[19]) The short-long-dashed line represents the results of calculations including both the Kramers factor,[20] with γ=1, and the τ_{delay}=30×10^{-21} s. A calculation with a transient time,[21] τ_{trans}, of 30×10^{-21} s, along with γ=1, is illustrated by the solid line.

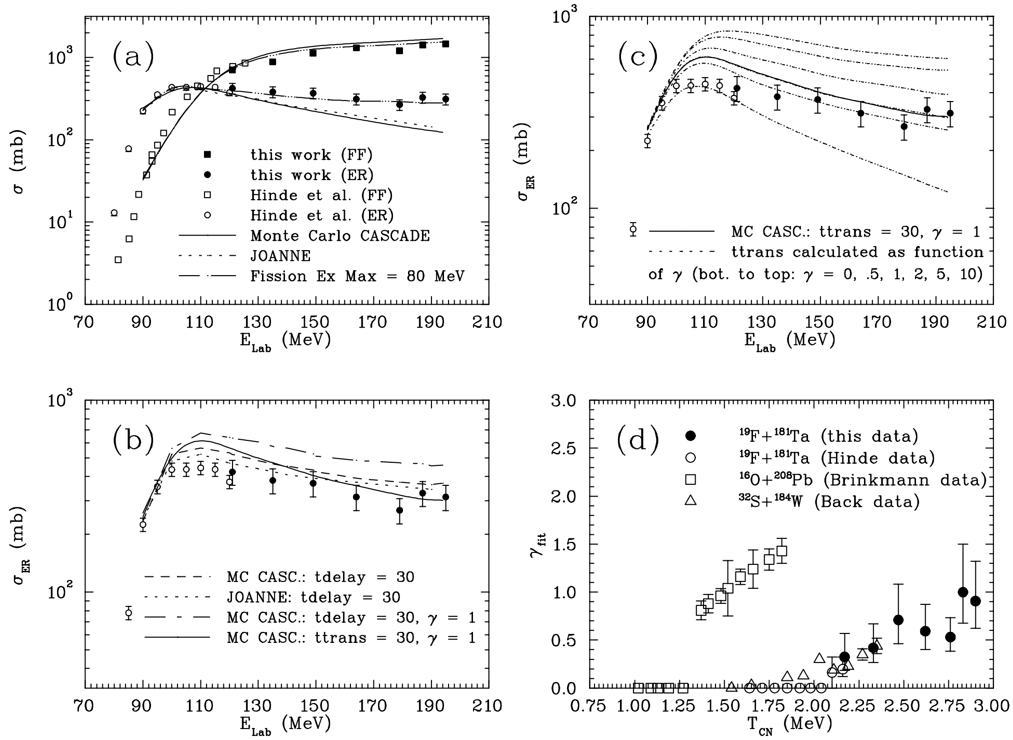

Figure 3.2-1. MC CASCADE and JOANNE calculations using several forms of fission hindrance. Also, results of viscosity-based analyses using an excitation energy independent nuclear dissipation coefficient, γ.

For the full viscosity analysis, dissipation was included in MC CASCADE in an approach similar to that of Butsch *et al.*[22] The fission width was modified by both the Kramers factor[20] and a simplified time-dependent expression.[9] Transient times used in the time-dependent expression were calculated as a function of γ.[21] Elapsed times were determined from time distributions governed by the total decay width, including fission. No other additions/changes to the code were necessary. In our initial analyses, γ was held constant at its input value for all excitation energies in order to allow for direct comparisons with earlier works.[13,16] Evaporation residue excitation functions calculated for γ=0, 0.5, 1, 2, 5 and 10 are shown in Fig. 3.2-1(c). Values of γ needed to reproduce the measured residue cross sections at each laboratory energy, γ_{fit}, were determined through interpolation. The results for γ_{fit} are illustrated in Fig. 3.2-1(d), along with the results of our own similar analyses

[18] R. Vandenbosch, Phys. Rev. C **50**, 2618 (1994).
[19] M. Thoennessen and G.F. Bertsch, Phys. Rev. Lett. **71**, 4303 (1993).
[20] H. A. Kramers, Physics VII, 284 (1940).
[21] K. H. Bhatt, P. Grangé, B. Hiller, Phys. Rev. C **33**, 954 (1986).
[22] R. Butsch *et al.*, Phys. Rev. C **44**, 1515 (1991).

of the $^{16}O+^{208}Pb$ and $^{32}S+^{184}W$ residue cross sections. The present results for γ are comparable, qualitatively, with the work of Back *et al.*[13] and Hofman *et al.*[16] Back *et al.*[13] have suggested that the splitting between the ^{224}Th and ^{216}Th systems is due to shell effects. Our results do not contradict that conclusion.

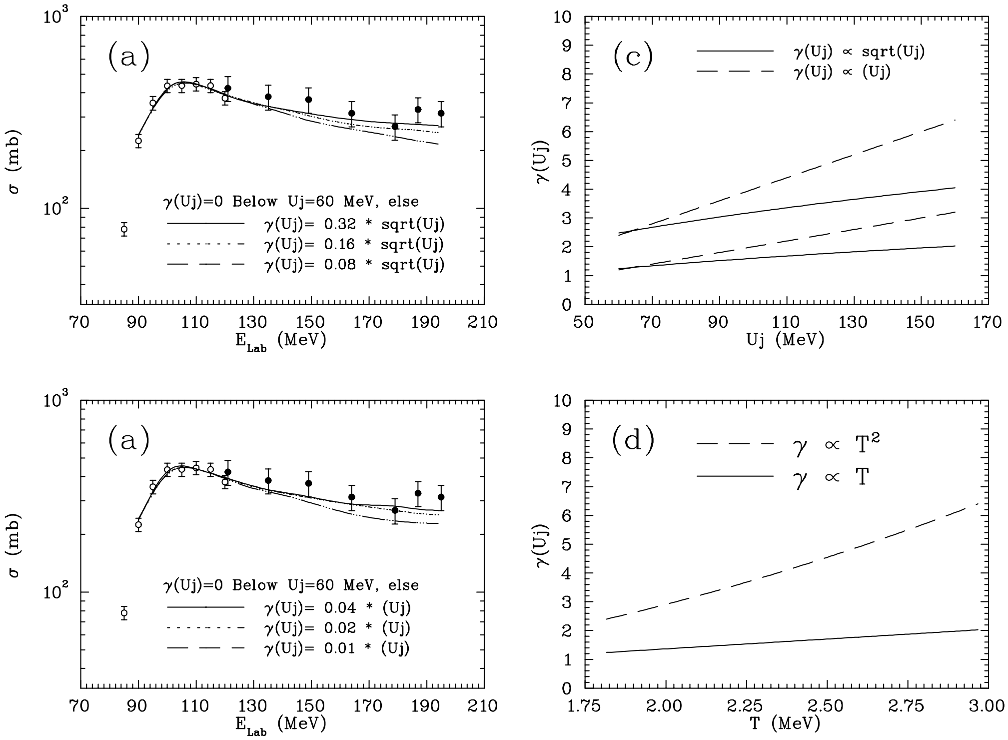

Figure 3.2-2. MC CASCADE calculations, including viscosity, using an excitation energy dependent nuclear dissipation coefficient, γ.

Presently, we are conducting a more rigorous analysis that includes an excitation energy dependence for γ within the calculations. The same statistical model parameters, a_n=A/11 MeV^{-1}, a_f/a_n=1.04 and k_f=1.00, were maintained in order to fit the near-barrier results without viscosity. For simplicity, a threshold for dissipation was estimated at U_j=60 MeV. Dependencies on the square root of U_j and on U_j are both being investigated, to approximate linear and quadratic dependencies on temperature, respectively. Some of our preliminary findings are illustrated in Fig. 3.2-2. The smallest amount of viscosity needed to achieve the maximum hindrance possible, *i.e.:* comparable to turning fission off completely, is depicted by the solid lines in Figs. 3.2-2(a) (T) and Fig. 3.2-2(b) (T^2). (The functional forms of the energy dependencies are noted in the figure legends.) Excitations functions with a 50% reduction in γ still result in reasonable reproductions of the data, qualitatively, and are illustrated by the dotted lines. The calculated cross sections are quite sensitive to further reductions in viscosity, as illustrated by the dashed lines which correspond to 75% reduction.

The upper and lower limits for the resulting energy dependencies for γ, as determined from our measured $^{19}F+^{181}Ta$ evaporation residue cross sections, are depicted in Fig. 3.2-2(c). Fig. 3.2-2(d) illustrates the corresponding limits for the dependence of viscosity on temperature (approximate: A=200, a=A/11 MeV^{-1}) of the emitting system. The lower and upper limits for γ(T) are given by the solid and dashed lines, respectively. The results show γ to be increasing moderately with temperature, consistent with the general expectations of one-body dissipation.[23]

Within the context of fission hindrance, it can be concluded that some dissipation is needed to reproduce our experimental residue cross sections. However, the exact energy dependence of γ is beyond the sensitivity of our results — and dependent also on the choice of statistical model parameters used in the calculations. In addition, although large values of γ are not required to reproduce the residue results, the possibility is not ruled out. The upper limits depicted in Fig. 3.2-2(c) and (d) should be viewed with caution. In the future, a simultaneous fit to the residue cross sections and as well as other observable would determine more precisely any dependence of γ on excitation energy (temperature).

[23] J. Blocki *et al.*, Ann. Phys. **113**, 330 (1978).

4 Nuclear and Particle Astrophysics

4.1 Progress in the ^{7}Be(p,γ)^{8}B measurement

E. G. Adelberger, A. R. Junghans, E. C. Mohrmann, K. A. Snover, T. D. Steiger, H. E. Swanson and TRIUMF Collaborators*

The cross section of the radiative proton capture of ^{7}Be at solar energies is of utmost importance for understanding the flux of high-energy solar neutrinos, which can be detected by large neutrino experiments e.g. SNO and Super-K. Our measurement of the cross section of ^{7}Be(p,γ)^{8}B is based on detecting the α particles following the β-decay of ^{8}B. For a precise determination of the cross section we use a nearly homogeneous proton-beam flux over the whole target area and a precision measurement of the total number of ^{7}Be target atoms. This avoids the large uncertainties associated with an inhomogeneous areal density which enters in a conventional measurement. The target, mounted on one end of a rotating arm, is irradiated in the proton beam and then rotated 180 degrees in front of a Si detector to count the α particles from the ^{8}B decay. During the counting time the integrated beam flux through an aperture of 3mm diameter is measured with a Faraday cup.

We have carried out several test experiments using radioactive ^{7}Be targets between 10 mCi and 27 mCi. The idea is to prove that every stage of the experiment has the required precision to reach our proposed final error limit on the cross section of ± 5%.

We have improved our experimental setup by also integrating the beam current which strikes the target, thus compensating for differences between the beam that strikes the target and the beam that strikes the aperture. To accomplish this, the target arm has been electrically isolated from the chamber. The arm is connected to a precision current integrator (BIC) and is biased to +300 V by means of a battery to reduce secondary electron losses. To eliminate leakage currents, the water cooling for the target arm is operated by an electrically isolated closed-loop chiller (NESLAB) using deionized water with a deionizer in the circuit which is kept under nitrogen atmosphere. The whole cooling apparatus is biased to the same potential as the arm, resulting in essentially zero leakage current. The typical discrepancy between the beam integration on the Faraday cup and on the target arm is smaller than 1%.

Of central importance for the principle of the measurement is the production of a homogeneous beam flux over an area larger than the target area (diameter 3mm). The beam is focused to approximately 1mm diameter on the target and then rastered by magnet coils which are driven by triangular waves of incommensurate frequencies (19.03 Hz in x and 41.00 Hz in y direction). The amplitudes determine the size of the swept area. To test the homogeneity of the beam flux we measure the beam current through apertures of 2mm, 3mm, and 4mm diameter. The ratios of the beam fluxes measured through these apertures should approach unity for swept areas larger than the apertures. With a deuteron beam of 770-keV energy we have demonstrated this homogeneity with a precision of ± 1%, shown in Fig. 4.1-1.

The homogeneity of the beam flux depends on the stability of the beam current delivered by the accelerator. Random fluctuations in the beam current are reduced by averaging over the time

*L. Buchmann, S. Park, J. Vincent and A. Zyuzin, TRIUMF, Vancouver, BC, Canada.

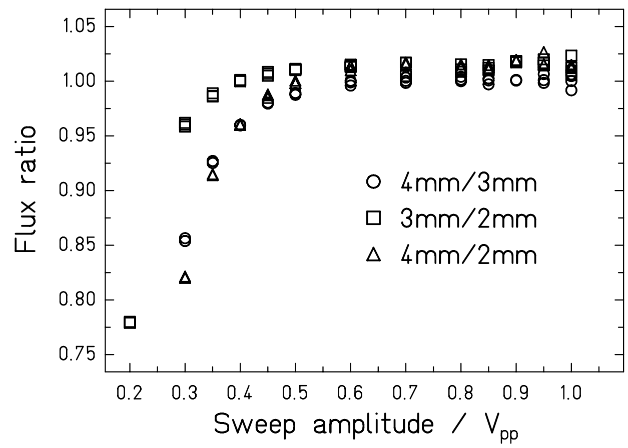

Figure 4.1-1. Ratio of beam fluxes through different size apertures, measured with a deuteron beam (E_d = 770 keV).

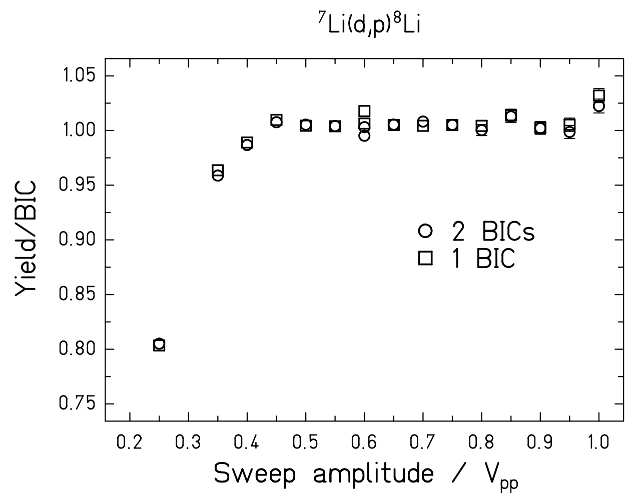

Figure 4.1-2. Yield per integrated beam of the reaction ^{7}Li(d,p)^{8}Li in a ^{7}Be target of 13 mCi. For the data marked 1 BIC the beam flux is measured only with the faraday cup, while for the data marked 2 BIC the beam intensity is measured on target.

of the measurement. It is impractical to run with a completely homogeneous beam flux since this corresponds to very large sweep amplitude and hence very small beam on target. Thus one must have some knowledge of the target uniformity. The necessary information was obtained by measuring the ratio of the reaction yield to the integrated beam passing through the 3mm aperture for the ^{7}Li(d,p)^{8}Li reaction, which was done with the ^{7}Be target in the same manner as the ^{7}Be(p,γ)^{8}B measurement. This ratio should become constant once the beam sweep is large enough to cover both target and aperture. An example of such a measurement is shown in Fig. 4.1-2. The similarity of Fig. 4.1-2 and Fig. 4.1-1 in the plateau region demonstrates that the ^{7}Li (and hence

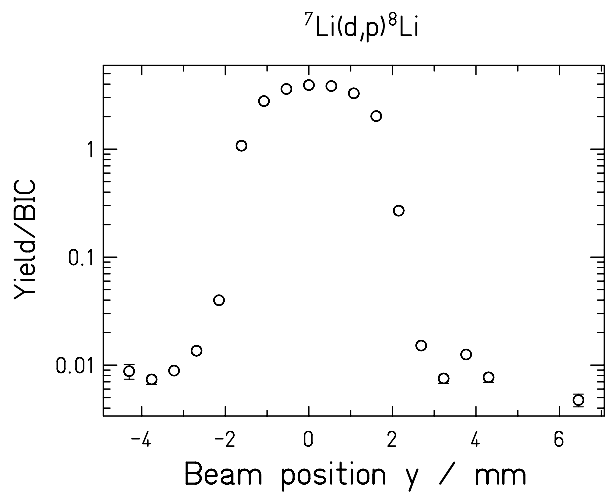

Figure 4.1-3. Scan of a ^{7}Be target (13 mCi) integrated over the y-direction.

presumably also the ^{7}Be) density distribution is reasonably uniform and concentrated in the central 3mm diameter region. In addition, we measure directly a scan of the density distribution. The data shown in Fig. 4.1-3 were obtained by sweeping the beam in the x direction and using the arm rotation to step through the target position in the y direction. These results demonstrate good alignment and localization of the target material. Similar scans with other ^{7}Be targets have shown a problem with ^{7}Be density tails extending to large radius, which is currently being worked on.

The total number of ^{7}Be target atoms has been determined by measuring the absolute activity of the target mounted on the target arm using a precisely aligned, collimated Ge detector. This detector has been calibrated to ± 1% using calibration sources ^{54}Mn, ^{125}Sb, ^{133}Ba, ^{134}Cs, and ^{137}Cs from Isotope Products Corp.

For 400-keV and 500-keV proton energy (c.m.) the α spectrum from ^{7}Be(p,γ)^{8}B has been measured with sufficient statistics to deduce cross sections. The lowest proton energy usable with our present setup of terminal ion source TIS and tandem accelerator is 300 keV. The α spectra show a cutoff due to noise at about 600-700 keV, as shown in Fig. 4.1-4. Noise from the motor controller and other sources has been shielded from the detectors or eliminated at the source. The small fraction of α particles below the cutoff will be determined by comparison of the measured spectra and the theoretical shape.

The absolute energy of the proton beam and its reproducibility have been determined to ± 1 keV by repeated measurements of sharp, well-known resonances in ^{19}F(p,$\alpha\gamma$)^{16}O at E_p = 484 keV and 872 keV, detecting the γ-rays with our large NaI spectrometer.

The energy width of two ^{7}Be targets (13 mCi, 27 mCi) has been measured using a ^{7}Be$(\alpha,\gamma)^{11}$C resonance at E_α =1.378 MeV again using the large NaI spectrometer, as shown in Fig. 4.1-5. The energy width of the resonance was found to be 6 keV and 10 keV respectively. The energy width of a pure ^{7}Be target with the given activity corresponds to about 20 percent of the measured values. This shows a consistent high purity of the metallic ^{7}Be targets.

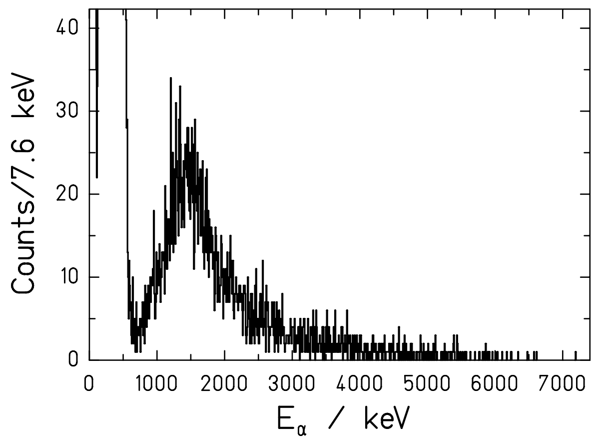

Figure 4.1-4. Measured α-spectrum with a 13mCi ^{7}Be target.

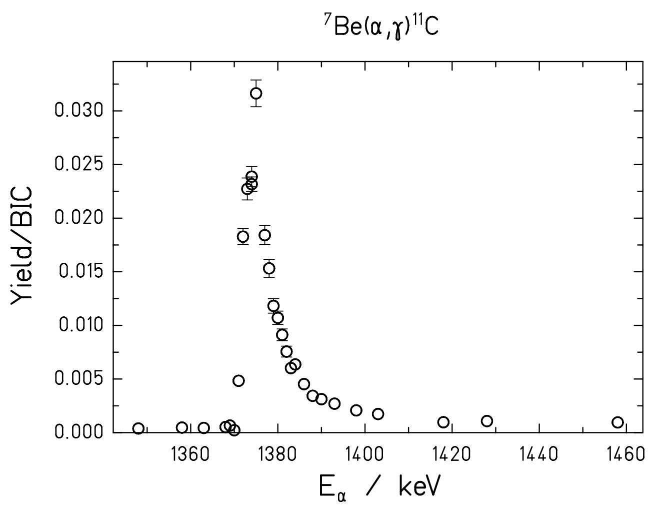

Figure 4.1-5. Measurement of the energy width for a ^{7}Be target (13 mCi).

For the experimental setup we have constructed a more rigid Ti target arm and an optional target mount directly in the line of the beam to measure the amount of backscattered ^{8}B nuclei using a catcher plate mounted on the arm (see Sec. 4.2). When these modifications are in place we will be ready to make the final production runs for the absolute cross section determination.

4.2 Measurement of ^{8}B backscatter for the ^{7}Be(p,γ)^{8}B experiment

E. G. Adelberger, A. R. Junghans, E. C. Mohrmann, K. A. Snover, T. D. Steiger, H. E. Swanson and TRIUMF Collaborators*

The ^{7}Be(p,γ)^{8}B cross section is being measured by bombarding a metallic ^{7}Be target with a proton beam and then moving the target to a counting position and detecting the α particles from the decay of ^{8}B. One important systematic concern in this measurement is the backscatter of ^{8}B atoms from the target during the bombardment phase. Any backscattered ^{8}B atoms will not be counted by the alpha detectors, resulting in a systematic underestimate of the ^{8}B yield.

Calculations with the computer code SRIM show that the effect of backscattering increases as the target thickness goes down, the atomic weight (Z) of the target backing material goes up, or the proton energy goes down. The dependences on the target thickness and Z have been verified in measurements by Weissman *et al.*[1] and Strieder *et al.*[2] for the backscattering of ^{8}Li produced in LiF targets by the ^{7}Li(d,p)^{8}Li reaction. For ^{7}Be targets, which typically have substantial chemical impurities, the backscattering also depends on the Z of the impurities.

Previous ^{7}Be(p,γ)^{8}B measurements have been potentially susceptible to backscatter because they employed high-Z Pt backings and had unknown chemical impurities in their targets.[3,4] However, these experiments did not address the issue of backscatter. A recent measurement (with two data points near $E_p = 1$ MeV) claims immunity from backscatter due to the nature of the implanted target used.[5]

Our experiment is expected to be moderately susceptible to backscatter. Though our Mo target backing has a significantly lower Z than the Pt backings used previously, our targets are thin due to their purity ($\sim$ 20% ^{7}Be) and we are attempting to go to low proton energies. Hence we are undertaking the first ever direct measurement of ^{8}B backscattering. Because the backscattering depends on target composition and thickness, it is important to measure the backscattering for the same target(s) used in the cross section measurement.

The backscatter measurement will be performed in the same chamber as the ^{7}Be(p,γ)^{8}B measurements. In this case, however, the ^{7}Be target will be mounted in a fixed position in place of the Faraday cup, and catcher plates will be mounted on both ends of the flipper arm to transport backscattered ^{8}B atoms to the α-counting position. During bombardment the proton beam will pass through the catcher plate (either through a thin foil or simply a small hole) and strike the fixed target. Both the target and the catcher plate will be electrically isolated to allow for beam integration. A special large-area alpha detector will be used, since the ^{8}B atoms will be spread over a sizeable area on the catcher plate.

The apparatus required for this measurement is currently under construction. It is expected that preliminary tests of the procedure will be conducted before summer '00, with complete ^{7}Be(p,γ)^{8}B and ^{8}B backscatter measurements to follow soon after.

---

*L. Buchmann, S. Park, J. Vincent and A. Zyuzin, TRIUMF, Vancouver, BC, Canada.

[1] L. Weissman *et al.*, Nuc. Phys. A **630**, 678 (1998).

[2] F. Strieder *et al.*, Euro. Phys. J. A **3**, 1 (1998).

[3] B.W. Filippone *et al.*, Phys. Rev. C **28**, 2222 (1983).

[4] F. Hammache *et al.*, Phys. Rev. Lett. **80**, 928 (1998).

[5] M. Hass *et al.*, Phys. Lett. B **462**, 237 (1999).

4.3 WALTA: The Washington Large-area Time-coincidence Array

J. G. Cramer, S. R. Elliott, B. Moorthy, C. Ouch, M. Roddy,* P. Schaffer,†
J. F. Wilkerson, J. Wilkes† and E. Zager†

Ultra-high energy cosmic ray particles that are protons with energies greater than $\sim 10^{20}$ eV cannot traverse great distances through the cosmos without losing energy to pion photoproduction in collisions with photons of the cosmic microwave background. The mean free path for this process is about 50 Mpc. Cosmic rays of similar energies that are electrons or gamma rays have similar energy loss processes with even shorter mean free paths. All known cosmic ray particles traveling cosmological distances should be limited to energies of less than about $\sim 10^{19}$ eV by such processes, yet a number of cosmic ray events with primary energies well above 10^{20} eV have been observed. This leads to the conclusion that the primary particles must have originated in our galactic neighborhood. However, the arrival direction of the few events seen so far does not indicate a nearby source. Furthermore there are few if any nearby astrophysical objects which could potentially accelerate a particle to these energies. This paradox is one of the major current mysteries in astrophysics.

We have formed a collaboration for the development of a distributed detector network. This system will support measurements of air showers from ultra-high energy cosmic rays and can also support a broad class of other physical measurements. We call the overall network NNODE (Northwest Network for Operation of Distributed Experiments), and we call the cosmic ray measurement component WALTA (WAshington Large-area Time-coincidence Array). The project is to be a direct physical science outreach program between faculty and students of the University of Washington and the science teachers and students of Washington-area middle schools and high schools (grades 7-12). The WALTA[1] part of the project is modeled on the ALTA initiative pioneered by the University of Alberta and currently being implemented in the Alberta Provincial School System. The local collaboration includes members of the Nuclear Physics Laboratory, physics department personnel in the cosmic ray and physics education groups, and a department of education faculty member from Seattle University. The project was described at the 1999 cosmic ray conference.[2]

Each WALTA/NNODE measurement module is envisioned to consist of a computer with an Internet connection, a GPS timing system, and measuring equipment. The measuring devices will be of several types. The WALTA modules will consist of scintillation paddles to be placed at the school to detect distributed particle showers produced at the top of the atmosphere by ultra-high energy ($\sim 10^{20}$ eV) cosmic rays. Groups from three other scientific disciplines have expressed some interesting possibilities of adding additional measurement units to the NNODE network.

This past year, we began the assembly of a prototype site for the cosmic ray detector. This was made possible by a DOE capital equipment grant we received to obtain the needed hardware for this development. We purchased but are awaiting the arrival of large scintillator modules and so have been testing detector configurations with smaller scintillator pieces available at NPL. We have bought GPS antennae and decoders and are implementing them. We have identified inexpensive,

---

*Education Department, Seattle University, Seattle, WA.
†Physics Department, University of Washington, Seattle, WA 98195.
[1]The WALTA web page can be found at http://www.phys.washington.edu/~walta/.
[2]E. Zager *et al.*, *Proceedings of the 26th International Cosmic Ray Conference*, Salt Lake City, Utah, August 17-25, 1999, to be published.

convenient, weatherproof enclosures for the detectors. At present we are experimenting with the phototube-scintillator geometry to determine the optimum signal-to-noise ratio for various cost effective configurations. We are also studying the noise levels associated with various high-voltage implementation schemes. We have also begun tests with LED's for detector calibration.

We purchased a low-voltage to high-voltage converting power supply (EMCO model K25N) and are performing tests on its operation. This supply converts a 24 V input to the 2000 V power required by the phototube. As this supply would be situated at the tube, it permits us to limit high voltage areas to within the inaccessible detector containment. As a result we won't have to distribute HV cables about school campuses. A further advantage of this system is its relatively low cost.

We have performed a number of simulations of a Seattle-area array using the CORSIKA code,[3] version 5.624. Fig. 4.3-1 shows a possible site layout with a simulated vertical 10^{19} eV event to provide some indication of the array response. In the figure, the squares are centered on sites which have no response to the event. The 5 sites responding to the event are indicated by circles. The area of each circle is proportional to the number of particles detected at the site. The number of detectors and their geometry, the detector spacing, and the trigger requirements are all parameters which are currently under study. Furthermore, site locations required to eliminate holes in the effective detector sensitive area are being identified. Subsequently, we will search for new candidate sites to fill such holes.

The project has employed two undergraduates whose activities are focused on this hardware development. This coming year we will also employ two students. One will develop the hardware further and the other will begin to implement data acquisition software. In addition a UW graduate student will join our efforts this spring.

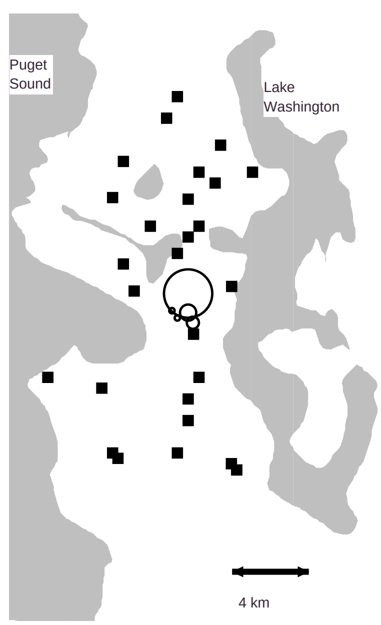

Figure 4.3-1. The proposed Seattle-area array with a superimposed 10^{19} eV event. See text for details.

[3] D. Heck *et al.*, 1998, Karlsruhe Report FZKA 6019; http://www-ik3.fzk.de/~heck/corsika/Welcome.html.

5 Ultra-Relativistic Heavy Ions

5.1 STAR event-by-event program status

D. J. Prindle, J. G. Reid, T. A. Trainor, D. D. Weerasundara* and the STAR Collaboration

The STAR EbyE program is a multifaceted analysis in which event-wise information is used to probe the QCD phase boundary and vacuum symmetry dynamics. Tom Trainor and Iwona Sakrejda (LBNL) co-convene this activity. There are presently seven major areas:

- Flow – residual large-scale azimuthal correlations arising in noncentral collisions are studied. The first two Fourier components (v_1, v_2) of the azimuthal distribution of particle number represent directed and elliptical flow respectively and give essential information on the equation of state of nuclear matter. The EoS in turn gives us information on the trajectory of collisions on the thermodynamic space (T, μ_B) and the relationship of these trajectories to the QCD phase boundary.

- Global variables analysis – large-scale measures (*e.g.,* total multiplicity and transverse momentum) are treated as thermodynamic variables, and collision events are treated as elements of a grand canonical ensemble. The object of study is to extract information about the QCD phase boundary by a comprehensive analysis of fluctuations in these variables. Details are given in an accompanying report (see Sec. 5.9).

- Two-point correlation analysis – Fluctuations in global variables as measured by variances and covariances are closely related to correlations in two-point measure spaces. A comprehensive program to characterize the correlation content of all relevant two-point spaces is closely coupled to global-variables analysis.

- SCA analysis – This effort attempts to characterize fully the correlation content of each event in the style of information theory using scale-local topological measures, of which the most important is dimension transport on scale.

- P- and T(CP)-violation searches – This effort seeks evidence for spontaneous parity or time-reversal symmetry violation on a QCD vacuum modified by high energy densities.

- High-p_t angular correlations – At p_t values significantly above 1 GeV/c we expect to find evidence of early momentum exchange between partonic degrees of freedom in angular correlations among high-p_t particles. Of particular interest is the distribution of minijets, relics of semi-hard interactions in the first fm/c of the collision.

- Low-p_t DCC searches – at very low p_t (near and below the pion mass) we expect to find indications of chiral symmetry restoration, an event-wise excess of low-p_t pions and/or a fluctuating nonzero isotensor distribution (fluctuation of the neutral-pion fraction).

For initial (year-one) analysis of STAR data we emphasize flow, global-variables analysis and two-point correlation analysis as baseline activities. Experience with NA49 analysis in these three areas (see accompanying articles) has been essential in developing the STAR EbyE program.

*BSQUARE Corp., Bellevue, WA 98005.

5.2 STAR global-variables analysis

J. G. Reid and T. A. Trainor

Event-by-event global-variables analysis is motivated by analogy with thermodynamic systems. The central problem is the state description of equilibrated systems for a given constraint system and description of the dynamics of small departures from equilibrium. The common problem we address is determining the correlation structure of a composite measure system $\vec{m}(x) = \{m_i\}$ of global event variables which serve as analogs to thermodynamic variables in a bulk-matter system. We emphasize correlation measures that characterize the variance structure of individual dynamical measures and pairs of measures relative to one another.

In order to simplify our initial approach to STAR global-variables analysis we adopt a gaussian fluctuation model corresponding to possible two-point correlations which are studied as a parallel aspect of EbyE analysis (see Sec. 5.3). We have previously constructed analysis techniques which can accommodate an arbitrary q-point correlation analysis as required, depending on the emerging complexity of EbyE analysis results. The gaussian assumption means that variance and covariance measures dominate global-variables analysis. In a typical analysis, represented by Fig. 5.2-1 we

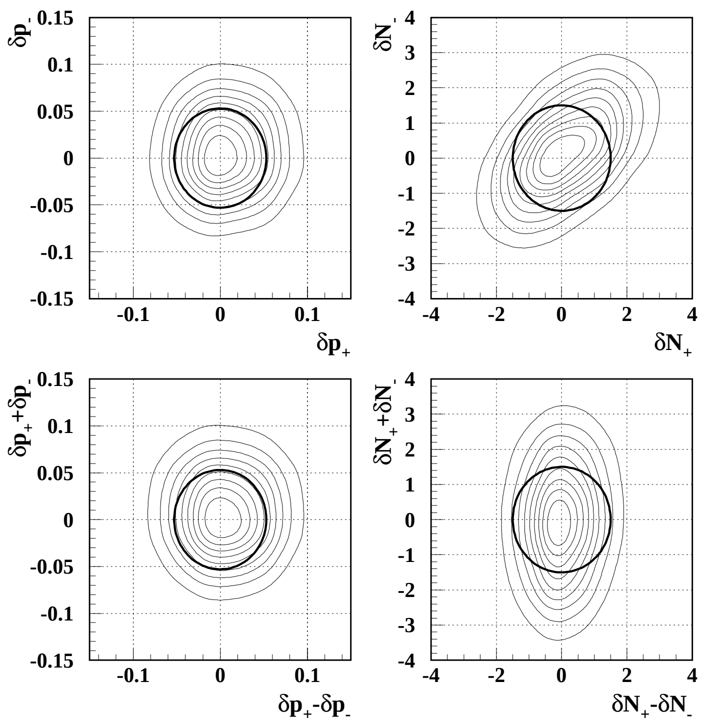

Figure 5.2-1. Measure-measure distributions illustrating a typical global-variables analysis. Measure pairs include total P_t and total multiplicity for positive and negative unidentified hadrons (examples taken from an NA49 preliminary analysis). Upper plots show elementary fluctuations in individual measures. Lower plots show fluctuations in sum and difference (or product and ratio) combinations. Momenta show essentially independent fluctuations in the two charge species, but multiplicities show the strong covariance expected as a result of resonance correlations. Dark circles indicate reference contours for an uncorrelated system.

study global event variables in pairs, extracting variances and covariances which are elements of a general covariance matrix for the system of global measures. We compare covariance matrix elements to references based either on the central limit theorem,[1] or on pair-mixing techniques.

[1]T.A. Trainor, Preprint hep-ph/0001148.

5.3 STAR two-point correlation analysis

J. G. Reid, J. Seger* and T. A. Trainor

As part of our design of the STAR event-by-event program we have initiated a series of simulations designed to provide interpretation of two-point analysis results. Figs. 5.3-1 and 5.3-2 represent preliminary results of this simulations program. A simple event generator throws particles into (m_t, y, ϕ) according to generic parent distributions (exponential, gaussian and flat respectively) but can be modified to include additional correlation content. Examples are 'dynamical' fluctuations, in which parent distribution parameters vary as gaussian random variables about a mean value with selected *rms* amplitude, 'volume' fluctuations in which all hadronic abundances are varied with an overall gaussian-random factor and resonance correlations in which selected mesonic and/or baryonic resonances are introduced which provide correlations among final-state particles.

Output of the MC generator is passed through a full simulation of STAR detector performance and track reconstruction to provide input to the EbyE correlation analysis system. Some results are shown in Figs. 5.3-1 and 5.3-2. Fig. 5.3-1 should show a flat distribution fluctuating about unity with an *rms* of a few *permil*. We see however that there is a small excess along the main diagonal, symptomatic of track splitting. This effect is well understood.

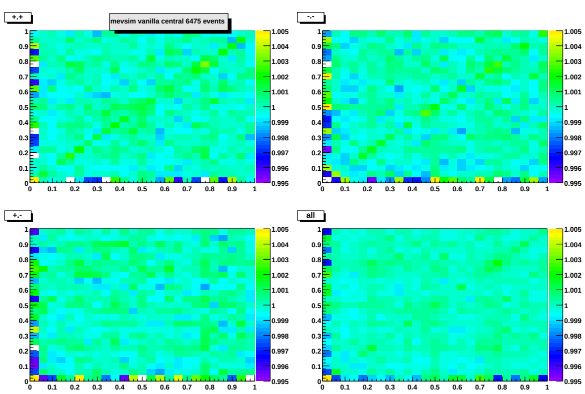

Figure 5.3-1. Two-point density ratios for four pair types obtained from minimally correlated Monte Carlo events. The ratios are flat within statistical fluctuations about unity, with the exception of small residual correlations along the main diagonals due to track splitting.

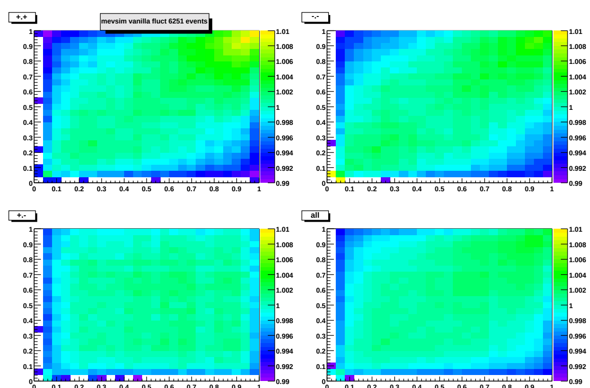

Figure 5.3-2. Two-point density ratios for four pair types obtained from Monte Carlo events containing 'dynamical' fluctuations in which the m_t-distribution slope parameter is event-wise varied about a mean value as a gaussian random variable with relative *rms* variation of 5%.

Fig. 5.3-2 represents the result for dynamical fluctuations in the parent distribution, modeling possible event-wise variations in collision dynamics associated with the QCD phase boundary. The structure for $+/+$ and $-/-$ pairs is anticipated. The absence of this structure in the mixed-charge distribution (lower-left panel) was puzzling given the intent of the MC design. It was discovered however that the program was actually throwing independent parameters for each particle type. The observed result properly indicated the event correlation structure – a good blind test for this analysis.

*Creighton University, Omaha, NE 68178.

5.4 STAR primary track definition

J. G. Reid, T. A. Trainor and the STAR Collaboration

Several aspects of heavy-ion physics analysis model a collision event ensemble as a grand canonical ensemble, with detected particles assumed to be emerging from a partially equilibrated thermodynamic system. Physics analysis of heavy-ion collisions therefore depends on identification of 'primary' particles – particles whose last interaction was part of a quasi-equilibrated hadronic cascade emerging from the collision event, as opposed to secondary particles resulting from weak and electromagnetic decays of unstable primaries far from the nuclear fireball. Examples of analysis topics requiring a well-defined primary-particle sample include anisotropic flow, hadronic spectra, global-variables and two-point event-by-event analysis and Hanbury-Brown - Twiss interferometry.

The problem of primary-particle identification becomes as a practical matter the problem of defining corresponding *primary tracks* in the STAR tracking detector system. We have developed a strategy for a self-consistent and stable definition of primary tracks for each event which involves a four-stage process. 1) Global tracks formed from one or several STAR tracking detector subsystems are optimally fit to a track model (Kalman filter) with due consideration for multiple Coulomb scattering and energy loss in material, including formation of a full covariance matrix for the track fit, and without regard for track point of origin. 2) A primary collision vertex position is determined using a select subset of all global tracks found in the event. 3) A loose momentum-dependent distance-of-closest-approach (*dca* relative to primary vertex) cut is applied to the resulting global-track population to define a population of primary-track *candidates*. 4) Each track in this candidate population is refit with the inclusion of the single primary-vertex point as an additional fit point. All resulting primary-track candidates with refit results are made available for physics analysis.

The central problem being addressed is identification of true primary particles by the relationships of certain global tracks (primary-track candidates) to the primary vertex. Therefore, the refit of global tracks with an included primary vertex point provides the single critical test of a primary-particle hypothesis. The population of primary-track candidates, including the χ^2 probability for the refit with primary vertex, requires development of cut systems to define optimal 'primary track' populations for each physics analysis. Cut systems depend on the χ^2 probability, final *dca*, track momentum and track quality parameters. Cuts also depend on the type of physics analysis in general, as any primary-track population is inevitably contaminated to a significant extent by weak-decay daughter particles, the fraction of which depends linearly on the adopted cut system. There are then tradeoffs among detection efficiency, spectrum distortion and alteration of the correlation structure of the primary track population. No cut system can be perfect, and optimized cut systems for various analysis topics must be interpreted as to their physics bias by simulations.

To achieve self-consistent precision physics results with the STAR detector the selection of primary track populations must be robust and optimal. A uniform cut architecture based on standardized methods and a central cut-parameter data base is being developed in common across several physics analysis groups. This common system is essential for consistent comparisons from one physics interest group to another.

5.5 NA49 two-point correlation analysis

J. G. Reid and T. A. Trainor

We now understand the direct connection between global-variables variance comparison measures and two-point density ratios.[1] A two-point density-ratio analysis first requires transformation of m_t to a variable x in order to 'flatten' distributions. This minimizes systematic errors in the correlation space due to gradients in the marginal distributions and insures uniform statistical errors. Comparisons are made between sibling pairs (formed from the same event) and mixed pairs (formed from different events). Mixed pairs are formed from 'nearest-neighbor' events – events which are proximate in a space of global event characteristics such as total multiplicity. The primary analysis space is the density ratio of sibling to mixed pairs for various pair types, such as like-signed and unlike-signed pairs. Spaces are typically binned in 25x25 bins for 100k events. Deviations from unity for ratio distributions are typically 1 *permil*. The bin number is chosen as a compromise between resolving quantum-interference structures and providing sufficient integration to insure reasonable S/N ratio for large-scale structures.

To optimize sensitivity in the density ratio we employ 'plaid' suppression (see Sec. 5.6) in which mixed pairs are formed from the same event set as sibling pairs, and specifically from event pairs that are carefully matched in their global characteristics. This reduces the statistical error in a two-point space to 2D Poisson statistics with negligible inter-bin error correlation (correlations observed as plaids in 2-D density plots). In Fig. 5.5-1, fits have been made to observed large-scale

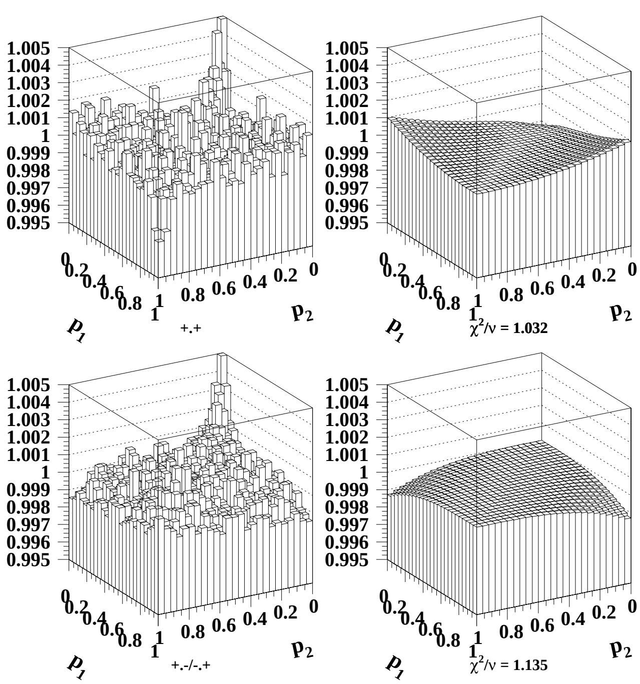

Figure 5.5-1. Two-point density ratio distributions for like-signed (++) and unlike-signed pairs (left top and bottom respectively) and corresponding fits to large-scale structure (right). Fits indicate similar shapes with opposite curvatures for the two pair types. These results can be interpreted in terms of an interaction between nuclear Hubble flow and local correlations of like-signed and unlike-signed particle pairs on the emission surface, with anticorrelation of like-signed pairs and correlation of unlike-signed pairs.

structures in these two-point spaces in the form of power-law expressions, with coefficients and exponents freely varying during the fit and interpretation is ongoing.

[1] T.A. Trainor, Preprint hep-ph/0001148.

5.6 Correlated error structure in two-point correlation analysis

J. G. Reid and T. A. Trainor

A common problem for correlation analysis is removal of unwanted correlations (statistical fluctuations, factorizable correlations, efficiencies) in favor of the 'signal' (object of study). Pair mixing of elements from marginal distributions (factorization reference) or from different events (mixed-event reference) are used to generate reference distributions which accomplish this goal. A mixed-pair reference should minimize the 1D statistical error which survives into the resulting 2D difference or ratio distribution. We have formulated a technique for constructing a mixed-pair reference which minimizes penetration of marginal statistical error into 2D pair distributions.

In forming a mixed-pair reference, sibling and mixed pairs should be generated using the same event population and event pairs with matching global characteristics (*e.g.,* total multiplicity). Statistical fluctuations are a form of correlation, and single-point statistical fluctuations in marginal distributions can be removed from the 2D pair distributions if a proper reference is formed which contains this correlation, leaving only true two-point statistical fluctuations in the comparison distribution. If events with different multiplicity or distribution shape are used to generate mixed pairs the assumptions which insure cancelation of single-point distribution statistical errors are invalid. Excessive correlated errors in the 2D distribution result, significantly reducing the effective statistical power of the data. In an analysis of 100k Pb-Pb collisions, events were separated into

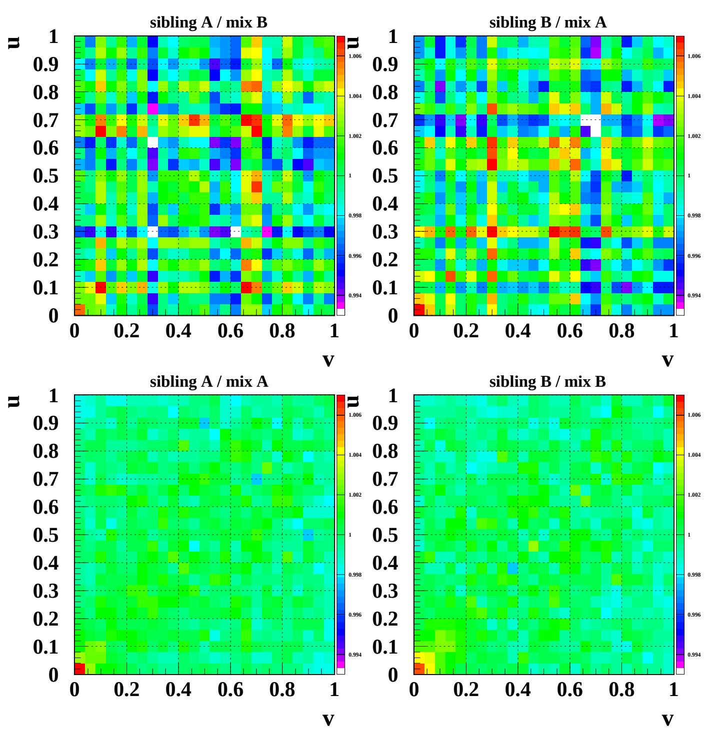

Figure 5.6-1. Sibling vs. mixed pair histogram ratios for different event sets (top) and same event sets (bottom) showing the characteristic plaid pattern for an ill-formed reference. In the case of pair spaces generated from the same single-point data, the single-point statistical fluctuations in those data cancel in the difference or ratio, revealing the true two-point statistical fluctuations of a 2D distribution (bottom) and the physics of interest. In the case where the sibling and mixed pair spaces are generated from *different* data, the fluctuations in the 1D distributions do not cancel and so dominate the error in the 2D space (top).

two groups – A and B. Identical analysis was carried out on each group, and the results were then combined to form sibling/mixed pair ratio distributions either as A/A and B/B or A/B and B/A. The results shown in Fig. 5.6-1 dramatically illustrate the importance of careful reference formation.

5.7 Autocorrelations and Hubble flow in heavy-ion collisions

J. G. Reid and T. A. Trainor

We formulate an extension of the usual treatment of two-particle momentum correlations to examine the possibility of non-chaotic or correlated particle emission from the hadronic freeze-out surface. We adopt a two-particle emission density which permits the description of nontrivial differences between pair autocorrelations for different pair types. We also adopt the idealization of nuclear Hubble flow as a maximally symmetric flow reference. Hubble flow is isotropic and homogeneous and represents a special form of radial flow in the context of a nuclear collision. Pair position autocorrelation determines how the nuclear flow is sampled by pair partners. If different pair types sample flow in a systematically different way there may be detectable differences in the two-particle momentum distributions.

As shown in the top left panel of Fig. 5.7-1 if there are no two-particle correlations on the source (independent particle emission) the emission density is factorizable (the usual assumption in an HBT analysis). If this independent-particle assumption is not valid however, as suggested by the top right panel in the figure, then a simple factorization on x_1 and x_2 is not appropriate. Guided by treatments of final-state interactions we instead factor the two-particle emission density into dependence on mean pair position x and on pair partner separation y, retaining the possibility of parametric dependence on mean and relative momenta. We then obtain for the two-particle Wigner density on phase space

$$S_2(x_1, x_2, p_1, p_2) \approx g_+(x,k)\, g_-(y,q)\, f_1(x_1,p_1)\, f_1(x_2,p_2). \tag{7}$$

where $g_-(y,q)$ is the autocorrelation density on pair relative position, with possible forms sketched in the bottom left panel of Fig. 5.7-1. For discussion purposes we represent the usual two-particle momentum distribution $P_2(\mathbf{p}_1, \mathbf{p}_2)$ as a sum of two terms $A(\mathbf{k},\mathbf{q}) + B(\mathbf{k},\mathbf{q})$, where the second (interference) term contains the usual HBT Fourier transform (= 0 in the case of mixed pairs), and the first term is ordinarily written as the product of two single-particle distributions $P_1(\mathbf{p}_1) \cdot P_1(\mathbf{p}_2)$. In the present case the generalization to a nonfactorizable autocorrelation density leads to the expression

$$A(\mathbf{k},\mathbf{q}) = m_1\, m_2\, e^{-\frac{m_1+m_2}{T}} \cdot \int d^4x g_+(x,k) \exp\left(\frac{2H}{T}\mathbf{k}\cdot\mathbf{x}\right) \cdot \int d^4y\, g_-(y,q) \exp\left(\frac{H}{2T}\mathbf{q}\cdot\mathbf{y}\right) \tag{8}$$

where the first factor is the usual Boltzmann distribution for the pair taken as a unit, the second factor represents blue shift of the pair mean momentum distribution, and the third factor represents a quadratic increase with increasing $|\mathbf{q}|$ (another form of blue shift) of the pair *relative* momentum distribution.

Dividing through by a reference distribution (factorization $P_1(\mathbf{p}_1) \cdot P_1(\mathbf{p}_2)$ of mixed pairs) we obtain the corresponding *noninterference* term for the two-particle correlator

$$a(\mathbf{k},\mathbf{q}) \approx 1 + \frac{1}{V} \int d^4y \left\{g_{obj}(y,q) - g_{ref}(y,q)\right\} \cosh\left(\frac{H}{2T}\mathbf{q}\cdot\mathbf{y}\right) \tag{9}$$

which would be unity in the absence of either nuclear Hubble flow or differing autocorrelations for different pair types. The presence of both conditions however produces a (positive or negative) quadratic deviation from unity in the correlator due to the leading term $<(\mathbf{q}\cdot\mathbf{y})^2>_{\Delta g}$ from the cosh factor as illustrated in Fig. 5.7-2.

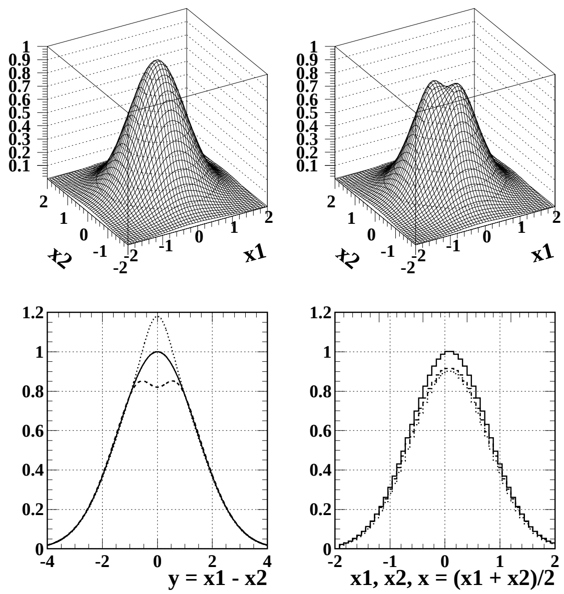

Figure 5.7-1. Two-particle emission densities are depicted for uncorrelated (top left) and anticorrelated (top right) pairs. Lower left panel shows autocorrelation densities on pair relative position y (four vector) for correlated (dotted), neutral (solid) and anticorrelated (dashed) systems. Lower right panel shows densities on pair mean position x and coordinates $x1$, $x2$.

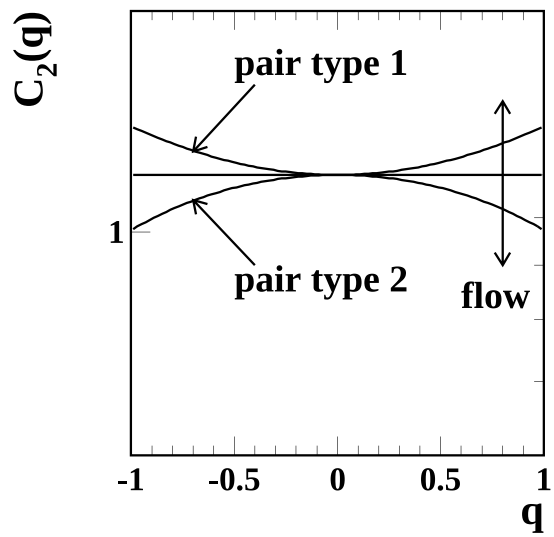

Figure 5.7-2. Two-particle momentum correlator (omitting the peaked contribution from quantum interference) showing the effects of nuclear Hubble flow combined with autocorrelations depending on pair type. Pair type 1 corresponds to anticorrelation, and pair type two corresponds to correlation in comparison to a mixed-event reference.

This new aspect of the two-point momentum correlator offers the possibility to examine the hadronization process at small scale on the emitting space-time surface. In effect, large-scale features of the two-particle momentum space may inform us about small-scale features of the emitting surface, although the mechanism is *not* quantum interference, but rather a classical dynamical effect analogous to cosmological Hubble flow and intergalactic red shifts used to map relative galaxy positions.

5.8 Small-scale structure of the hadronic freezeout surface in Pb-Pb collisions

J. G. Reid and T. A. Trainor

We have extended the usual treatment of two-particle momentum correlations to examine the possibility of non-chaotic or correlated particle emission from the hadronic freeze-out surface (see Sec. 5.7). Here we consider the consequences for Pb-Pb collisions at the SPS and implications of an NA49 EbyE analysis of $<p_t>$ fluctuations and two-point momentum correlations (see Sec. 5.5). We obtained an expression for the noninterference component of the two-point momentum correlator as

$$a(\mathbf{k},\mathbf{q}) \quad \approx \quad 1 + \frac{1}{V} \int d^4y \, \{g_{obj}(y,q) - g_{ref}(y,q)\} \, \cosh\left(\frac{H}{2T}\mathbf{q}\cdot\mathbf{y}\right). \tag{10}$$

which would be unity in the absence of nuclear Hubble flow *or* autocorrelation densities depending on pair type. If we further assume that the autocorrelation density difference is localized to a fraction of the nuclear volume ($\rightarrow r/R \ll 1$) and that there is a significant degree of correlation between configuration space and momentum space opening angles (kinematic constraints or small mean free path for hadrons emitted from an opaque freezeout surface) then we obtain for the correlator projected onto (p_t, p_t)

$$\begin{aligned} a(p_{t1},p_{t2}) \quad \approx \quad & 1 \mp \epsilon \, \frac{\hat{\beta}_\perp^2}{8T^2} \, (r/R)^2 \, \{1-(r/R)^2\} \; , \{2k^2 \, (1- <\cos(\phi)>_{\Delta g}) \\ & + q^2 \, (1+ <\cos(\phi)>_{\Delta g})/2\} \qquad <\cos(\phi)>_{\Delta g} \in [0,1] \end{aligned} \tag{11}$$

The value of $<\cos(\phi)>_{\Delta g}$ can be established from experiment by comparing the amplitudes of observed quadratic dependences on $k = (p_{t1} + p_{t2})/2$ and $q = p_{t1} - p_{t2}$. This value may be affected by kinematic constraints from a hadronic precursor decay or by nuclear opacity effects.

Due to the finite mean free path of pions in nuclear matter throughout much of the collision process the mean value of the pair opening-angle $\cos(\phi)$ may be significantly different from zero, and possibly close to unity (an 'opaque' source). Implications of opacity for source space-time structure is a very active area of research. On the other hand, we expect from phenomenological descriptions and infer from multiplicity correlations[1] that a significant fraction ($\approx 50\%$) of final-state pions derives from meson and baryon resonance decays, implying that pair momenta may be correlated in direction and magnitude by few-body kinematic constraints. This could also drive $<\cos(\phi)>_{\Delta g}$ to values approaching unity.

Results from our NA49 analysis may indicate nontrivial autocorrelations depending on pair type combining with nuclear Hubble flow to produce large-scale quadratic structures primarily q^2 dependent with negligible k^2 dependence, suggesting that correlated pair momenta are restricted to small opening angles. If this is due to kinematic restrictions posed by precursor hadron decay it presents the very interesting possibility that nuclear Hubble flow influences the decay kinematics of individual hadrons.

[1]J.G. Reid (NA49) private communication.

5.9 Event-by-event analysis and the central limit theorem

T. A. Trainor

Event-by-event analysis of heavy-ion collision events provides an essential means to study the QCD phase boundary. A universal feature of phase boundaries is the appearance of increased measure variances compared to a reference system. In a recent paper[1] I have developed an extended system of global-variables variance comparison measures based on the central limit theorem. I find that the central limit theorem is, in a broader interpretation, a hypothesis about the scale invariance of *total* variance for a measure distribution, which relates to the scale-dependent symmetry properties of the distribution. I further generalize this concept by connecting the scale dependence of the full covariance matrix describing gaussian fluctuations for all dynamical measures relevant to a collision on the one hand to a matrix of scale-dependent covariance integrals defined on two-point measure spaces on the other.

The central limit theorem applied to N-fold sampling of a parent (single-particle) transverse momentum distribution (*e.g.,* to form collision events) gives for the variance of the event-wise $<p_t>$ in terms of the parent-distribution variance the following elementary relation

$$N\sigma^2_{<p_t>} - \sigma^2_{p_t} = 0,$$

the validity of which depends on assumptions 1) that the parent is static and 2) that the samples are independent. Assumption 2) is certainly violated (by quantum correlations, final-state interactions and instrumental effects), but in ways that can be simulated precisely. We then look for additional interparticle correlations and evidence that the parent distribution varies event-wise: dynamical fluctuations indicating that each collision (or a subset of the total) evolves with unique dynamics.

The principal elements of this work are as follows:

- Collision events are viewed as elements of a Grand Canonical Ensemble. Global event variables are assumed to fluctuate according to a gaussian fluctuation model as a null hypothesis.

- The degree of equilibration achieved in the final state is determined by comparison of event-wise fluctuations with an equilibration model such as the statistical model. One then asks whether any excess fluctuations present in the final state are due to phase-boundary effects.

- Precision determination of variance and covariance differences requires reference values supplied by the central limit theorem and/or a baseline correlation hypothesis (*e.g.,* quantum correlations).

- Fluctuations and correlations are related at several levels. Fluctuation measures such as variance and covariance are related to two-point correlation measures in a nontrivial way. The details of this relationship are now clarified.

- Variance (per-bin variance) is identified as a scale-dependent quantity, as illustrated in Fig. 5.9-1. A generalization is made to total variance (per-bin variance times bin number).

[1]T.A. Trainor, Preprint hep-ph/0001148.

- The Central Limit Theorem provides a convenient maximum-symmetry reference for variance comparisons. The CLT is reinterpreted as a statement of scale-invariance of total variance, as illustrated in Fig. 5.9-2.
- Finally, the central limit theorem is generalized to a hypothesis concerning the scale invariance of total covariance matrices.

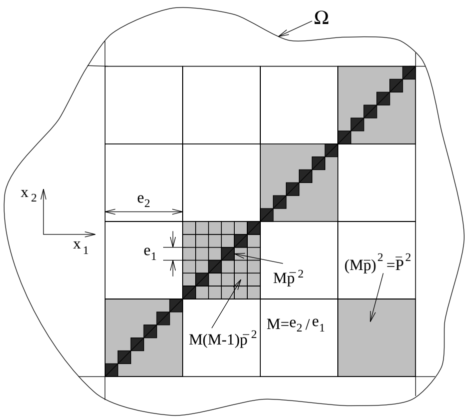

Figure 5.9-1. This figure illustrates the central limit theorem as a comparison between per-bin variance in a larger bin (light squares) and N times the per-bin variance in the smaller bins (dark squares). Any excess variance (violation of the CLT) comes from off-diagonal bins corresponding to net two-point correlations within a specific scale interval.

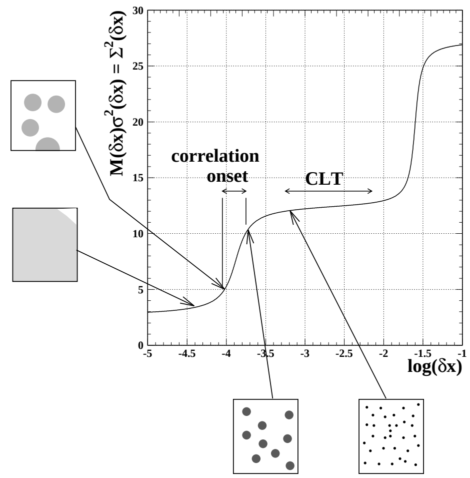

Figure 5.9-2. This figure illustrates that the *total* variance Σ^2 for a measure distribution is scale invariant over scale intervals for which the CLT is satisfied. For a maximally symmetric system such intervals are bounded by the system size and/or 'correlation onsets,' restricted scale intervals in which reside the 'quasiparticles' of a dynamical system.

I illustrate this situation for a pair of dynamical measures – event-wise total transverse momentum P_t and multiplicity N. The difference between covariance matrices $\mathbf{K}(p, n, \delta x)$ evaluated at the particle scale $\delta x_1 = a$ and event scale $\delta x_2 = L$ are explicitely expressed and related to a matrix of correlation integrals $\mathbf{A} = \{A_{ij}\}$ (*e.g.*, $A_{pp} \approx \int p_1 p_2 \cdot \{\rho_{2,obj}(\delta x_1, \delta x_2;) - \rho_{2,ref}(\delta x_1, \delta x_2;)\} dp_1 dp_2$).

$$\begin{aligned}
\mathbf{K}(p,n,L)/N(a,L) - \mathbf{K}(p,n,a) &= \begin{pmatrix} N\sigma^2_{\langle p_t\rangle} - \sigma^2_{p_t} + 2\bar{p}\sigma^2_{<p>N} & \bar{p}\sigma^2_{<p>N} + \hat{p}^2(\sigma^2_N/N - \sigma^2_n) \\ \bar{p}\sigma_{<p>N} + \hat{p}^2(\sigma^2_N/N - \sigma^2_n) & \hat{p}^2(\sigma^2_N/N - \sigma^2_n) \end{pmatrix} \\
&= \mathbf{A}(a, L; (p,n) \otimes (p,n))/N \\
&= \frac{1}{N} \begin{pmatrix} A_{pp} & \hat{p}A_{pn} \\ \hat{p}A_{pn} & \hat{p}^2 A_{nn} \end{pmatrix}
\end{aligned}$$

Note that the matrix element corresponding to A_{pp} in the covariance matrix difference contains the elementary form of the central limit theorem (previous page) as one component. This generalized treatment of the central limit theorem and covariance matrices points the way to a detailed description of the scale-dependent symmetry dynamics of a complex measure system.

5.10 Scale-local measures and jet correlations - where is the pQCD?

J.G. Reid and T. A. Trainor

We want to understand how and to what degree the cascade structure of perturbative QCD (pQCD) is transmitted to hadrons in jet production by analyzing energy and multiparticle angular correlations for produced hadrons relative to the jet axis. It is predicted that because of the self-similar structure of a pQCD gluon bremsstrahlung cascade one should observe the *remnants* of a recursive or fractal pattern (intermittency) in hadron populations derived from jet fragmentation.

A variety of jet shape and correlation measures has been developed to characterize both event-wise and inclusive jet energy and multiplicity angular distributions. The application of scaled factorial moments to multiparticle spectra in search of 'intermittency' or power-law scaling behavior already has a significant history. We have developed a system of scale-local correlation measures which contains factorial moments and other shape measures as special cases and some accompanying analysis techniques which permit precision differential correlation studies, especially important near the distribution boundary scale, which may improve sensitivity to pQCD effects.

We have made a comparison[1] between scale-local correlation measures and some conventional measures applied to jet data, including a factorial-moment analysis of Delphi jet angular correlations[2] and application of two jet-shape measures to H1 data[3] (the latter comparison is not described here). We provide interpretations of the experimental results from a scale-local perspective and suggest methods to improve the Delphi and H1 jet analyses. We observe that scale-dependent correlation structure is sharply limited in these data, restricted primarily to large-scale jet shape and width fluctuations.

Fig. 5.10-1 shows the original Delphi data analyzed in terms of factorial moments plotted in the form $\log(F_q(\delta\theta))$, vertical factorial moments defined on a single angle bin of variable width $\delta\theta$ centered on the jet axis, logs of these moments scaled by a factor q and plotted *vs* bin width. Scaling the logs by the factor q yields the vertical information I_q^V, a scale-local measure from which dimension transport can be obtained directly as $\Delta d_q = \partial I_q / \partial \log(\delta\theta)$ and included in the figure.

Fig. 5.10-2 shows scale-local measures for the simple case of a simulated peaked object distribution contracted to smaller width compared to its original form taken as a reference (see Sec. 5.11). This is a multi-bin horizontal analysis of a single distribution in the terminology of intermittency analysis, as opposed to a single-bin vertical analysis of many distributions in an ensemble, as in the Delphi analysis. We have shown that for the conditions of the Delphi analysis and this simulation the horizontal and vertical informations are directly comparable.

Comparison of the two figures shows considerable similarity in shapes and magnitudes, leading to an interpretation of the Delphi results as indicating simple large-scale jet width fluctuations, with any recursive or fractal structure sharply limited. In particular, the initial rise in I_q^V with decreasing scale (bin width) should not be interpreted as indication of fractal structure corresponding to some scaling exponent. This type of structure has to be present with any type of distribution width change

[1] *Scale-local Measures and Jet Correlations – Where is the pQCD?*, T.A. Trainor and J.G. Reid, Preprint, Nuclear Physics Laboratory (1999).

[2] B. Buschbeck, F. Mandl, Preprint hep-ph/9905367, *Phys.Lett.* **B457** 368-382 (1999).

[3] H1 Collaboration, Preprint hep-ex/9901010 (1999).

or fluctuation. The fact that the informations or factorial moments quickly saturate to constant values with decreasing scale is a clear indication that no substantial scale-invariant phenomena are present.

We find by these simulations and the use of well-understood scale-local measures that at scales significantly below the jet boundary scale nontrivial correlations in the Delphi data are apparently constrained below the *percent* level in some information measures, leading to the question where are the recursive correlations expected from pQCD branching in gluon bremsstrahlung? The Delphi results are consistent with the interpretation that the first few stages of gluon radiation survive hadronization in the form of large-scale jet width fluctuations. Smaller-scale bremsstrahlung lower in the radiation hierarchy is apparently absorbed in the hadronization process. In effect hadronization can be represented as a bandwidth limitation on wavenumber. Only the lowest-order long-wavelength structure in the glue field survives into the hadronic final state. It would be interesting to characterize the transfer function of hadronization in terms of gluonic degrees of freedom by a precision analysis of jet correlations.

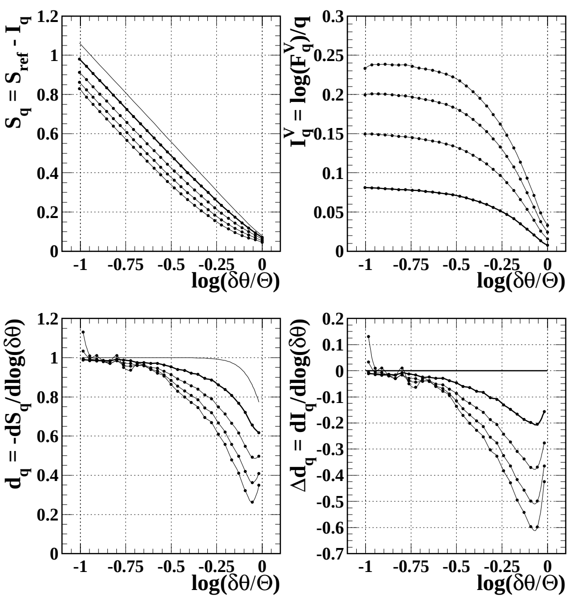

Figure 5.10-1. Upper right panel shows a replot of the results of a Delphi vertical factorial moment analysis expressed as informations of rank 2-5. The upper left plot shows the reconstructed corresponding entropies. The lower right panel shows the dimension transport inferred from the informations and the lower left plot the corresponding scale-local dimension. These curves can be compared with Fig. 5.10-2.

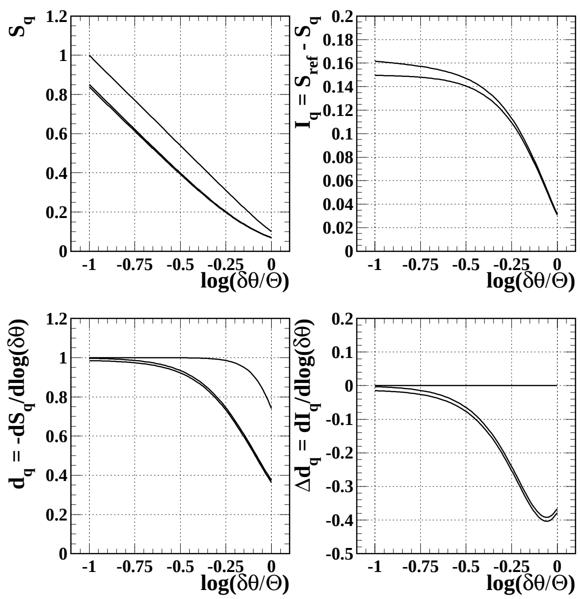

Figure 5.10-2. These panels show results similar to Fig. 5.10-1 but for a single peaked distribution reduced in width compared to the original as reference. The upper right panel shows information corresponding to a simple change in distribution width. Connections between this horizontal analysis of width variation and the Delphi vertical analysis of shape fluctuations are noted in the text.

5.11 Jet correlations model analysis

J. G. Reid and T. A. Trainor

We have carried out simulations illustrating application of scale-local topological measures to jet correlation analysis. The primary distributions chosen represent idealized angular distributions of final-state hadrons about a jet axis. For illustrative purposes we generate two similar distributions of 1M points each: a triangle distribution and a gaussian, having identical widths. Although these distributions are easily distinguishable by eye they are numerically quite similar.

This analysis is based on a scale-local information expression given by

$$I_q(E, E_{ref}, e) = \frac{1}{q-1} \log \left(\left\langle \sum_{i=1}^{M_1(e)} q_i(e) \{p_i(e)/q_i(e)\}^q \right\rangle_\phi \right). \tag{12}$$

where p_i represents bin contents for the object distribution (triangle or gaussian), q_i represents bin contents for the reference distribution (in this case a uniform distribution), e represents a bin size (scale), q represents the information *rank* index and $<>_\phi$ represents a dithering process to reduce aliasing. Information is a logarithmic representation of the effective size reduction of an object distribution (E) relative to a reference (E_{ref}) due to a degree of correlation content.

From the information distribution on scale a dimension transport distribution can be extracted as

$$\Delta d_q(E_{obj}, E_{ref}, e) = \frac{dI_q(E_{obj}, E_{ref}, e)}{d \log e}. \tag{13}$$

Dimensionality is a primary symmetry measure for a distribution. A maximally symmetric distribution has a dimensionality of maximum magnitude distributed over the largest scale values consistent with a constraint system. Increased correlation corresponds to transport of dimensionality as a conserved quantity to lower scale. Equilibration corresponds to dimension transport to higher scale. Whereas information integrates correlation contributions on scale, dimension transport represents a true scale-local differential correlation measure.

Two object distributions and their information distributions on scale are shown in Fig. 5.11-1. The reference for each is a uniform distribution on the *support* of the object distributions – the occupied bins. The information distributions indicate as a function of decreasing scale how the width reductions of the object distributions relative to the reference are accumulating. The informations saturate at some lower scale value because there is no small-scale correlation content in these distributions.

The two dimension-transport distributions (upper panels) in Fig. 5.11-2 show a reduction in dimensionality at large scale due to the relative size reductions. This dimensionality is transported as a conserved quantity to smaller scale (beyond the scale interval plotted). The most important distribution is the difference between dimension transports for the two object distributions in the lower-right panel (the information differences in the lower-left panel are included for completeness). The dimension transport differences offer an optimal scale-local basis for direct quantitative comparison of correlation content. We observe difference values of a few percent, reflecting the close numerical similarity of the two distributions. However, these differences are statistically very significant, reflecting integrated point counts of $\approx 1M$ in the object distributions.

This exercise is meant to illustrate the general application of scale-local measures to jet correlation analysis. In the case of real data one is searching for width fluctuations, systematic width differences between gluon and quark jets and evidence for hierarchical structure in the hadronic final state due to gluon bremsstrahlung cascades in the partonic regime. This last is an essential component of any program to understand hadronization and to interpret the final state in terms the dynamics of a prehadronic precursor system – a quark-gluon plasma.

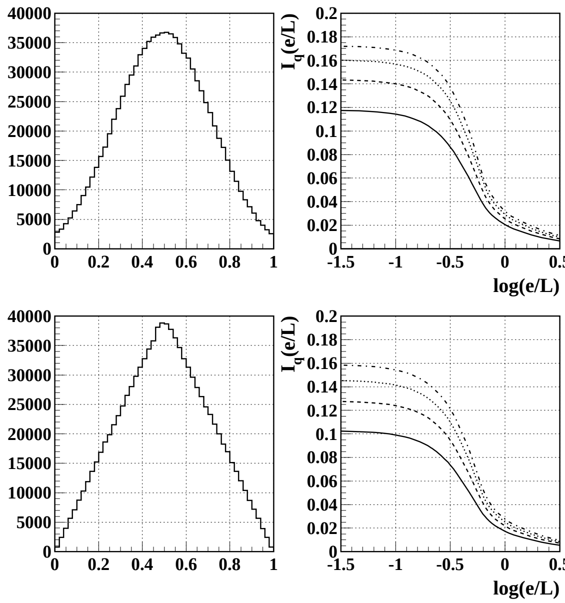

Figure 5.11-1. Comparison of two peaked distributions (gaussian and triangle) of 1M points each (left). Information for ranks $q = 2, 3, 4, 5$ is shown (right), with $q = 2$ as the solid curve.

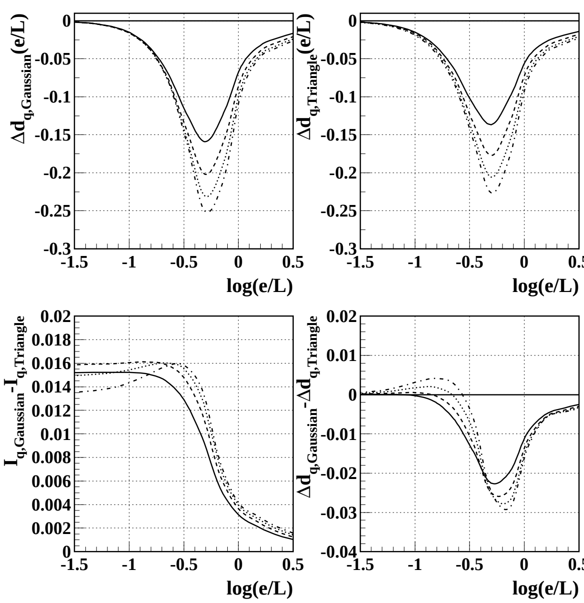

Figure 5.11-2. Dimension transport for two peaked distributions relative to a uniform distribution (top). Information and dimension transport differences for two distributions (bottom).

5.12 Data set viewer (DSV): status and plans

D. J. Prindle, J. G. Reid and T.A. Trainor

We have previously described a system for visualizing relativistic heavy ion collisions.[1] Non-trivial data sets representing such collisions typically have more than three interesting aspects requiring visualization of various projections of the dataset, and optimum visualization may require transformations from one variable set to another. We therefore sought a convenient and flexible way to define projections and transformations without modifying the core visualization package. Relativistic heavy ion collision visualization is more complex than conventional high energy physics visualization because of the greatly increased multiplicity of display objects (particles, tracks and momentum vectors). This complexity adds a requirement that the display be able to inhibit data elements so that features of interest become more visible.

DSV (Data Set Viewer) can be thought of as an extension to QCDisplay,[2] a program to verify tracking in NA49. QCDisplay has various ways of inhibiting the display of data, including turning objects off completely, rendering them only when the view is not being modified and rendering a subset of the items depending on color indices and cut planes. DSV enhances the data-hiding capabilities of QCDisplay by using vector expression to determine the visibility of each display object. The new aspect of DSV is a flexible interface between the data source and QCDisplay. This graphical user interface (GUI) is created using tcl (tool command language) scripts representing the data set as a source and QCDisplay as a destination. The user can navigate the dataset hierarchy, select a column from a table and drag it to an item in QCDisplay to establish a map. Source vectors can be directly copied to QCDisplay, combined with other source vectors via mathematical expressions or sent to a tcl procedure or C command for more complicated manipulation. There are also tabular displays available for examining data numerically. The QCDisplay mapping is automatically invoked when a new event is selected.

DSV is currently installed on an AFS partition at RHIC. Binaries are available for Linux, Solaris and HP-UX platforms. The current data I/O packages can read XDF format files as well as plain ascii text files. A package capable of attaching to a DSPACK server and extracting most types of information from it is also available, although for technical reasons this requires a special version of DSV. DSV is widely used as an event display within STAR but is not currently used as a more general data display package. There are no 1D or 2D views (histograms) available. We plan to include at least a minimal interface to BLT graphs soon. The DSV tcl scripts are now being re-written so that interactively defined mappings are savable and easily customized. Finally, because STAR is moving from XDF format files to ROOT format files we are introducing two methods to access ROOT data. The first is a socket interface to a ROOT session requiring the user to start ROOT and DSV sessions and connect them. This will provide the possibility of having a ROOT data server running on a machine remote from the DSV display. The second access to ROOT files will be to read them via a DSV I/O package. This will require changes in the ROOT file format which are currently being implemented by the ROOT team.

[1] Nuclear Physics Laboratory Annual Report, University of Washington (1999) p. 48.
[2] Nuclear Physics Laboratory Annual Report, University of Washington (1996) p. 44.

5.13 DSV: applications

D. J. Prindle, J. G. Reid and T. A. Trainor

We have used DSV to study output from several event generators where the spatial scale is a few tens of fermis. Most event generators write their output as text files, and we use the text reading feature of DSV to visualize these data. The event generators we have examined most completely are VENUS and NEXUS (Klaus Werner, University of Nantes) and VNI (Klaus Kinder-Geiger, late of Brookhaven National Laboratory). These event generators record the space-time freezeout coordinates of the particles as they are produced in the MC process. We typically employ rapidity-like variables to place small-scale or early-time features on an equal footing with large-scale and late-time evolution. In the case of event generators large scale means tens of fermis. VENUS and NEXUS share similar behaviors, including creating certain particle types at rather specific times late in the collision evolution. Visually this manifests as a shell of produced particles in configuration space. A sampling of these images can be found at http://www.star.bnl.gov/afs/rhic/star/doc/www/imagelib/event_images/index.html.

VNI is a parton cascade MC that can in principle record all the particles in existence at any given time. This can provide many files recording different time slices of the same event. Using the scripting features of DSV we can cycle through all these files, creating images of each time slice. Assembling these in a sequence we can visualize the time evolution of a partonic cascade as interpreted by VNI as a movie. Some of these movie sequences can be viewed at http://www.star.bnl.gov/STAR/html/ebe_l/star-ebe.html.

DSV was originally written to examine detector data for QA purposes. Tracks typically extend for several meters, but the measured points on tracks are usually determined to a few hundred microns. We have found many tracking anomalies in STAR which provide critical input to software development. Some early problems have included tracks with an extraneous point added after a gap of several pad planes which are then pulled to lower momentum and split track segments which are very short, giving rise to extraneous high-momentum particles and producing spurious correlations in HBT analysis.

Examining TPC laser track data in STAR we look for deviations in reconstructed point positions of a few hundred microns over track lengths of two meters as a test of tracking and system geometry, especially drift speed accuracy. It is also possible to determine very precisely the tilt and offset of the central cathode plane. A selection of images of STAR simulation and data events can be found at http://www.star.bnl.gov/afs/rhic/star/doc/www/imagelib/event_images/index.html.

DSV images have appeared in a variety of public media, including Newsweek and Scientific American, as well as the CERN Yearbook cover, GSI calendar, APS calender and a number of European commercial news media. We have recently generated two image sets for the NA49 experiment at CERN. The first uses the clip plane feature of DSV to create 200 images with tracks increasing further in length from the target in each image. The effect shows all the tracks from a collision event (about 1000) expanding toward the viewer through the tracking detector system. The second set of images maintains the same top view of 25 different collision events. Formulated as an endless strip movie this collection illustrates the large-scale and statistical variations in typical NA49 event types. Both projects are intended for public display.

5.14 HBT physics at STAR

J. G. Cramer and STAR HBT Physics Working Group

Technical difficulties in the planned Summer-1999 startup of the RHIC facility, which arose from damage to components of the accelerator during 20 Atm -pressure tests of the RHIC vacuum system, have delayed the beginning of the physics program with the STAR detector by approximately a year. This unexpected delay, while painful, has provided the STAR HBT Physics Working Group (HBT PWG) with an opportunity. We have been able to refine the analysis software that has been developed for the STAR program and to investigate other opportunities for physics that the data from STAR will provide.

The HBT Physics Working Group (a group of approximately 20 physicists led by co-convenors J.G. Cramer and M.A. Lisa) has made very significant progress in the past year in preparing for the initial operation of STAR. In the Fall of 1999 the HBT PWG initiated biweekly telephone conferences that have continued up to now and that focus on problems and progress in preparing for the initial running of STAR.

A major accomplishment in the past year ahs been the development and testing of a new C++ -based object-oriented analysis framework for HBT analysis (StHbt), initially developed by M. Lisa and tested by the group. This framework is intended to operate either within the ROOT software analysis platform that is the STAR standard, or alternatively as a stand-alone package that can be operated on local computer systems that need not be linked to the BNL facilities. At BNL, because of recent hacker attacks, there is now rising emphasis on software security, with strong encryption login procedures being implemented and off-site use of facilities discouraged. In this climate, the HBT PWG's decision to develop a stand-alone analysis framework looks very wise indeed.

Here we list major projects that have been undertaken by the HBT PWG in the past year.

- Development and description of micro-DST file formats for off-line and remote HBT analysis of STAR data. Extensions of this format have been developed that contain "hidden" information from simulation codes.
- Development of techniques for simulating Bose-Einstein and Fermi-Dirac correlations in identical particles, Coulomb correlations in charged particles, and correlations arising from strong final-state interactions and resonances between particles.
- Development of a Coulomb correction module that employs the best procedure for describing Coulomb final state interactions of particles emitted from finite-size sources. This module performs 2-dimensional interpolation over tables of Coulomb corrections determined by Monte Carlo 6-dimensional integration over Coulomb wave functions.
- Development of procedures for dealing with the problem of track-splitting in the STAR detector environment. The splitting of a single track into two tracks by the tracking software presents a significant source of background and error for HBT analysis, and the HBT PWG has an ongoing program for reducing the impact of this problem with a variety of techniques.
- Development of techniques for extracting the maximum amount of HBT-related source geometry information from single STAR events. Here a significant problem is the characterization

of the uncorrelated background for a single event, and the HBT PWG has investigated a number of approaches to dealing with this problem. It is still not clear whether a meaningful HBT "radius" can be extracted from single RHIC collision events.

- Development of procedures for performing correlation analysis on pairs of secondary neutral particles that are reconstructed from decays into charged particles, e.g., pairs of K_0 mesons.
- Development of procedures for performing correlation analysis on unlike pairs of final-state particles with differing masses (e.g., p-Λ^0 correlations). Simulations indicate that such analyses may be possible using data from the first year of STAR operation.
- Development of an extension of the StHbt analysis framework that can be applied to three-particle and multi-particle HBT analysis.

As this is being written, the third "Mock Data Challenge" is beginning at Brookhaven. Many of the techniques listed above will be tested in the next few weeks with new simulations.

In summary, the STAR HBT Physics Working group has mounted an active program for performing Bose-Einstein and other correlation analyses on the data that will be produced by the STAR detector beginning in the Summer of this year. We look forward to a busy and productive year.

5.15 Energy loss in thin layers of argon

H. Bichsel

The study of the energy loss spectra of fast particles in Ar gas has been continued.[1] A full description is given in STAR Note SNO418, accessible at http://www.star.bnl.gov, under "general documents." It describes the evolution of the straggling functions for segments (layers) x from 1 mm to 15 mm. Since the convolution method (PAI) is used,[2] the details of the functions can be seen clearly. Separate peaks associated with various features of the single-collision cross-section disappear gradually. An example is shown in Fig. 5.15-1; energy losses below 20 eV (peaks a, b, c) are due to single collisions, the peaks d and e are due to two collisions corresponding to the peaks a and b, while peak c is broadened due to the convolution for two collisions to such an extent that it cannot be seen at about 40 eV.

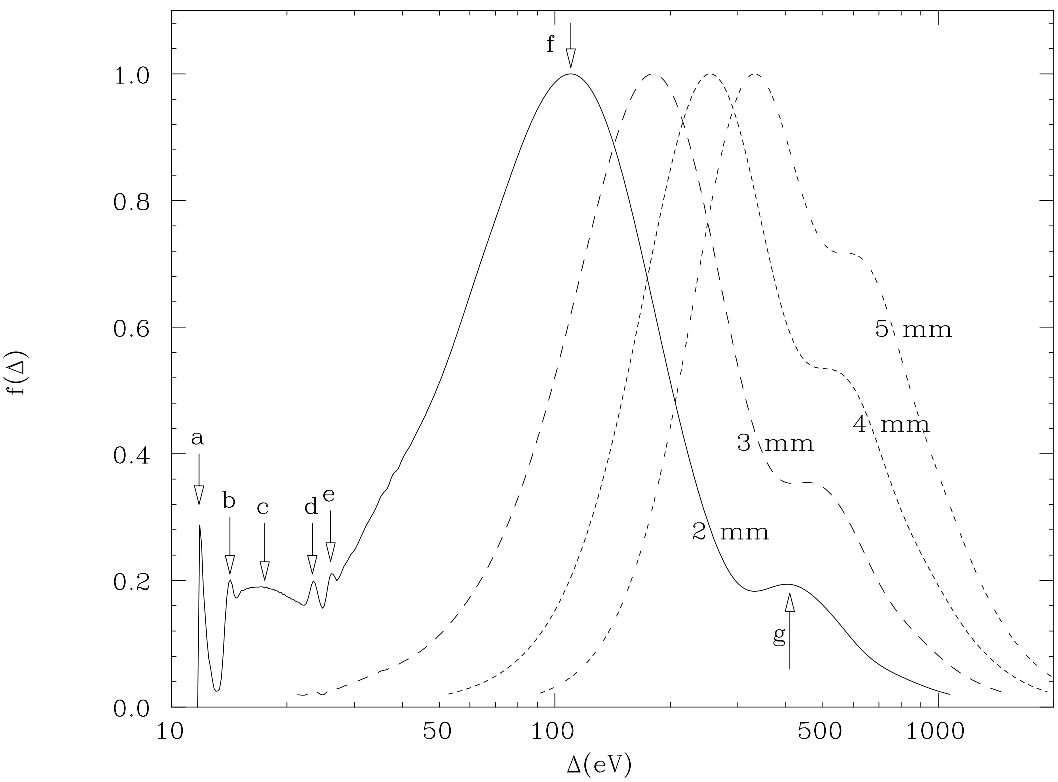

Figure 5.15-1. The peak at f is due to multiple collisions with energy losses less than 50 eV, and peak g is due to single energy losses to an L-shell electron.

[1]Nuclear Physics Laboratory Annual Report, University of Washington (1993) p. 56; (1994) p. 42; (1995) p. 46; (1996) p. 49.

[2]H. Bichsel, Rev. Mod. Phys. **60**, (1988) 662.

At 15 mm, a smooth function similar to a Landau-Vavilov function is obtained, solid line, in Fig. 5.15-2. It is compared to the Vavilov function (dotted line) and a Vavilov function “stretched” to have the same width and position as the convolution function (dash-dotted line).

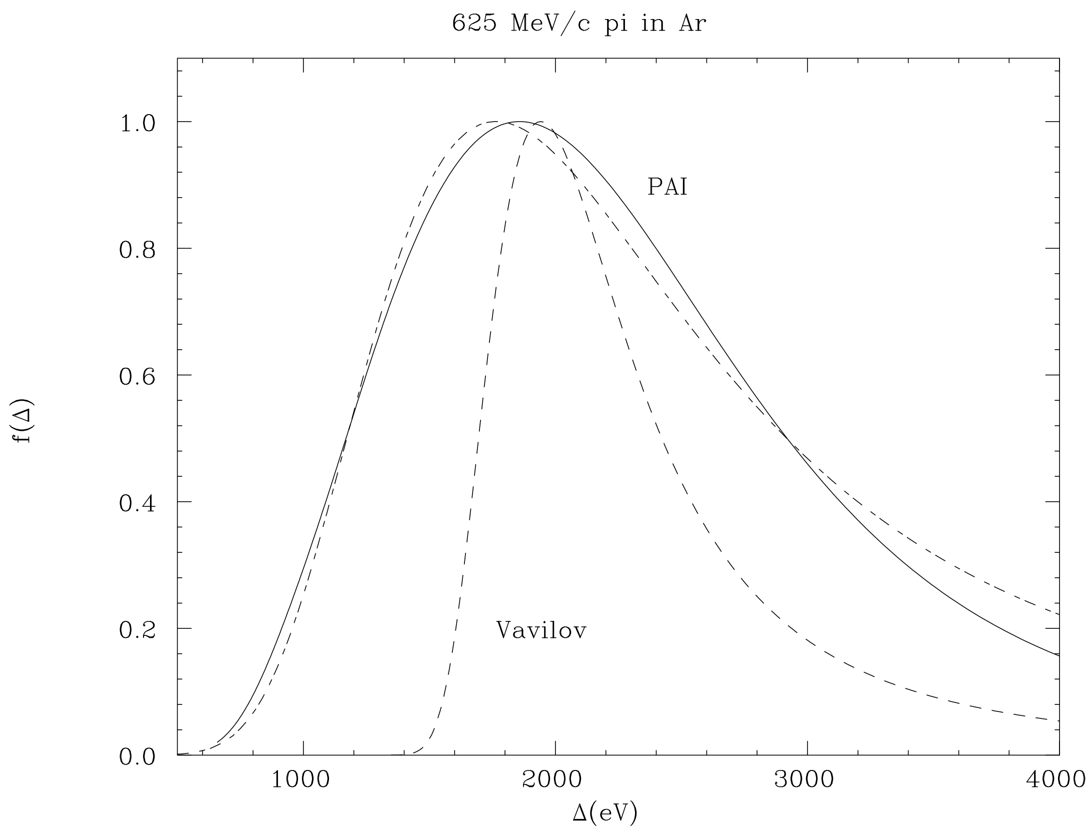

Figure 5.15-2. The most probable energy loss for the convolution function (PAI) is $\Delta_p = 1.86$ keV, the fwhm is $w = 1.75$ keV, for the Vavilov function $\Delta_p = 1.94$ keV, $w = 0.73$ keV.

6 Atomic and Molecular Clusters

6.1 High energy fragmentation of C_{60}

R. Vandenbosch and D. I. Will

We have previously studied the inclusive ("singles") and two-fragment coincidence distributions of collisional fragmentation[1] of C_{60} by H_2. It was found that the fragmentation of C_{60} can proceed via extraction of carbon chains with at least as many as eight carbons, and the remaining partner can still retain its fullerene structure. This process is competitive with the more commonly assumed dimer emission, and when sequential decay processes are included can account for the yield of even-n fullerenes down to n=32.

Below n=30 one sees a sizeable yield of fragments for all n, including odd as well as even n. Some of the lighter of these n<30 fragments can be attributed to the direct or sequential decay products of the longer chain partners to the fullerence products mentioned above. The n>10 fragments must mostly come from a different process, often assumed to be multifragmentation. This multifragmentation process is thought to be analogous to multifragmentation observed in nuclear reactions at higher bombarding energy. For C_{60} also multifragmentation seems to become relatively more important compared to binary fragmentation as the bombarding energy increases. We have therefore decided to study multifragmentation using a heavier target (Ar, M$\sim$40) to increase the energy available in the c.m. system.

The emphasis in this study is to look at three-fragment events where at least two of the fragments are sufficiently heavy to not come from sequential evaporation. Since we are using reverse kinematics, all of the reaction products from C_{60} incident on an Ar target are focused in a narrow cone in the forward direction. We use two electrostatic deflectors to analyze the reaction products. The first deflector looks at relatively light fragments, which have a low electric rigidity. They are deflected by ninety degrees into a channeltron detector. The heavier fragments, in the n=14 to 30 region, have a much higher electric rigidity and can escape from the first deflector through a hole in one of the plates. The second deflector has two exit slits, each of which is followed by a channeltron detector. In this deflector we can look at two fragments closer in mass, such as 14 and 15 or 18 and 19, etc. These examples correspond to some of the more intense mass peaks in the singles mass spectrum.

Preliminary results have been obtained for 45 kev C_{60} + Ar ($E_{c.m.}$=2370 ev). The relative yield of different light fragment masses in triple coincidence with n=18 and n=19 fragments has been determined for light fragment masses with n=2 to n=9. The three-fragment coincidence yield varies only weakly with light fragment mass over this size range. An enhancement of the yield of light fragments with an odd number of carbons is observed, perhaps related to the fact that the sum of the number of carbons of the two observed heavy fragments is odd.

[1] R. Vandenbosch, B.P. Henry, C. Cooper, M.L. Gardel, J.F. Liang, and D.I. Will, Phys. Rev. Lett. **81**, 1821 (1998).

6.2 Evidence for gas phase Si_2O_5 dianion

R. Vandenbosch

Recently we devised a new method for producing doubly-charged negative ions in the gas phase.[1] It is based on fragmentation of a singly-charged anion incorporating an electropositive atom. The singly-charged anion is fragmented after acceleration in a gas target. In a small fraction of the collisions the electropositive atom is removed as a positive ion leaving a dianion. We showed that C_9 dianions could be produced by fragmentation of the CsC_9 anion.

There is a recent theoretical prediction that Si_2O_5 can bind two extra electrons to make a stable dianion.[2] We are trying to test this prediction using our fragmentation method. We sputter a Na_2SiO_3 sample (with Ag binder) by bombardment with a Cs ion beam. The mass spectrum of the sputtered anions is very complex, but a peak is found at A=159 consistent with the $NaSi_2O_5$ singly charged negative ion. This ion is accelerated to an energy of 36 keV and fragmented in a H_2 gas target. The negative ion spectrum is analyzed with a ninety degree electrostatic deflector followed by a Channeltron detector. Prominent peaks in the deflector spectrum correspond to singly-charged SiO_2, SiO_3, and Si_2O_5 anions. A much weaker peak is found at the position corresponding to the Si_2O_5 dianion. This peak grows in magnitude relative to the SiO_2 and SiO_3 peaks as the discriminator level on the signals from the Channeltron is raised. This is the behavior expected for the more energetic dianions as compared to the SiO_2 and SiO_3 monoanions. Further experiments are planned to confirm this identification.

[1] R. Vandenbosch, D.I. Will, C. Cooper, B. Henry, and J.F. Liang, Chem. Phys. Lett. **274**, 112 (1997).
[2] T. Sommerfeld, M.K. Scheller and L.S. Cederbaum, J. Chem. Phys. **104**, 1464 (1997).

7 Electronics, Computing and Detector Infrastructure

7.1 Offline analysis and support computer systems

M. A. Howe, R. J. Seymour and J. F. Wilkerson

The Lab's network is a switched fabric blending over 90 ports of 100baseTX ethernet, thirty 10baseT ports, and our existing legacy 10base2 net. We use an HP 800T 8-port switch to partition the network to distribution hubs based upon speed and office location. One HP port is a full duplex 100baseFX fiber uplink to the campus routers. A secondary 5-port Hawking switch provides a full duplex connection between the two Alphaservers and the HP switch.

We continue to accrete desktop/side systems in the form of G4 Macintoshs for SNO/EWI/NCD tasks, and 450-MHz generic PCs as Windows98-based normal desktop workstations.

Our offline computing and analysis facility consists of:

- Our principal central compute-server base: a pair of dual-CPU Digital AlphaServer 4000/466s running Digital Unix, each with a gigabyte of ram and a StorageWorks 4 gigabyte system disk. This year we added a 288 gigabyte RAID system. With dual Mylex controllers, its eight 36-gig drives provide 216 gigs of user space, one 'parity' drive, and an active hot-swap drive. We've partitioned it to provide 70 gigs of non-RAID scratch space for SNO data tapes, with the remaining 146 gigs as a RAID-5 set for general user space. Our single DLT4000 tape drive has been supplemented with a single DLT8000 drive to handle the backup load of 260 gigs online on the Alphas. All other Unix and VMS systems route their backup load through the RAID system.
- Our VMS cluster, holding at three VAXstation 3100s, three 3200s and a single Alpha 3000/400. The cluster shares 26 gigabytes of disk space. In addition, we have a standalone OpenVMS AlphaStation 433au with a dedicated 27 gigs.
- The Ultra-Relativistic Heavy Ion group's seven Hewlett Packard 9000 Unix systems, all running HP-UX v10.2, sharing 62 gigabytes of distributed disks. Two of the systems are serving as workstations at STAR. One of the HPs is the lab's World Wide Web server (www.npl.washington.edu).
- The SNO and emiT group have Macintoshes, Power Computing 200 MHz PowerPC Mac clones and a growing number of Apple G4 systems. They also have a Sun SparcStation 20 running Solaris 2.5.1 to provide CADENCE circuit layout facilities to our electronics shop, two Sun Ultras and two SparcStation 2s.
- A dual-processor 400MHz Pentium II system running Red Hat Linux v6.2 serving as the development platform for our next data acquisition system (see Sec. 7.6). For compatibility with RHIC's RCF facility, we also have Red Hat Linux on a 233 MHz Pentium II system.
- We still share two VMS VAXstation 3200s providing Email and CPU cycles for the Institute for Nuclear Theory and the Physics Nuclear Theory group. We have a Sun Sparc 5 for Slow Controls software development for STAR, a VAXstation 3200 serving as the Linac's control and display system, three PDP-11/23s and six PDP-11/21s built into the Linac for cryogenics, vacuum and resonator control, and four PCs serving as controllers for the rest of the accelerator systems' interlocks, safety and vacuum system.

7.2 VAX-based data acquisition computer systems

M. A. Howe, R. J. Seymour and J. F. Wilkerson

For in-house particle data, we use three CAMAC/MBD-11/VAX/VMS-based acquisition systems.

They consist of Digital Qbus-based VAXStation 3200/GPXs running VMS v4.7a using VWS/UIS as their windowing software. Each VAXstation supports a BiRa MBD-11 controlled CAMAC crate. Our primary system is attached to a dozen dedicated 200 MHz Tracor Northern TN-1213 ADCs. Those ADCs and other CAMAC modules are coincidence-gated by a UWNPL-built synchronization interface, which includes monitor (Singles) and routing-Or capabilities. The system also has a bank of 32 10-digit 75 MHz NPL-built scalers.

Our principal VAXStation's dual BA-23 cabinet has an MDB-11 DWQ11 Qbus-to-Unibus converter driving a Unibus expansion bay. The system's Qbus peripherals include a CMD CQD-220/TM SCSI adapter for a Seagate ST41650 1.38 gigabyte disk, an Iomega Jaz 1 gigabyte removable disk and an occasional TTI CTS-8210 8mm tape drive. We also use a DEC IEQ11 IEEE-488 bus controller and a DEC DRV11-J parallel interface to control the scalers and IEEE-bus equipment. The Unibus bay contains a DR11-C parallel interface for the experiment controller, an LPV11 Printronix lineprinter controller and a Unibus cable continuing on to the MBD-11.

The other acquisition systems each consist of a VAXstation 3200/GPX's BA-23 cabinet and an Able Qniverter providing a Unibus cable direct to stand-alone MBD-11s. Unlike the principal system, these do not directly control non-CAMAC-based equipment.

One of the systems also has a CMD SCSI adapter for a 4 gigabyte hard drive, a Jaz drive and an 8mm tape system. That system is frequently used for near-line analysis and for media conversion from the Jaz platters to 8mm archival tapes.

All three systems run acquisition software based upon TUNL's XSYS, with major modifications to their DISPLAY program.

Development of the VAXs' eventual replacement systems is described in Sec. 7.6 of this report.

7.3 Electronic equipment

E. R. Eames, G. C. Harper, A. W. Myers and T. D. Van Wechel

Along with the normal maintenance and repair of the Nuclear Physics Laboratory's electronic equipment, projects undertaken by the electronics shop included the following:

1. The SNO NCD MUX boards have been fabricated and are currently being stuffed with components.
2. The ten delay line boxes for the SNO NCD MUX boards have been completed.
3. The controller for the SNO NCD MUX boards has been designed. The controller board layout is being done commercially.
4. The DAC boards that set the threshold voltages for the SNO NCD MUX boards and set the high voltage for the NCDs are currently being laid out.
5. The Shaper/ADC boards for the emiT and SNO NCD experiments have been constructed and are currently nearing completion of final testing.
6. Three Shaper/ADC boards were constructed for Los Alamos with Altera chips modified to replace the scalers with time tag registers.
7. The majority of the cables required for the SNO NCD electronics interface are completed.
8. Prototypes of the low power emiT preamp modules and a 4 channel mother board have been constructed for testing of performance and high voltage durability.
9. Several repairs were made to the sputter source in the Physics building that is used to plate insulators for the NCD tubes.
10. A high voltage and low voltage power supply control/monitor system was designed and constructed for the compact 20 MeV gamma-ray source that is used for energy calibration at the SNO.[1]

[1] Nuclear Physics Laboratory Annual Report, University of Washington (1998) p. 23.

7.4 Electronics upgrade

D. W. Storm

We received a capital equipment grant in the summer of 1999 for electronics. The grant was divided into four parts:

1. Test equipment.
2. URHI computer upgrade.
3. WALTA prototype.
4. Experimental program upgrade.

To date we have acquired about 70% of the test equipment, including a digital oscilloscope, an rf spectrum analyser, a low frequency spectrum analyser, and circuit board preparation equipment. We have about 65% of the electronics for the experimental program. This is primarily NIM electronics. We have obtained scintillator and some of the photomultiplier high voltage power supplies for the WALTA prototype, and we are in the process of procurement of the computers for the Relativistic Heavy Ion program.

7.5 The data acquisition electronics for the emiT and SNO NCD experiments

M. C. Browne* A. W. Myers, R. G. H. Robertson, T. D. Van Wechel and J. F. Wilkerson

The design of the electronics for the SNO Neutral-Current Detector has been completed except for the global trigger ID board and some details for the high voltage control. The NCD preamplifiers have been completed, and the MUX boards have been produced and are currently being stuffed with components. The controller board and the DAC boards that set and monitor the individual channel thresholds and set the high voltage for biasing the NCDs are currently being laid out.

The operation of the SNO NCD system has been changed slightly since last year.[1] As described previously it is impossible to get digitizer data for sequential decays in a single counter that are separated by less than the readout time of the digitizer, which is about one second. The assaying of U and Th alpha chains requires the time correlation of events with a 0.145 second half life. The scopes have been re-configured to make a one stage buffer. Each 4-channel scope services all 96 inputs (8 MUX boxes) with the equivalent scope inputs connected in parallel to 24 multiplexed channels. One of the scopes digitizes most of the pulses, with the active scope selected via a signal from the computer via VME and Control. A scope is triggered at its AUX TRIG input from Control, which routes the OR of 8 MUX-BOX-TRIGGERED inputs to the appropriate scope, for example Scope "A". That interrupts the continuous storage to the scope's circular buffer once the right number of points have been digitized. The scope then issues a service request (SRQ) over GPIB and waits to be read out. The time for readout depends on the service routine but may be 1 second or more per scope. During the time from the initial trigger to the end of readout the Main Trigger Out TTL signal (=SCOPE AVAIL) at the rear panel is LO and the scope ignores new triggers. If a second event arrives before Scope "A" becomes available the second scope "B", is triggered and digitizes the event.

Shaper/ADC boards[2] in revision C have been manufactured and stuffed, and are currently nearing completion of final testing. There are two versions of the shaper/ADC boards; the emiT shaper has a four-stage integrating shaping network with a 1 μs time constant and a 50 μs pole zero-compensation network, and the SNO NCD version of the board has a four stage integrating shaping network with a 4 μs time constant and no pole-zero compensation. Revision C sets the convert status register at the end of the ADC conversion to assure that an ADC cannot be read early. Also the floating scaler has been eliminated since it is redundant to the individual channel scalers. Several shaper/ADC boards have been built for Los Alamos, some with a custom programmed Altera chip that replaces the scalers with 48 bit time tag registers with 50 ns resolution.

For the emiT experiment prototypes of the low power preamps and a 4-channel motherboard have been constructed and tested. The low power preamp boards will be manufactured commercially and board layout for the 16 channel preamp mother board will commence shortly. The fiber-optic transmitters have been constructed. Also a temperature measurement circuit has been developed that fits on a board with the same footprint as the fiber-optic transmitter boards.

*Los Alamos National Laboratory, Los Alamos, NM 87545.
[1]Nuclear Physics Laboratory Annual Report, University of Washington (1999) p. 20.
[2]Nuclear Physics Laboratory Annual Report, University of Washington (1999) p. 55.

7.6 Status of advanced object oriented real-time data acquisition system

M. A.Howe, F. McGirt* and J. F. Wilkerson

Work is proceeding at NPL to develop an advanced object oriented real-time data acquisition (DAQ) system. The ultimate goal of this project is to implement a multiple platform, fast, scaleable, distributed DAQ system suitable for both small and large experiments. By using a client/server model to totally separate the hardware controlling computers (the servers) from the user interface computers (the clients), we are building in the flexibility to have multiple server computers taking and processing data while being controlled by a remote client and/or viewed by multiple remote monitoring clients. We will support both the common crate-based DAQ hardware systems (VME and CAMAC) as well as PC-based DAQ cards. The server and client frameworks are designed in such a way that it is easy to add support for new DAQ objects as the need arises.

Both the client and the server are written in C++ using the gnu compiler running under the Linux operating system. The graphic user interface uses the Qt, which provides a cross platform widget set for both Windows and Unix. For communication between the client and server, we are using CORBA (Common Object Request Broker Architecture). CORBA is industrial standard client/server software that makes Internet communication between objects very easy to implement.

Good progress has been made on the framework code for the hardware servers. The servers, after being set up by the controlling client, do all data acquisition and processing. They have no external user interface at all, only a low-level programming interface. Objects existing at the server level implement all of the functionality of the hardware objects that they represent. The server level objects that have been implemented so far include the low-level PCI driver, the VME 617 crate controller, and VME FIFO hardware buffer cards. Work is progressing on a VME crate object that will encapsulate an interface to all of the VME cards. A mechanism to allow the hardware objects to pass data from one to another and to data processing objects is finished. Work has begun on a histogram data processing object.

Significant progress has also been made on the main client, which provides an easy to use graphic user interface to the hardware servers. To set up a hardware configuration, the user selects a hardware or data processing element from a list of available objects in a catalog dialog and drags that element to a configuration window. The desired object is created on the server when the drag is completed, and appears in the configuration window as an icon. Each icon is a proxy for the 'real' object that exists on the server. It acts as an 'observer' of that object and so can show the object's status. The data flow between objects is set up at run time by dragging lines from object to object. Double clicking on an icon brings up a dialog for controlling and/or viewing the status of the represented server object. Work is progressing to add an automatic updating feature so that all icons and dialogs can provide real-time status of that object.

In the near future we will be polishing the core framework and adding support for many more types of DAQ cards. In addition, we are developing objects for processing, formatting, storing, and viewing the data.

*Los Alamos National Laboratory, Los Alamos, NM 87545.

7.7 Performance overview of a 7-channel silicon microstrip detector

A. L. Caraley, A. R. Junghans, T. L. McGonagle and R. Vandenbosch

The strip detector used for the ^{40}Ca + ^{208}Pb fusion barrier distribution experiment is a 7-channel totally depleted silicon microstrip detector[1] with a full depletion voltage of +20V. During the first two months of operation it was observed to have a leakage current between .5 μA and .7 μA. when +27V were applied across the 12 MΩ resistor pre-amp connected to the detector's back-plane. An energy signal and a timing signal were collected from the back-plane. Rather than using a pre-amp for each of the seven strips, delay-lines were used between adjacent strips and each end of the detector was connected to one of two additional pre-amps. A strip position signal was created from the relative timing between signals from each end of the detector. Typical peak-to-valley resolution between individual strips was 1000:1. During initial setup, the CFD delays of all three pre-amps were established using a ^{252}Cf fission fragment source.

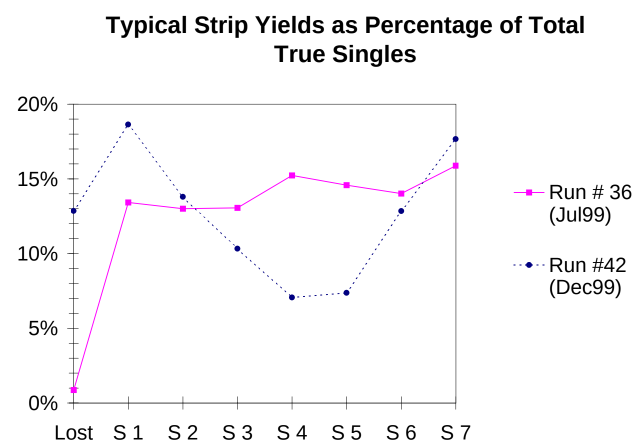

Figure 7.7-1. Typical strip yields, showing deterioration.

The detector was used to collect coincident fragments at 5 beam energies during the months of July and August of 1999, and subsequently at 9 more energies in December of 1999. The first sign of performance problems for the detector was an increase of leakage current from .5 μA to over 1 μA within the first two days of data collection in December 1999. The strip detector continued to be plagued with a high leakage current, reaching values as high as 2.9 μA, throughout the nearly three weeks of its use in December. The rate of rise for the detector leakage current became so great near the end of scheduled beamtime that several bias adjustments per two hour run became necessary in order to maintain the +20V net bias. A correlation between the presence of beam and rising leakage current was observed during this time. Off-line analysis of the data collected revealed a loss of counts in the detector, particularly from the middle strips, even though full depletion voltage had been maintained. This is illustrated in Fig. 7.7-1 where individual strip singles efficiencies from a typical December run are compared to those from a run from July. For the figure, 'Lost' refers to events without a valid position signal, while 'S 1' through 'S 7' refer to the individual strips. Data analysis also showed sagging elastic peak energies and an overall deterioration of energy resolution

[1]Micron Semiconductor Limited, Lancing, Sussex, England.

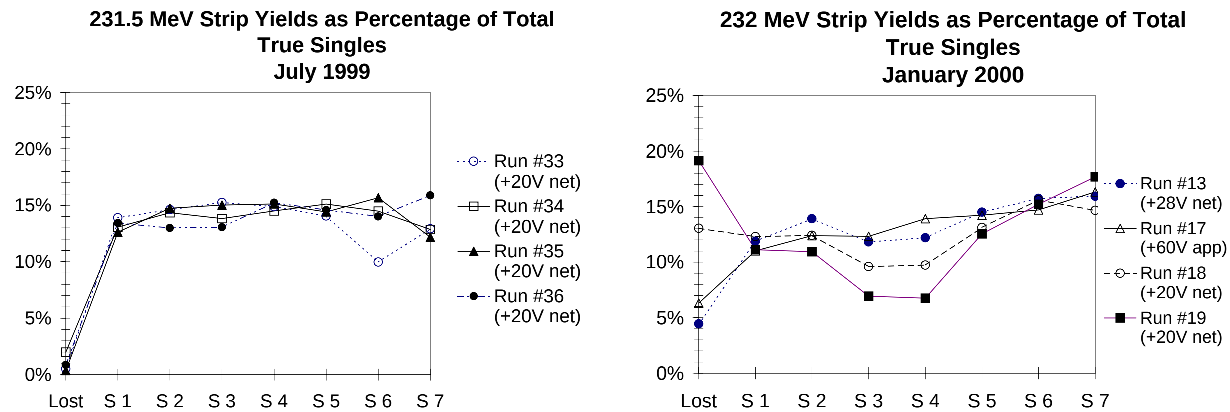

Figure 7.7-2. Comparison of July 1999 and January 2000 strip yields.

for the middle strips. The beamtime scheduled for January was used to conduct tests in an effort to determine the cause of the dramatic decline of the strip detector collection efficiency.

January testing began with a run using a ^{241}Am source to measure the solid angle of the entire detector as well as those of the individual strips. Count rates agreed with those observed during the initial set-up in July, and the solid angles calculated were as expected from the experimental geometry. Different CFD delays were then used for additional runs. Only a reduction of the CFD delays to 1/10 their "run-time" values resulted in any observable change in strip relative detection efficiencies. Even if severely damaged by radiation, a silicon detector would not be expected to produce such a large change in signal risetime, and therefore a "mis-match" between the CFD delays and the risetime of the actual signals is not considered to be responsible for the observed reduction of detection efficiency.

Following the alpha source runs, several hours of runs were taken using the ^{208}Pb target with the ^{40}Ca beam at 232 MeV. The effect on leakage current of having beam in the chamber was immediate. For the first run with beam, the leakage current rose from 1.75 μA to 2.2 μA in 15 minutes. The effect of turning the beam off had just as an immediate effect, with leakage current dropping visibly the moment beam was off, and continuing to recover for as long as the beam remained off. In addition, data collected after the detector had not been subjected to beam for a couple of hours showed a much higher strip efficiency than data collected after the detector had been in operation with beam for several hours. The bias settings for these runs included maintaining a net bias of +30V, setting a constant applied bias of +60V, and maintaining a net bias of +20V. Strip efficiency improved with higher levels of bias. Four of the January runs at 232 MeV energy provide the comparison shown in Fig. 7.7-2 to four 231.5 MeV runs from July 1999.

The final two tests done in January explored the possible existence of a beam-related source of electrons in the vicinity of the detector. Each test began with a period of running at +20V net with beam until the leakage current began to rise and the detector exhibited a loss of efficiency in the middle strips. At this point a run was done with beam with the ^{241}Am source in place, effectively blocking the beam. Count rates for the alpha source showed a much lower detection efficiency for the middle strips. When the beam was shut off, however, the relative efficiency for the middle strips began to improve, and continued to improve until all strips were the same. The chamber was then opened and magnets were installed on the apparatus holding the strip detector. The previous test was then repeated. The initial irradiation, however, did not produce the same level of poor performance in the detector as it had previously. Also, relative strip efficiency seen while hitting the back of the alpha source with beam was nearly that seen for the alpha source alone.

Although neutron and proton radiation are typically much more damaging to silicon than electrons, these last two tests point to electrons as the cause of the detector performance problems. The cause of these secondary electrons, as well as the sensitivity of this particular detector to them, is still being investigated.

8 Van de Graaff, Superconducting Booster and Ion Sources

8.1 Van de Graaff accelerator operations and development

G. C. Harper, C. E. Linder, A. W. Myers and T. D. Van Wechel

The tandem was entered 29 times this year.

Nine brief tank openings were for the purpose of ascertaining the optimum distribution of ball bearing column section shorts to allow operation with very low terminal voltages (see Sec. 8.3).

Seven openings were to change the gas and the magnet in the Terminal Ion Source (TIS) for the production of different ion species.

Four openings were for changing the terminal configuration from stripper to TIS, or for the reverse.

On 7/16/99 the LE cold trap overfilled and froze its O-ring. This let air into the beam tube to an estimated pressure of 200 microns before automatic valves could close. At the time of the accident the tandem terminal voltage was 8.5 Mv. This damaged beam tube No. 1, by creating point electron sources that stimulated X-ray emission, causing beam instabilities that hamper LINAC operation. (The O-ring seal has since been replaced by a metal seal.)

These emission points were more or less precisely located by dragging a small shorting bar (referred to as a "boat") the length of the LE column with the terminal set at a high enough voltage to excite the problem X-rays, while continuously monitoring local X-ray levels. When the boat shorted certain planes X-ray emission would drop off significantly. The resistors in those planes found to be X-ray instigators were then reduced to half value, keeping the particular plane potentials below field emission levels.

Four openings were required for boat testing and plane shorting before there was a satisfactory reduction of X-rays.

One opening was made to replace the LE tube grid, which was first thought to be the problem. It was not.

There was one tank opening for each of the following:

1. To refoil.
2. To repair the vertical steerers and the HE column current pickup. (One opening.)
3. To repair the terminal computer.
4. To remove a column resistor shunt, which had fallen out of the resistor string and lodged between two rings with the connector pins pointing out towards the floor, making a spark gap that effectively limited terminal voltage to 3 MV.

We replaced no chain idlers or pick-up pulleys this year.

During the year from March 1, 1999 to February 29, 2000 the tandem pellet chains operated 2178 hours. The DEIS operated 331 hours, and the SpIS 739 hours. Additional statistics of accelerator operations are given in Table 8.1-1.

Activity	Days Scheduled	Percent
Molecular research, deck ion sources only	32	9
Nuclear physics research, TIS and tandem	69	19
Nuclear physics research, ^{4}He or below, tandem only	3	1
Nuclear physics research, heavy ions, tandem only	3	1
Nuclear physics research, ^{4}He or below, tandem and LINAC	0	0
Nuclear physics research, heavy ions, tandem and LINAC	+38	+10
Subtotal, molecular or nuclear physics research	145	40
Machine development, maintenance, or crew training	+138	+37
Grand total	283	77

Table 8.1-1. Tandem accelerator operations
March 1, 1999 to February 29, 2000.

8.2 Booster operations

J. F. Amsbaugh, G. C. Harper, M. A. Howe, D. W. Storm and D. I. Will

During the period March 1, 1999 to Feb 28, 2000, the booster was operated for 28 days. This is a continuation of the trend last year when we ran 31 days.

Only ^{40}Ca was accelerated.

We spent quite a bit of time diagnosing and repairing a bunch phase lock instability that appeared during one of the ^{40}Ca runs. There is a feedback system that adjusts the low energy buncher phase to maintain phase lock between the LINAC clock and the beam entering the LINAC. Normally this system requires occasional adjustments in the operating point to keep the control loop functioning, but otherwise works reliably. Following a vacuum accident in the low energy tube of the tandem, which occured when the tandem was at 8.5 MV, the timing of the bunches entering the LINAC shifted often and substantially enough that the feedback system could not maintain phase lock for more than a few minutes. We traced the source of this instability to discharges in the low energy tube, and the magnitude of these discharges was indicated by x-rays of 10 to 20 mR/hr detected outside the tandem tank. The discharges fluctuated in intensity even when the tandem was running steadily. We believe that the discharges altered the field pattern in the low energy tube, where the ions are moving slowly, and so influenced the time of flight through the tandem significantly. The fluctuations in the intensity of the discharges corresponded to fluctuations in the time of flight beyond the range of the phase locking electronics. The amount of voltage change from the discharges was not so much, however, that the energy regulator of the tandem failed. We were able to locate some of the main sites of these discharges and short out the tube sections, as described in Sec. 8.1. After this was done we were able to accelerate ^{40}Ca again with the LINAC.

There was no extensive maintenance on the LINAC. All resonators are presently operable.

We continue to operate the low beta resonators at an average field of 3.0 MV/m and the high beta ones at average of 2.4 MV/m.

The helium compressors continued to run with no failures this year. Our oldest compressor now has run for 115k hours, and the other two have run for 79k hours in one case and 56k hours in the other case. The compressor with over 100k hours is one of the three originally installed before the booster was completed in 1987.

8.3 Tandem terminal ion source

G. C. Harper, C. E. Linder, A. W. Myers and T. D. Van Wechel

The terminal ion source (TIS) was used in several experiments during this reporting period, all for the ^{7}Be(p,γ)^{8}B experiment. Most of the runs used ^{1}H$^+$ at terminal voltages from 0.3 MV to 1.5 MV. The remaining runs used either ^{2}H$^+$ at terminal voltage of 1.4 MV or ^{4}He$^+$ at a terminal voltage of 1.37 MV. The list of experiments run with the TIS to date is given in Table 8.3-1.

The tank was only opened for routine servicing for the terminal ion source this reporting period. On one occasion the tank was opened to replace a source canal which had sputtered away. The boron-nitride insulator and the pyrex discharge bottle were also replaced at this time. Additional openings were required for changing ion species or the tube gradient.

Development for this year included modeling of the toroidal electrostatic deflector. The toroidal deflector was designed to have optical properties as similar as possible to those of a double focusing magnet. When tested it was found that the deflector had focusing power that was unbalanced in the vertical and horizontal planes or had second order effects that were more significant than expected. Transport of an ion beam from the deflector was difficult at all energies tested. We plan to do further tests using unbalanced electrode voltages after careful modeling with an electrostatics design program.

We continue to use 0.5 inch diameter chrome-plated steel ball bearings inserted between the anti-corona rings of the column to short out various planes of the beam tube. We have found this to be an extremely fast way to alter the gradient for optimum beam transmission at these low energies.

Future plans for terminal ion source use are to procure a non-inclined field tube in either new or used condition. A non-inclined field tube would not add the transverse perturbations which have made tuning the very low energy (100 keV to 300 keV) ion beam very difficult.

ION	ENERGY RANGE (kev)	EXPERIMENT	BEAM CURRENT (μamps)
^{1}H$^+$	300-1400	^{7}Be(p,γ)	10-20
^{2}H$^+$	770, 1000	^{7}Li(d,p)	15-18
^{3}He$^+$	5500	^{6}Li(^{3}He,n)	28
^{4}He$^+$	1370	^{7}Be(α,γ)	12

Table 8.3-1. Table of ion species and TIS experiments.

8.4 Cryogenic operating experience

J. H. Elms, G. C. Harper, M. A. Howe, D. W. Storm and D.I. Will

The superconducting booster LINAC is cooled by liquid helium from a Koch Process Systems, Inc.,[1] Model 2830S Helium Refrigerator. During a shutdown due to power outage, water ice diffused to the cold end and blocked the coaxial Refrigerator Delivery Tube between the 2830S and the 1000 liter dewar. The blockage had little effect on J-T operations but reduced wet engine efficiency severely. To clear this ice the dewar was isolated and warmed above room temperature for the first time since 1990. The RDT was removed, derimed and repumped. During this period the 2830S continued operating at liquid helium temperature with its cold end high-to-low-pressure bypass valve cracked open to act as an impromptu J-T. The following table summarizes maintenance[2] for 1999 January 1 to 1999 December 31:

Item	In Use	Major Services	Times Performed
Helium Refrigerator			
Cold Box	94%	warm/pump/purge	2
Main Dewar	96%	warm/pump/purge	1
Top Expander	∼7000 Hrs	warm/pump/purge	6
	∼130 RPM	belts and valve seals	1
		wrist pin and cam follower brngs	1
		flywheel and crank pin bearings	1
		main piston seals	3
Middle Expander	∼6000 Hrs	warm/pump/purge	8
	∼100 RPM	belts and valve seals	1
		wrist pin and cam follower brngs	1
		flywheel and crank pin bearings	1
		main piston seals	3
Wet Expander	∼2000 Hrs	warm/pump/purge	4
	∼50 RPM	belts and valve seals	1
		wrist pin and cam follower brngs	1
		flywheel and crank pin bearings	1
		main piston seals	1
		repaired DC drive motor controller	1
Distribution System	92%	warm, pump, purge lines	4

This final table shows screw compressor history here as of 2000 March 21:

Item	Total	1999	Status	Maintenance
RS-1	115,052 hours	8694 hours	running	none
RS-2	57,547 hours	0 hours	phases shorted	core removed 1993
RS-2a	55,990 hours	8663 hours	running since 1993	none
RS-3	22,752 hours	0 hours	shorted to ground	core removed 1990
RS-3a	79,554 hours	3979 hours	running since 1990	none

[1] The cryogenic division of Koch was bought by Cryogenic Plants and Services, a division of Pro-Quip Corporation, affiliate of Linde, AG.

[2] Nuclear Physics Laboratory Annual Report, University of Washington (1999) p. 60.

9 Outside Users

9.1 Degradation of solar cells in space radiation environments

B. E. Anspaugh*

The purpose of this task is to establish a method of calculating the degradation of dual- and triple-junction solar cells in space radiation environments.

The electrical characteristics of several cells of each type and from three separate suppliers have been measured to establish their pre-irradiation electrical parameters. The cells are irradiated with both electrons and protons to several energies and fluences, and electrical characteristics measured after each irradiation. These characteristics will be plotted as curves of electrical degradation vs. fluence for each energy and particle type. The degradation curves will be used as input to a computer program for calculating radiation damage coefficients as a function of energy and shielding protection (coverglass thickness) in an omnidirectional radiation environment. The results will be folded into another computer program which will allow the calculating of solar cell degradation of the dual- and triple-junction solar cells in any electron and/or proton space radiation environment.

Cell degradation as a function of 10-MeV proton irradiation is a key set of data in the above calculations.

On November 19, 1999 we irradiated 16 cells with 10 MeV protons at the NPL. The cells were irradiated to a fluence of $2. \times 10^{12}$ protons/cm^2. The cells were irradiated in two runs, 8 cells per run. We achieved a uniform beam over all the cells by interposing a gold scattering foil in the beam line. The gold foil used was 51.6 microns thick. The foil to target plane distance was approximately 4 meters and resulted in a calculated uniformity over the target plane of $\pm 2\%$. Another set of irradiations was performed on January 18, 2000, using the same procedure. These cells were irradiated to 7 different fluences ranging from $5. \times 10^{10}$ to $3. \times 10^{12}$ protons/cm^2. Results are not yet available.

*Jet Propulsion Laboratory, 4800 Oak Grove Drive, Pasadena, CA 91109.

9.2 Scientific Imaging Technologies (SITe) CCDs in the space radiation environment

M. Blouke, J. Janesick, G. Soli and A. Reinheimer*

Solar flare protons are of primary concern to CCDs operating in interplanetary space. Protons, in addition to producing total dose damage in CCD oxides, also create displacement damage in the bulk silicon. SITe SF023A CCDs were irradiated at the NPL during the previous year. This note models displacement damage allowing CCD performance in the space radiation environment to be accurately predicted.[1]

The SF023A is a split-frame-transfer CCD. This means that the image is split at the CCD center and read out through serial registers at the top and bottom of the CCD. The heavy curve shown in Fig. 9.2-1 is from a region-of-interest near the center of the CCD, before charge can be lost from shifting the signal charge from row to row. The light curve is from a region-of-interest near the serial registers, after row shifting has taken place. Parallel Charge Transfer Efficiency, CTE, is measured by the shift in the X-ray peak energy shown in Fig. 9.2-1. X-ray generated charge is lost to proton generated traps in the bulk silicon. The shift in the X-ray peak energy indicates a CTE > 0.99999, the $>$ being due to the error in the X-ray-peak fits. A CTE of 1 would indicate that no charge was lost.

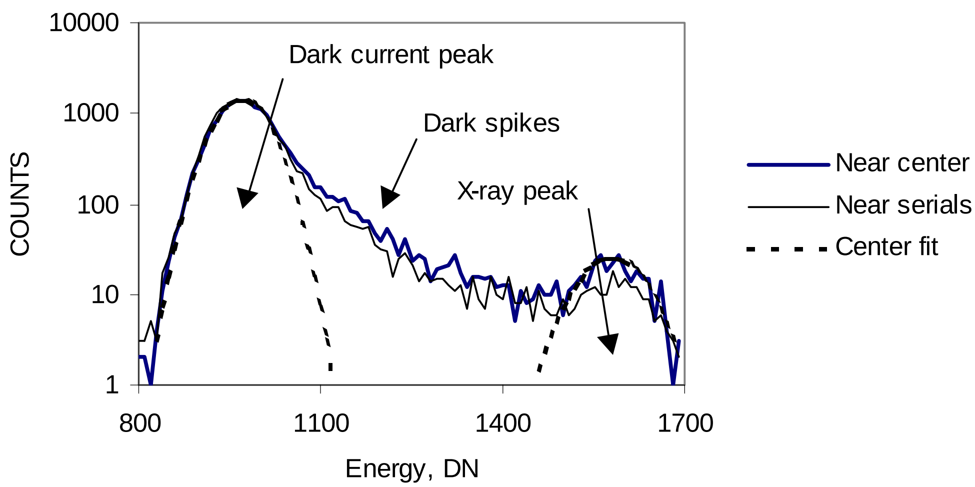

Figure 9.2-1. Device SF023A (09-A1) operating at +8° C with a 10 s row shift time after being irradiated with 1.25×10^9p/cm^2 at 8 MeV.

The SF023A (09-A1) operating with a 10 s row shift time at +8°C, shows a factor of 162 improvement in parallel CTE over the old SITe TK512 CCD. A factor of 6.5 comes from[2] the decreased pixel area in the SF023A and a factor of 25 comes from running the CCD with a 10 s row shift time at +8°C (6.5 x 25 = 162). The same CCD (09-A1) has a CTE of 0.9998 running slow and cold, with a 360 s row shift time at 80°C, for the factor of 25 improvement. A 625 ms

*All authors at Scientific Imaging Technologies, Inc., Beaverton, OR 97075.

[1] J. Janesick, G. Soli, T. Elliott and S. Collins, "The effects of proton damage on charged coupled devices," in Charged Coupled Devices and Solid State Optical Sensors II, Proc. SPIE 1447.87 (1991).

[2] Nuclear Physics Laboratory Annual Report, University of Washington (1999) pp. 62-63.

integration time was required to allow the X-ray peaks to be seen above the dark spikes. Fe-55 5.9 keV X-rays were used, indicating an energy calibration of 2.6 electrons per DN.

Carrier emission from proton generated traps is enhanced by strong electric fields.[3] The amount of dark current generated from a single trap can increase orders of magnitude in electric fields greater than 105 V/cm. CCDs with smaller pixels have higher electric fields. For comparison to the old SITe TK512 CCD, dark spikes are defined as the dark current at a dark spike density of 100 counts in the region-of-interest. The TK512 proton generated, dark spike damage factor, at 0°C at the 100 count level, is 10.8 pA/cm^2-krad. The dark spike counts for the SF023A are shown in Fig. 9.2-1, but the dark spike damage factor was computed from data without the X-ray source. The SF023A dark spike damage factor, adjusted to 0°C at the 100 count level, is 124 pA/cm^2-krad, an increase of more than a factor of 10 over the old SITe TK512 CCD. Newer CCD star-tracker cameras that use CCDs with smaller pixels for improved CTE need to handle more dark spikes.

Running multi-pinned-phased (mpp) to hold the signal charge away from the surface, eliminating surface dark current, the old TK512 has a dark current damage factor at room temperature of 62 pA/cm2-krad. The SF023A, adjusted to room temperature, has a 37 pA/cm^2-krad damage factor, shown as the dark current peak in Fig. 9.2-1.

The Tandem Van de Graaff particle accelerator at the University of Washington Nuclear Physics Laboratory was used to accelerate protons into SITe SF023A CCDs. In order to expose the CCDs to a uniform fluence of protons, gold scattering foils were used to spread the proton beam out over the CCDs. The scattering foils were placed in the beam pipe 130” up-stream from the CCDs.

The proton detector was exposed through a (1/493) cm^2 collimator in order to maintain a silicon surface barrier detector count rate less than 1 x 10^4 protons per second (to avoid pulse pileup) and a 4 krad exposure time of about 10 minutes. The proton count was accumulated in a preset scalar that turned off the proton beam at a preset total count where counts times 493 equals the total fluence.

[3] P.W. Marshall, C. J. Dale, E. A. Burke and G. P. Summers, IEEE Trans. Nucl. Sci. **36**, 1831 (1989).

10 Nuclear Physics Laboratory Personnel

Faculty

Eric G. Adelberger	Professor	
Hans Bichsel	Affiliate Professor	
John G. Cramer	Professor	
Peter J. Doe	Research Professor	
Hiroyasu Ejiri[1]	Visiting Professor	
Steven R. Elliott	Research Assistant Professor	
George W. Farwell	Professor Emeritus	
Jens H. Gundlach	Research Associate Professor	
Isaac Halpern	Professor Emeritus	
Blayne R. Heckel	Professor	
Michael V. Romalis	Assistant Professor	
R.G. Hamish Robertson	Professor;	Scientific Director
Kurt A. Snover	Research Professor	
Thomas D. Steiger	Research Assistant Professor	
Derek W. Storm	Research Professor;	Executive Director
Thomas A. Trainor	Research Professor	
Robert Vandenbosch	Professor Emeritus	
William G. Weitkamp	Professor Emeritus	
John F. Wilkerson	Professor	

Postdoctoral Research Associates

Stefan Baessler[2]
Manojeet Bhattacharya
Anne L. Caraley[3]
Alice Araz Hamian
Ryuta Hazama[4]
Arnd R. Junghans
Qingjun Liu
Stephen M. Merkowitz
Ulrich Schmidt
Gregory Smith[5]
Josephus P. S. van Schagen[6]

[1]Research Center for Nuclear Physics, Osaka University, Osaka, Japan.
[2]Q-Das GmbH, Niederliebersbach, Germany.
[3]Indiana University, Bloomington, IN.
[4]Japan Fellow.
[5]Skagit Community College, Mt. Vernon, WA.
[6]WRQ Co., Seattle, WA.

Predoctoral Research Associates

Qazi Rushdy Ahmad
Michael Browne[7]
Theresa Bullard
Ki-Young Choi
Charles Duba
Robert Fardon
Karsten Heeger
Bruce Henry[8]
Charles David Hoyle
Qiling Huang[9]
Dan Kapner
Graeme Lufkin[9]
Antonino Miceli[9]
Erik Mohrmann
Hans Pieter Mumm
John Orrell
Jeffrey Reid
Kathryn Schaffer
Miles Smith
Sarah Veatch
Eric Zager[9]

Professional staff

The professional staff are listed with a description of their recent major efforts.

John F. Amsbaugh	Research Engineer	Mechanical design, Vacuum systems
Thomas H. Burritt	Research Engineer	Construction SNO NCD's
James E. Franklin	Research Engineer	Construction SNO NCD's
Gregory C. Harper	Research Engineer	Electronic and mechanical design Accelerator upgrades and operation
Mark A. Howe	Research Engineer	Software for DAQ, control systems
Carl E. Linder	Research Engineer	Electrical systems, Tandem operations
Duncan J. Prindle, Ph.D.	Research Scientist	Heavy Ion software
Richard J. Seymour	Computer Systems Manager	
H. Erik Swanson, Ph.D.	Research Physicist	Precision experimental equipment
Timothy D. Van Wechel	Electronics Engineer	Electronic design, construction, maintenance
Douglas I. Will	Research Engineer	Cryogenics, Ion sources

Technical staff

James Elms	Instrument Maker
Allan Myers	Electronics Technician
Hendrik Simons	Instrument Maker, Shop Supervisor
Willie White[10,12]	Electronic Shop Helper
Steven Zsitvay[11]	Instrument Maker

[7] Los Alamos National Laboratory, Los Alamos, NM.
[8] Microsoft Corp., Redmond, WA.
[9] Department of Physics, University of Washington Seattle, WA 98195.
[10] Seattle, WA.
[11] Physical Plant, University of Washington, Seattle, WA.

Administrative staff

Barbara J. Fulton	Administrator
Karin M. Hendrickson	Fiscal Specialist

Undergraduate Helpers

Daniel B Allred
Misty Bentz[12]
Jon Bumgardner
Nathan Collins
Paul Duffell
Clara Eberhardy
Adrian Fehr
Elysa Kuznetz
Jeff Leonard[12]
Merisa Mackey[12]
Angus MacNab[12]
Bhasker Moorthy
Manish Naidu[12]
Chris Paul[12]
Antonio Ramos[12]
Kyle Sundqvist
Lincoln Webbeking
Kevin Ayers[12]
Michael Bradley[12]
Daryl Carlson[12]
Erik Curre[12]
Ellen Eames
Adam Elias
Laura Grout
Joshua Leingang
Nels Lindberg
Tami McGonagle
Christy McKinley
Robert O'Neill
Cheth Ouch
Annika Peter
Christopher Scannell
Tien Troung[12]
Matthew Wilson[12]

[12]Left during 1999.

11 Degree Granted, Academic Year, 1999-2000

Preparation for Deployment of the Neutral Current Detectors (NCDs) for the Sudbury Neutrino Observatory (SNO). Michael C. Browne, North Carolina State University and University of Washington, (1999).

12 List of Publications from 1999-2000

Published papers:

"Limits on the annual modulation of WIMPs-nucleus scattering with large-volume NAI(T1) scintillators," K. Fushimi, H. Ejiri, K. Hayashi, R. Hazama, T. Kishimoto, N. Kudomi, K. Kume and H. Ohsumi, Astro. Phys. **12**, 185 (1999).

"Electron detachment and fragmentation in collisions between 1.25 keV/carbon C_8^- and C_{60}^- clusters and H_2," M.L. Gardel, R. Vandenbosch, B.P. Henry, C. Cooper and D.I. Will, Euro. Phys. J D **7**, 79 (1999).

"Low-background ^{3}He proportional counters for use in the Sudbury Neutrino Observatory," M.C. Browne, and SNO collaborators (including P.J. Doe, C.A. Duba, S.R. Elliott, K.M. Heeger, R.G.H. Robertson, M.W.E. Smith, T.D. Steiger, and J.F. Wilkerson), IEEE Transactions in Nucl. Sci. **46**, 873 (1999).

"Strangeness measurements in the NA49 experiment with Pb projectiles," S. Margetis and the NA49 collaborators (including J.G. Cramer, J.G. Reid and T.A. Trainor), J. Phys. G **25**, 189 (1999).

"Xi and anti-Xi+ production in Pb+Pb collisions at 158-GeV per nucleon," J. Bachler and the NA49 collaborators (including J.G. Cramer, J.G. Reid and T.A. Trainor), J. Phys. G **25**, 199 (1999).

"Reconstruction over a large rapidity interval of lambda, antilambda and K0(S) in the NA49 experiment," H. Appelshauser and the NA49 collaborators (including J.G. Cramer, J.G. Reid and T.A. Trainor), J. Phys. G **25**, 469 (1999).

"A rotating torsion balance to measure Newton's constant," J.H. Gundlach, Meas. Sci. Technol. **10**, 454 (1999).

"The NA49 large acceptance hadron detector," S. Afanasiev and the NA49 collaborators (including J.G. Cramer, J.G. Reid and T.A. Trainor), Nucl. Instrum. Methods A **430**, 210 (1999).

"Metallic ^{7}Be target of small diameter," A.Y. Zyuzin, L.R. Buchmann, J.S. Vincent, K.R. Buckley, N.P. Bateman, K.A. Snover, J.-M. Casandjian, T.D. Steiger, E.G. Adelberger and H.E. Swanson, Nucl. Instrum. Methods A **438**, 109 (1999).

"Time reversal in polarized neutron decay - the emiT experiment," G.L. Jones and emiT collaborators (including H.P. Mumm, R.G.H. Robertson, T.D. Steiger and J.F. Wilkerson), Nucl. Instrum. Methods A **440**, 648 (2000).

"The giant-dipole resonance in hot Sn nuclei," M.P. Kelly, K.A. Snover, J.P.S. van Schagen, M. Kicinska-Habior and Z. Trznadel, Nucl. Phys. A, **649**, 123c (1999).

"GDR decay and bremsstrahlung emission in ^{12}C + ^{58,62}Ni reactions," M. Kicinska-Habior, Z. Trznadel, M.P. Kelly, K.A. Snover, and J.P.S. van Schagen, Nucl. Phys. A, **649**, 130c (1999).

"Systematics of the nuclear giant dipole resonance," D. Kusnezov, Y. Alhassid and K.A. Snover,

Nucl. Phys. A, **649**, 193C (1999).

"Centrality dependence of directed and elliptic flow at the SPS," A.M. Poskanzer and the NA49 collaborators (including J.G. Cramer, J.G. Reid and T.A. Trainor), Nucl. Phys. A **661**, 344 (1999).

"A systematic study of two particle correlations from NA49 at the CERN SPS," R. Ganz and the NA49 collaborators (including J.G. Cramer, J.G. Reid and T.A. Trainor), Nucl. Phys. A **661**, 448 (1999).

"Collective transverse expansion in central Pb+Pb collisions at the SPS," H. Appelshauser and the NA49 collaborators (including J.G. Cramer, J.G. Reid and T.A. Trainor), Part. Nucl. Phys. **42**, 311 (1999).

"Universal pion freeze-out phase space density," D. Ferenc, U. Heinz, B. Tomavsik, U.A. Wiedemann and J.G. Cramer, Phys. Lett. B **457**, 347 (1999).

"Event-by-event fluctuations of average transverse momentum in central Pb+Pb collisions at 158-GeV per nucleon," H. Appelshauser and NA49 collaborators (including J.G. Cramer, J.G. Reid and T.A. Trainor), Phys. Lett. B **459**, 679 (1999).

"Two protons correlations from 158-A/GeV Pb+Pb central collisions," H. Appelshauser and NA49 collaborators (including J.G. Cramer, J.G. Reid and T.A. Trainor), Phys. Lett. B **467**, 21 (1999).

"Statistical model for fragmentation of C_{60}," R. Vandenbosch, Phys. Rev. A **59**, 3584 (1999).

"Measurement of the response of the Russian-American Gallium experiment to neutrinos from a ^{51}Cr source," J.N. Abdurashitov and SAGE collaborators (including S.R. Elliott and J.F. Wilkerson), Phys. Rev. C **59**, 2246 (1999).

"Fission fragment folding angle distributions for the system ^{11}B+^{237}Np, ^{12}C+ ^{236}U, and ^{16}O+^{232}Th in the energy range $1.1 < E/V_b < 2.1$," S. Kailas, D.M. Nadkarni, A. Chatterjee, A Saxena, S.S. Kapoor, R. Vandenbosch, J.P. Lestone, J.F. Liang, D.J. Prindle, A.A. Sonzogni and J.D. Bierman, Phys. Rev. C **59**, 2580 (1999).

"Measurement of the solar neutrino capture rate with Gallium metal," J.N. Abdurashitov and SAGE collaborators (including S.R. Elliott and J.F. Wilkerson), Phys Rev. C **60**, 055801 (1999).

"Short-range tests of the Equivalence Principle," G.L. Smith, J.H. Gundlach, E.G. Adelberger, B.R. Heckel and H.E. Swanson, Phys. Rev. D **61**, 022001 (1999).

"The giant dipole resonance width at high excitation energy: does it saturate?" M.P. Kelly, K.A. Snover, J.P.S. van Schagen, M. Kicinska-Habior and Z. Trznadel, Phys. Rev. Lett. **82**, 3404 (1999).

"Positron-neutrino correlations in the $0^+ \rightarrow 0^+$ decay of ^{32}Ar," E.G. Adelberger and the ISOLDE collaborators (including H.E. Swanson and H. Bichsel), Phys. Rev. Lett. **83**, 1299 (1999).

"Improved test of the Equivalence Principle for gravitational self-energy," S. Baessler, B.R. Heckel, E.G. Adelberger, J.H. Gundlach, U. Schmidt and H.E. Swanson, Phys. Rev. Lett. **83**, 3585 (2000).

"Measurement of the solar neutrino capture rate by SAGE and implications for neutrino oscillations

in vacuum," J.N. Abdurashitov and SAGE collaborators (including S.R. Elliott and J.F. Wilkerson), Phys. Rev. Lett. **83**, 4686 (1999).

"Aspects of fast-ion dosimetry," H. Bichsel, T. Hiraoka and Omata, Radiation Research, **153**, 208 (2000).

"Limits on the annual modulation of WIMPs-nucleus scattering with large-volume NAI(T1) scintillators," K. Fushimi, H. Ejiri, K. Hayashi, R. Hazama, T. Kishimoto, N. Kudomi, K. Kume and H. Ohsumi, Rev. Sci. Instrum. **12**, 185 (1999).

"Event-by-Event analysis and the QGP phase transition," T.A. Trainor, *Proceedings of the Workshop Particle Distributions in Hadronic and Nuclear Collisions*, eds. M. Adams, R. Betts, T. Imbo, W.-Y. Keung and U. Sukhatma (World Scientific, Singapore) (1999).

"Event analysis using scaled topological measures in NA49," D.D. Weerasundara, *Proceedings of the Workshop Particle Distributions in Hadronic and Nuclear Collisions*, eds. M. Adams, R. Betts, T. Imbo, W.-Y. Keung and U. Sukhatma (World Scientific, Singapore) (1999).

"Probing the QCD phase boundary with finite collision systems," T.A. Trainor, *Proceedings of the 15th Winter Workshop on Nuclear Dynamics*, eds. W. Bauer and G.D. Westfall (Kluwer Academic/Plenum Publications, New York) (1999).

"^{3}He Neutral current detectors at SNO," S.R. Elliott, M.C. Browne, P.J. Doe, C.A. Duba, J.V. Germani, K.M. Heeger, A.W.P. Poon, R.G.H. Robertson, M.W.E. Smith, T.D. Steiger, P.M. Thornewell and J.F. Wilkerson, in *New Era in Neutrinos Physics*, eds. H. Minakata and O. Yasuda, Universal Academy Press Inc., Tokyo, Japan p. 235 (1999).

"Searches for new long-ranged forces: Equivalence Principle violation and planck-scale physics," E.G. Adelberger, S. Baessler, J.H. Gundlach, B.R. Heckel, C.D. Hoyle, S.M. Merkowitz, G.L. Smith and H.E. Swanson, in *Physics Beyond the Standard Model*, eds. P. Herczeg, C.M. Hoffman and H.V. Klapdor-Kleingrothaus, World Scientific Publ. Co., Singapore, p. 717 (1999).

"*Gravitational Physics: Exploring the Structure of Space and Time*," J.B. Hartle, E.G. Adelberger, A.V. Ashtekar, B.K. Berger, G.T. Horowitz, P.F. Michelson, R. Narayan, P.R. Saulson, D.N. Spergel, J.H. Taylor, S.A. Teukolsky and C.M. Will), National Academy Press, Washington, DC (1999).

Papers submitted or to be published:

"Positron-Neutrino correlations in ^{32}Ar and ^{33}Ar decays: Probes of scalar weak currents and nuclear isospin mixing," A. Garcia and the ISOLDE collaborators (including E.G. Adelberger, H.E. Swanson and H. Bichsel), submitted to Hyperfine Interactions.

"High-Voltage Microdischarge in Ultra-Low-Background ^{3}He Proportional Counters," K.M. Heeger, S.R. Elliott, R.G.H. Robertson, M.W.E. Smith, T.D. Steiger and J.F. Wilkerson, in press, IEEE Transactions of Nucl. Sci.

"Background Studies for the Neutral Current Detector Array in the Sudbury Neutrino Observatory," K.M. Heeger, P.J. Doe, S.R. Elliott, R.G.H. Robertson, M.W.E. Smith, T.D. Steiger and

J.F. Wilkerson, in press, IEEE Trans. Nucl. Sci.

"A low-noise ^{3}He ionization chamber for measuring the energy spectrum of a cold neutron beam," S.D. Penn, E.G. Adelberger, B.R. Heckl, D.M. Markoff and H.E. Swanson, submitted to Nucl. Instrum. Methods.

"The Sudbury Neutrino Observatory," J. Boger and the SNO collaborators (including Q.R. Ahmad, T.H. Burritt, P.J. Doe, C.A. Duba, S.R. Elliott, J.E. Franklin, A.A. Hamian, K.M. Heeger, M. Howe, A. Meyers, R.G.H. Robertson, M.W.E. Smith, T.D. Steiger, T. Van Wechel and J.F. Wilkerson), in press, Nucl. Instrum. Methods in Physics Research A.

"Data analysis techniques for extracting Gamow-Teller strengths from 0° (p,n) data," C.D. Goodman, M. Bhattacharya, M.B. Aufderheide, S.D. Bloom and P. Zuprawski, submitted to Nucl. Instru. Methods.

"A compact ^{3}H(p,γ)^{4}He 19.8-MeV Gamma-Ray Source for Energy Calibration of the Sudbury Neutrino Observatory," A.W.P. Poon, R.J. Komar, C.E. Waltham, M.C. Browne, R.G.H. Robertson, N.P. Kherani and H.B. Mak,in press, Nucl. Instrum. Methods in Physics Research A.

"New limit on the D coefficient in polarized neutron decay," L.J. Lising and emiT collaborators (including H.P. Mumm, R.G.H. Robertson, T.S. Steiger and J.F. Wilkerson), to be submitted to Phys. Rev. C.

"Isoscalar, isovector, orbital, and spin contributions in M1 transitions in mirror nuclei," Y. Fujita, B.A. Brown, H. Ejiri, K. Katori and H. Ueno, submitted to Phys. Rev. C, Feb. 2000.

"A measurement of Gamow-Teller Strength for ^{176}Tb $\rightarrow$ ^{176}Lu and the efficiency of a solar neutrino detector," M. Bhattacharya, C.D. Goodman, R.S. Raghavan, M. Palarczyk, A. Garcia, J. Rapaport, I.J. van Heerden and P. Zupranski, submitted to Phys. Rev. Lett.

"Shape of the ^{8}B alpha and neutrino spectra," C.E. Ortiz, A. Garcia, R.A. Waltz, M. Bhattacharya and A.K. Komives, submitted to Phys. Rev. Lett.

"Nuclear spin isospin responses for low energy neutrinos," H. Ejiri, accepted, Physics Reports.

"In-target chemistry during the production of ^{15}O and ^{11}C using ^{3}He reactions," K.A. Krohn, J.M. Link and W.G. Weitkamp, in press, Radiochim. Acta.

"Spectroscopy of Double-Beta and Inverse-Beta Decays from ^{100}Mo for Neutrinos," H. Ejiri, J. Engel, R. Hazama, P. Krastev, N. Kudomi and R.G.H. Robertson, preprint (Nov. 1999).

"Event-by-Event analysis and the central limit theorem," T.A. Trainor, preprint, hep-ph/0001148, (2000).

Invited talks, abstracts and other conference presentations:

"The GDR at high excitation energy; does the width saturate?" K.A. Snover, *Riken Symposium on Selected Topics in Nuclear Collective Excitations (Nucolex99)*, Tokyo Japan, March 1999, Riken symposia series, N.D. Dang, ed., Riken Review 23, July 1999, p. 111 (invited paper).

“Catching some Zs: The solar neutrino problem, neutral currents, and SNO,” T.D. Steiger, *Particle Astrophysics Seminar*, Univer. of Mich, Ann Arbor, MI, March, 1999.

“Probing the QCD phase boundary with finite collision systems,” T.A. Trainor, invited talk, University of Oregon, Eugene, OR, April, 1999.

“The role of scaling in statistical analysis,” T.A. Trainor, invited talk, University of Oregon, Eugene, OR, April, 1999.

“NA49 Event-by-Event analysis,” J.G. Reid, *Quark Matter ’99* Torino, Italy, May, 1999.

“Results from current solar neutrino experiments,” J.F. Wilkerson, invited review talk, *Particles in Collision Conference*, Ann Arbor, MI, June 1999.

“Neutral Current Detection in the Sudbury Neutrino Observatory,” K. Heeger, *National Nuclear Physics Summer School*, UCSD San Diego, CA, June/July, 1999.

“Neutral-current detection at SNO: Something new under the Sun?” T.D. Steiger, invited talk, *INT Workshop on Neutrino Physics*, University of Washington, Seattle, WA, July, 1999.

“Neutrino studies by double beta decays,” H. Ejiri, *Workshop on Neutrino Physics*, invited paper, Seattle, WA, July, 1999.

“Neutrino mass and oscillations,” R.G.H. Robertson, invited talk, *Lepton-Photon ’99 International Conference*, Stanford, CA, August, 1999.

“The Washington Large Area Time Coincidence Array,” E. Zager and WALTA collaborators (including J.G. Cramer, S.R. Elliott and J.F. Wilkerson), *Proceedings of the 26th International Cosmic Ray Conference*, Salt Lake, Utah, August, 1999.

“Background studies for the Neutral-Current Detector Array in the Sudbury Neutrino Observatory,” K.M. Heeger, to be published in *TAUP99, 6th International Workshop on Topics in Astroparticle and Underground Physics*, College de France, Paris, France, Poster, September, 1999.

“Neutrino detection using lead perchlorate,” P.J. Doe, S.R. Elliott, C. Paul and R.G.H. Robertson, to be published in *TAUP99, 6th International Workshop on Topics in Astroparticle and Underground Physics*, College de France, Paris, France, September, 1999.

“University of Washington Lab Report to SNEAP,” G.C. Harper, *Symposium for Northeastern Accelerator Personnel*, Knoxville, TN, October, 1999.

“Tandem terminal ion source,” G.C. Harper, *Symposium for Northeastern Accelerator Personnel*, Knoxville, TN, October, 1999.

“High-Voltage Microdischarge in Ultra-Low-Background ^{3}He Proportional Counters,” K. Heeger *IEEE Nuclear Science Symposium*, Seattle, Washington, USA, October, 1999.

“Review of neutrino oscillation experimental results,” S.R. Elliott, American Physical Society, Asilomar, CA, Bull. Am. Phys. Soc. **44**, 11 (1999).

“STAR event-by-event physics program,” T.A. Trainor and STAR collaborators, American Physical Society, Asilomar, CA, Bull. Am. Phys. Soc. **44**, 21 (1999).

"The solar neutrino problem and neutral current detection at SNO," S.R. Elliott, Pacific Northwest National Laboratory, Richland, WA November, 1999.

"The solar neutrino problem and neutral current detection at SNO," S.R. Elliott, University of Wisconsin, Madison, WI, February, 2000.

"The solar neutrino problem and neutral current detection at SNO," S.R. Elliott, TRIUMF, Vancouver, Canada, February, 2000.

"DSV - A general visualization tool for HEP event data," D. Prindle, *International Conference on Computing in High Energy Physics - CHEP2000*, Padova, Italy, February, 2000.

"Zooming in on hadronization or the dynamical structure of 0 and 1," T.A. Trainor, *RHIC 2000*, Park City, UT, March, 2000.

"The giant dipole resonance at high excitations energy; does the width saturate?" K.A. Snover, invited talk, American Physical Society, Asilomar, CA, Bull. Am. Phys. Soc. **44**, 28 (1999).

"Status of the SNO experiment," J.F. Wilkerson, invited talk, *3rd International Symposium on Symmetries in Subatomic Physics*, Adelaide, Australia, March, 2000.

"Nuclear spin isospin responses and spectroscopy of β-β rays from ^{100}Mo for neutrino studies in nuclei," invited paper, *Carolina Symposium on Neutrinos Physics - Its Impact on Particle Physics, Astrophysics, and Cosmology*, Columbia, SC, March, 2000.

Conference presentations by collaborators of NPL personnel:

"Multiparticle dynamics of Pb+Pb collisions at the CERN SPS," G. Roland and NA49 collaborators (including J.G. Cramer, J.G. Reid and T.A. Trainor), presented at *27th International Symposium on Multiparticle Dynamics (ISMD 97),* Frascati, Italy, Sept. 1997, Phys. Proc. Suppl. **71**, 261 (1999).

"Overview of hadronic observables measured by NA49 at the CERN/SPS in central Pb-208 + Pb collisions at 158-GeV/nucleon," P. Foka and the NA49 collaborators (including J.G. Cramer, J.G. Reid and T.A. Trainor), *29th International Conference on High-Energy Physics (ICHEP 98)*, Vancouver, British Columbia, Canada, July, 1998, published in High Energy Physics **2**, 1491 (1999).

"Can doubly strange dibaryon resonances be discovered at RHIC?" R.L. Ray and NA49 collaborators (including J.G. Cramer, J.G. Reid and T.A. Trainor), American Physical Society, Austin, TX, Bull. Am. Phys. Soc. **44**, in press.

"Two proton correlations from Pb+Pb central collisions," F. Wang and the NA49 collaborators (including J.G. Cramer, J.G. Reid and T.A. Trainor), presented at the *15th Winter Workshop on Nuclear Dynamics*, Park City, UT, January 1999.

"Solar neutrino results from SAGE," J.S. Nico and SAGE collaborators (including S.R. Elliott and J.F. Wilkerson), *Proceedings of the xth International School on Particles and Cosmology*, Baksan Valley, Kabardino-Balkaria, Russia, April 1999, to be published by World Scientific Publishing Co. Pte. Ltd.

“Systematic study of hadronic observables in nucleus nucleus collisions at the CERN SPS,” R. Ganz and the NA49 collaborators (including J.G. Cramer, J.G. Reid and T.A. Trainor), Tampere, Finland, July, 1999.

“Double beta decays of ^{100}Mo by ELEGANT V at Oto Cosmo Observatory,” N. Kudomi, H. Ejiri, K. Fushimi, K. Hayashi, T. Kishimoto, K. Kume, B. Kuramoto, H. Ohsumi, K. Takahisa, Y. Tsujimoto and S. Umehara, *TAUP99, 6th International Workshop on Topics in Astroparticle and Underground Physics*, September, 1999, College de France, Paris, France.

“Search for WIMPs with the large NaI (T1) scintillator of ELEGANT V,” S. Yoshida, H. Ejiri, K. Fushimi, K. Hayashi, M. Komori, N. Kudomi, K. Kume, H. Kuramoto, K. Matsuoka, H. Ohsumi, K. Takahisa, Y. Tsujimoto, and S. Umehara, *TAUP99, 6th International Workshop on Topics in Astroparticle and Underground Physics*, September, 1999, College de France, Paris, France.

“The parity non-conserving neutron spin-rotation in liquid helium,” D.M. Markoff and PNC collaborators (including B.R. Heckel, E.G. Adelberger, S. Baessler, U. Schmidt and H.E. Swanson), American Physical Society, Asilomar, CA, Bull. Am. Phys. Soc. **44**, 16 (1999).

“Time reversal in polarized neutron decay - the emiT experiment,” K.P. Coulter and emiT collaborators (including H.P. Mumm, R.G.H. Robertson, T.D. Steiger and J.F. Wilkerson), American Physical Society, Asilomar, CA, Bull. Am. Phys. Soc. **44**, 17 (1999).

“The TRIUMF parity violation experiment,” R.J. Woo and the TRIUMF collaborators (including A.A. Hamian), American Physical Society, Asilomar, CA, Bull. Am. Phys. Soc. **44**, 17 (1999).

“If 5 isospin mixing in the $0^+ \to 0^+$ β decay of ^{32}Ar,” A. Komives and other collaborators (including E.G. Adelberger, M. Bhattacharya and H.E. Swanson), American Physical Society, Asilomar, CA, Bull. Am. Phys. Soc. **44**, 67 (1999).